Spring 2017

SEQUENCE STRATIGRAPHIC CORRELATION OF THE BOW ISLAND MEMBER OF THE THERMOPOLIS FORMATION USING SURFACE OUTCROP AND SUBSURFACE DATA, LIBERTY AND HILL COUNTIES, MONTANA

Michael Vineyard
Montana Tech

SEQUENCE STRATIGRAPHIC CORRELATION OF THE BOW ISLAND MEMBER OF THE THERMOPOLIS FORMATION USING SURFACE OUTCROP AND SUBSURFACE DATA, LIBERTY AND HILL COUNTIES, MONTANA

by

Michael Vineyard

A thesis submitted in partial fulfillment of the

requirements for the degree of

Master of Science in Geoscience:

Geology Option

Montana Tech

2017

Abstract

The Bow Island Member of the Thermopolis Formation in Montana is a low-pressure gas producer, which formed due to the first (Kiowa-Skull Creek) transgressive–regressive cycles of the Cretaceous Western Interior Seaway.

The Bow Island Member and its correlative units (Viking and Muddy Formations) have been extensively exploited for oil and gas throughout Canada and Wyoming, but remains relatively unmapped in Montana. The area of stratigraphic study is located at section 15, T36N, R5E Liberty County, Montana. This area located on Dafoe Ranch exhibits a moderately exposed stratigraphic section of Cretaceous Thermopolis Formation. The Bow Island Member lies between the Skull Creek Shale Member and the Shell Creek Shale Member of the Thermopolis Formation. The measured stratigraphic section of the Bow Island is approximately 270 feet. The section shows a progradational parasequence set of five coarsening upward sequences deposited in an offshore to uppershoreface depositional environment. Very fine to coarse-grained sandstone sequences are separated by mudstone flooding surfaces. The sequence boundary between a highstand systems tract and a transgressive systems tract is marked by a sandstone containing black chert pebbles. The previously recognized bed of chert-pebble lag gravel marks a position of erosion and the Albian eustatic drop in sea level. The unconformity marked by the middle Bow Island top is interpreted as second order and the parasequences are interpreted as fourth to fifth order.

Well-log data from exploratory and producing wells are used to conduct subsurface and sequence stratigraphic mapping of the Bow Island Formation. Correlation of 814 wells located near East Butte and the surrounding area into Liberty and Hill counties are used to map surfaces recognized in outcrop to the subsurface. Four informal units correlated are: Bow Island top, middle Bow Island, lower Bow Island, Skull Creek Shale. Four structure contour maps, four isochore maps and two 3D visualizations are shown to illustrate the Bow Island in a 35-township area in north central Montana. Most of the controls for gas production in the area are structural, a new subsurface domal structure is detailed in the 3D visualizations. Stratigraphic traps within the Bow Island could not be determined from log rasters.

The PANalytical TerraSpec Halo Mineral Identifier was used to identify minerals within samples obtained from the exposed beds of the sediments in the Bow Island Member to determine the cause for decreased production in wells drilled in the area. Illites and micas are the predominant minerals throughout the column. A combination of processes (particle plugging, clay swelling, change in pH) lead to decreased permeability within the member.

Keywords: Bow Island, Stratigraphy, Subsurface, Mineralogy

Acknowledgements

I would like to thank my wonderful wife Catie for her patience and continued support during graduate school. Dr. Larry Smith for his guidance and help throughout my graduate career. Dr. Curtis Link and Dr. Chris Gammons for their help as the graduate committee.

Table of Contents

List of Tables

List of Figures

1. Introduction

The Lower Cretaceous Bow Island-Viking Member of northern Montana and southern Alberta and Sakatchewan, Canada formed as a product of transgression and regression events of the Western Interior Seaway. The Bow Island is comprised of upward coarsening cycles of offshore to foreshore deposits and a succession of tidal flat, estuarine, and lagoonal deposits (Pedersen, 2001). The Bow Island Member is characterized by Pedersen (2001) as having an overall progradational-retrogradational architecture. Sandstones and mudstones within the Bow Island represent a wedge shaped coarse clastic interval that prograded from the Cordilleran orogenic belt eastward to the Western Canadian foreland basin where the lower Bow Island was deposited in a offshore to lower shoreface environment, the middle Bow Island was deposited in an offshore to foreshore depositional environment, and the upper Bow Island was deposited in tidal flat/estuarine environment (Peterson, 1966).

In the study area (Figure 1), the Bow Island Member lies conformably above the Skull Creek Shale Member of the Thermopolis Formation and lies unconformably below the Shell Creek Shale Member of the Thermopolis Formation. The Western Interior Seaway was an epeiric sea that separated North America during the Cretaceous (Figure 2). The Bow Island is equivalent to members of the Blackleaf Formation in western Montana and the Muddy Formation in Colorado and Wyoming. In Canada, the Bow Island is equivalent to the Viking Formation (Figure 3).

In Montana, the Bow Island Member is a shallow low-pressure gas producer which was found as a secondary play while targeting deeper horizons. The Bow Island produced 1.3 BCF throughout Montana in 2015 (Montana Board of Oil and Gas, 2016; last accessed 25 October, 2016; appendix A). According to MBOG data, 1073 wells are producing oil and gas currently

from the Bow Island throughout Montana (Montana Board of Oil and Gas, 2016; last accessed 25 October, 2016). The Bow Island has not been studied as extensively in Montana as it has in Alberta, likely due to production being limited to mostly shallow natural gas in the study area (Figure 1).

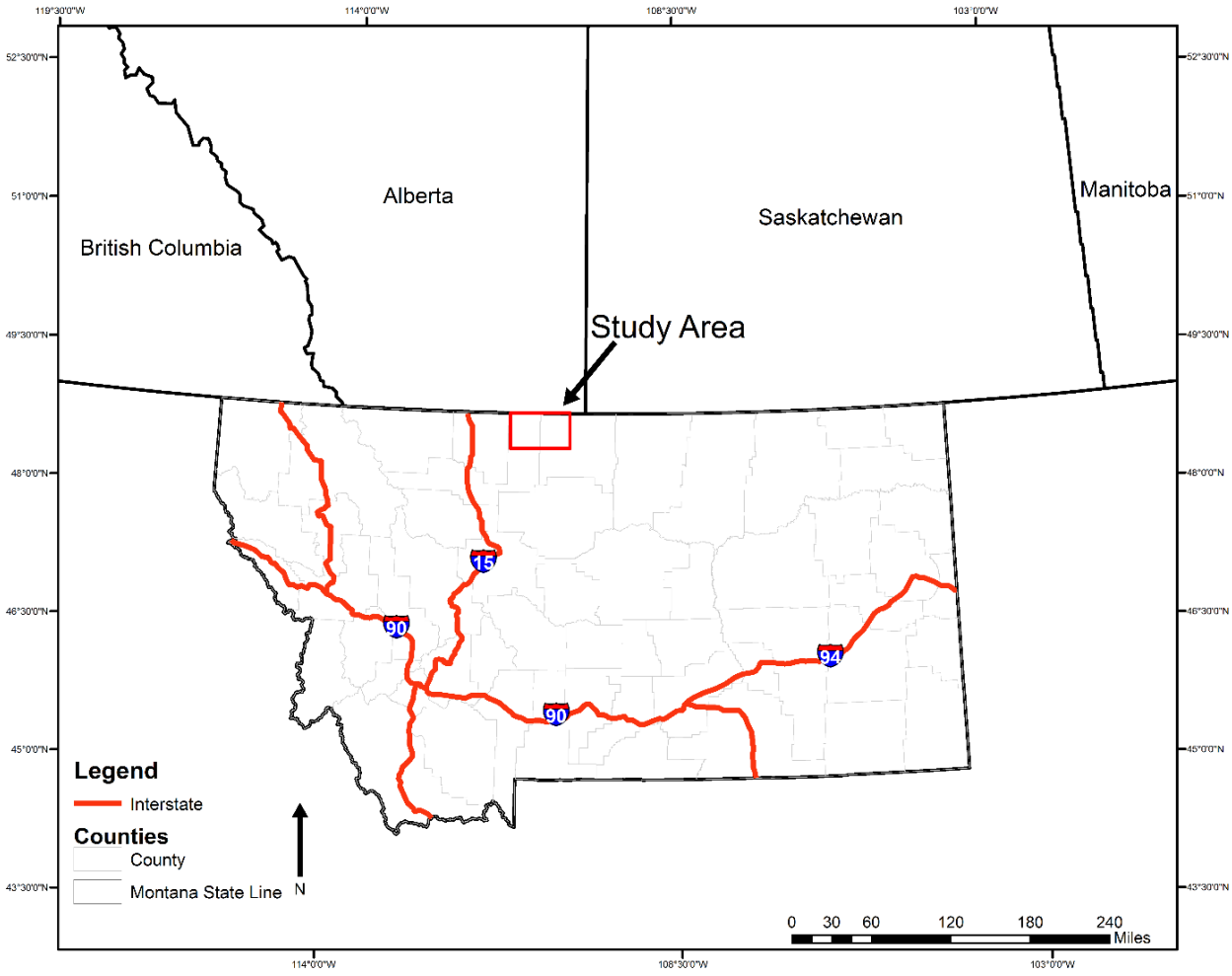

Figure 1: Location of the study area highlighted by the red box.

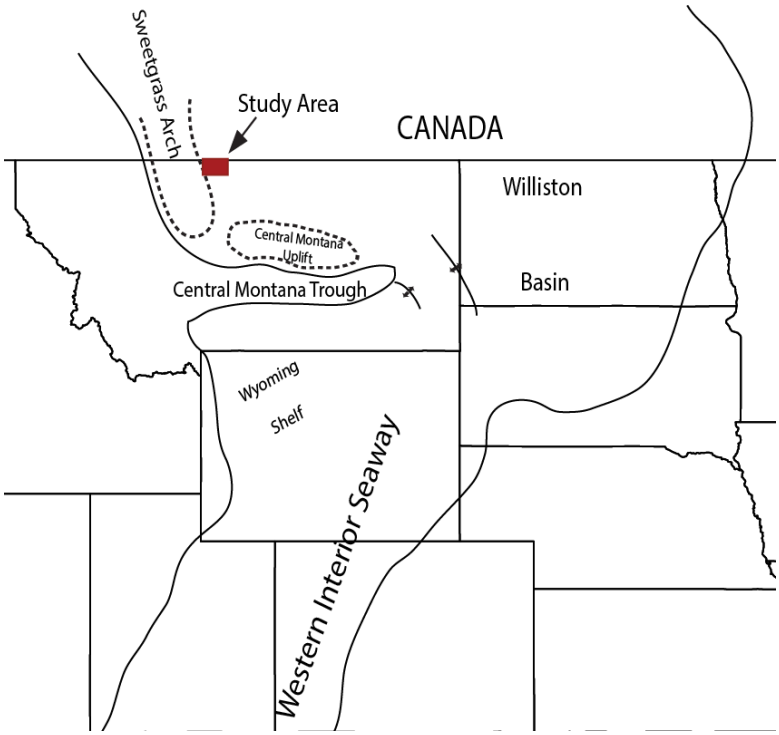

Figure 2: General location of the Western Interior Seaway. The red box in north central Montana illustrates the location study area. (modified from Peterson, 1966).

1.1. Overview of Previous Work

Until recently, the Bow Island was not a focus of studies as it had been in the past. Before work that Porter et al. (1997) conducted, the Bow Island in Montana had not been part of a work study for nearly 30 years. Croft (2012) chose to conduct a wide scale mapping project of the Bow Island throughout north central Montana. Prior to that, the Bow Island was seen as a large potential natural gas producer in Montana and was the subject of many reports conducted by the USGS and the Billings Geological Society (Cobban and Reeside 1952; Cobban, 1955; Cobban and Erdmann, 1959; Cobben et al., 1976). The reports looked to identify depositional environments, clarify nomenclature of members within the Bow Island, and characterize the hydrocarbon potential of the Bow Island.

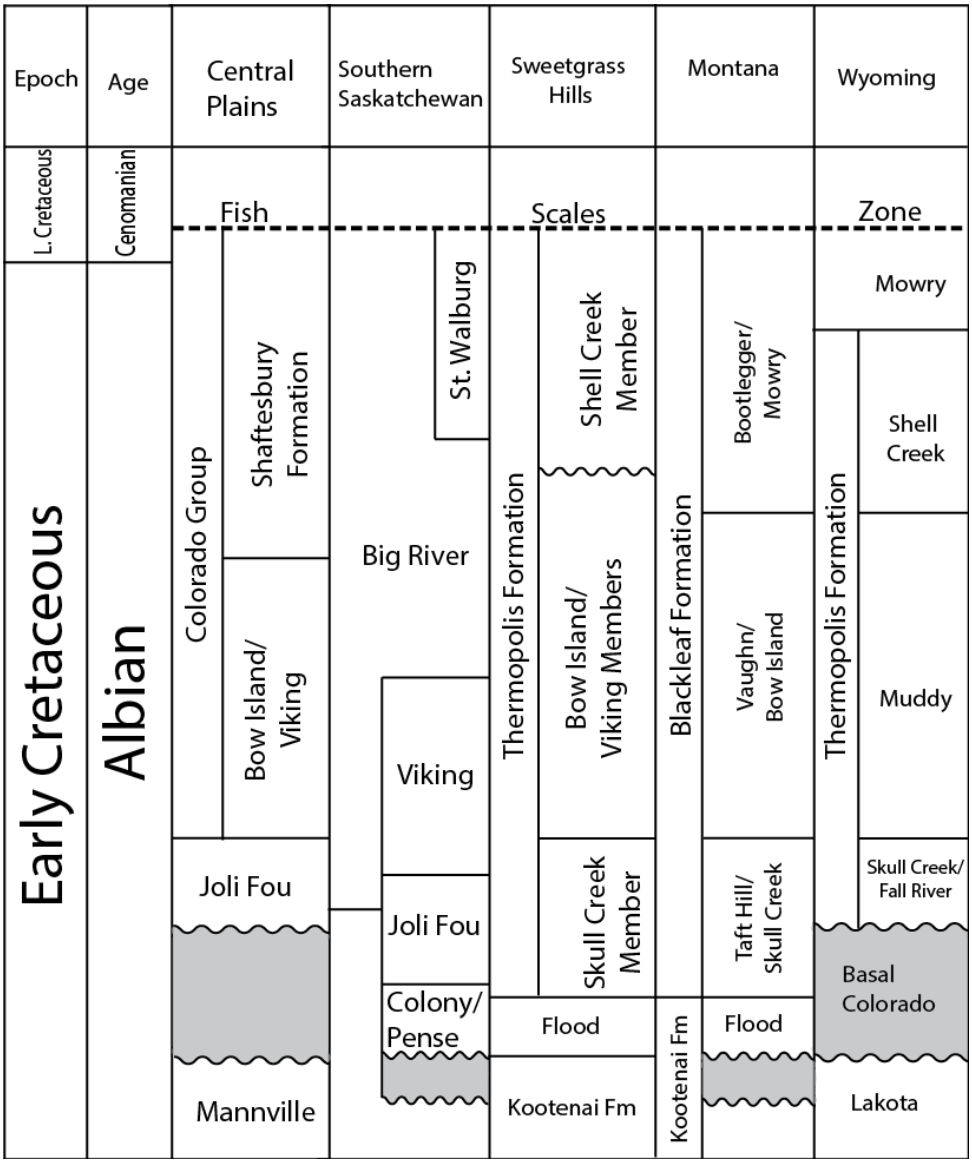

Figure 3: Stratigraphic nomenclature for the Bow Island Formation, equivalent units, and enclosing strata for differing locations (modified from Reinson et al., 1994). Sweetgrass Hills nomenclature was is used in this project.

1.1.1. Stratigraphy

Stratigraphic terms for Lower Cretaceous strata in the northern plains of Montana and Canada were developed from outcrop and the subsurface. The Colorado Group was initially observed in the front ranges of the Rocky Mountains and named by Weed (1899). Weed (1899)

divided the groups into what he called the ancient sedimentary rocks. He was the first to divide the Colorado Group into two units: the Benton shale and the Niobrara limestone. He mentions that the limestone is a shale that contains limestone concretions and is in turn classified as a limestone. That name was changed to the Colorado Shale by Fisher (1909). The Blackleaf Formation, initially defined and named after Blackleaf Creek, Montana by Stebinger (1918), was chosen as a subdivision of the Colorado Shale by Cobban (1955). The Bow Island was originally named from a subsurface unit taken from a well drilled by the Canadian Pacific Railroad northwest of Bow Island, Alberta (Glass, 1997; Croft, 2012). The Viking was first named by Slipper (1918) to describe a gas bearing sandstone encased in shale in east-central Alberta. Subsurface correlations of those strata from the southern plains of Canada to approximately the geographic border of Montana and Wyoming were such that the Viking interval was used in Montana (Reinson et al. 1994).

Cobban (1955) does not use the term "Bow Island" but instead called the Bow Island interval the "glauconitic sandstone unit". He highlights the fact there may be as many as five sandstone units in each well and describes them as a shale with interbedded sandstone units that may attain thicknesses as great as 40 feet. He also mentions layers of black coated, gray chert pebbles and that the sandstones produce gas on the east flank of the Kevin-Sunburst dome. In Cobban (1959) he changes the name of the glauconitic sandstone unit to the Taft Hill Member of the Blackleaf Formation, named after the small town of Taft Hill, a prominent bench near the outcrop area. In Cobban (1959) he changes the name of the red speck zone to the Vaughn Member of the Blackleaf Formation, named after the small town of Vaughn. The Vaughn Member is typically classified as continental in origin and is considered an equivalent to the Taft Hill Member.

Peterson (1966) created a summary of the history of the Sweetgrass Arch to attempt to relate the sedimentary events of northern Montana to those of other areas throughout Montana. Peterson (1966) used the Blackleaf Formation stratigraphic terminology which was then divided into four subunits: A lower sandy unit, an overlying glauconitic sandstone and gray shale unit, a nonmarine sequence of bentonitic beds and clayey sandstone, an upper marine sandy unit of thin-bedded sandstone and gray shale containing fish scales. Peterson (1966) proposes that gas is the primary product of the Blackleaf Formation because of the shallow depth and lack of total organic content (TOC) maturity.

Lopez (1995, 2002) mapped the geology of the Sweetgrass Hills, which included several stratigraphic columns and a large geologic 1: 100,000-scale map that covered an area from the Kevin Sunburst Dome to east of East Butte of the Sweetgrass Hills. In his report he summarized the sedimentary beds ranging from the Mississippian Madison Group to Quaternary glacial till. He presented the section in 36E 5N as the Blackleaf Formation and subdivided it into: the Bootlegger member, the Taft Hill member, and the Flood member. Lopez (1995) determined that there were seven coarsening upward sequences within the measured section of the Blackleaf and equated the lower sandstones of the Blackleaf to the Bow Island. He characterized the lower sandstones of the Blackleaf to be petroleum productive and emphasized their importance in oil and gas production throughout the Sweetgrass Hills area.

In Wyoming, Eastern and Central Montana, the Blackleaf Formation is correlated to the Thermopolis Formation. In Montana, the Thermopolis is subdivided into three units, the lower Skull Creek Shale, an informal middle sandy member (Bow Island), and the Shell Creek Shale (Porter et al., 1997). The Skull Creek Shale lies conformably below the Bow Island Member and was deposited during a high stand systems tract of the Western Interior Seaway. The Skull Creek

Shale was deposited as a thick series of mostly mud beds. Sediment supply was derived from the developing Sevier Highlands to the west. The Skull Creek Shale is correlative with the Taft Hill Member in the eastern portion of Montana and the Joli Fou Formation to the north. This unit contains the pebbly sandstone with black cherty pebbles. Porter et al. (1998) mentions that the pebble unit is likely correlative to the Muddy/Newcastle interval of the Black Hills Formation and the Cyprian sandstone of the Little Rocky Mountains.

The Shell Creek Shale is a clay shale above the last sandstone of the Bow Island, and indicates a sequence boundary from a highstand systems tract to a transgressive systems tract (Reinson et al., 1994). Porter et al. (1998) mentioned that the Shell Creek Shale could be correlated to the upper portion of the Taft Hill Member of the Blackleaf Formation or the upper portion of the Thermopolis Formation. The Shell Creek increases in thickness southward and eastward from southern Alberta into central Montana and continues into northern Wyoming Porter et al. (1998).

Porter et al. (1997) chose to use the Thermopolis Formation nomencalture based on stratigraphic continuity and lithologic characteristics of the units throughout Wyoming, Montana and Canada. Her correlations differ from those that Croft (2012) and Reinson et al. (1994) worked from in that his entire section is considered to be the Bow Island Formation whose average thickness in logs is approximately 650 feet (Figure 4). Porter et al.'s (1997) correlations consider the Bow Island to be a member of the Thermopolis Formation whose average thickness in logs is approximately 270 feet. Figure 4 shows the correlations by different authors of the same log; notice the difference in naming schemes and formation elevations. Given the flux of many names, various authors have mentioned the difficulties with working in one stratigraphic

nomenclature (Condon, 2000; Bremer, 2015). Accordingly, stratigraphic terminology from Porter et al. (1997) will be used in this project (Figure 3; Figure 4).

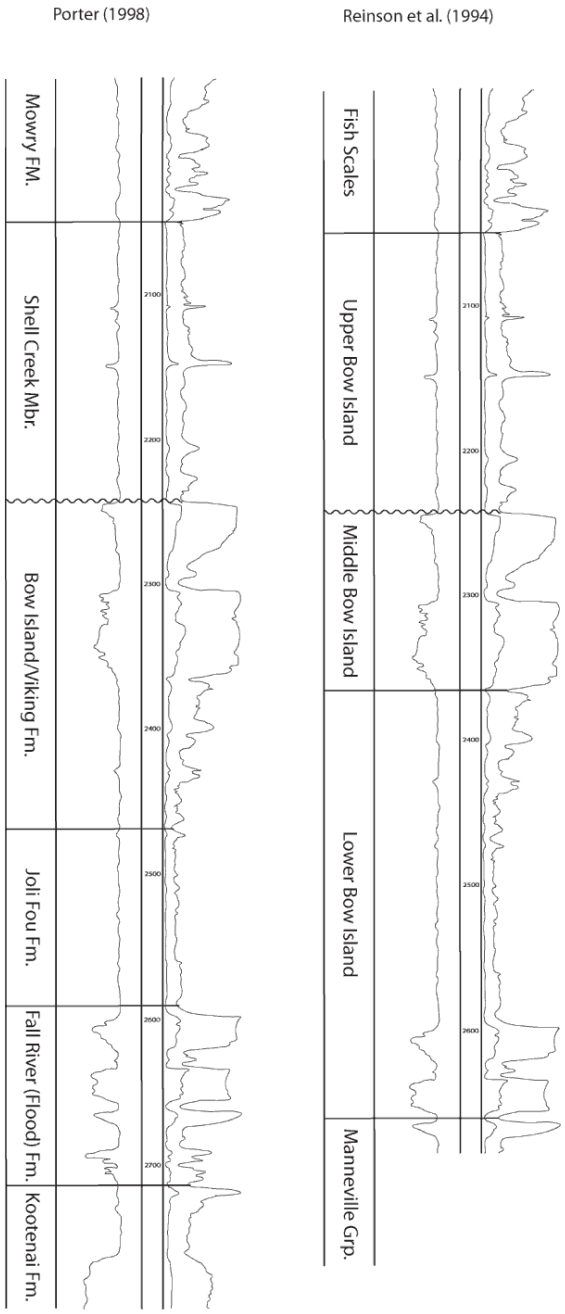

Figure 4: Comparison of different correlations : 25-051-21235; SWNE 7-T37N-R6E (from Croft, 2012). Croft continued with the picks that Reinson et al. (1994) had established.

1.1.2. Sequence Stratigraphy

Reinson et al. (1994) conducted a large-scale project that mapped the Viking Formation (Bow Island) throughout Alberta, Saskatchewan, and Manitoba (Figure 5). Reinson et al. (1994) undertook the project with the objective of creating a creating a general regional stratigraphic relation of the Viking clastic wedge, primarily in the subsurface foreland basin of the Western Canada Sedimentary Basin south of latitude 60° to the USA-Canadian border. Reinson et al. (1994) discussed the major sea level fluctuations that were evident within the Viking (Bow Island). He also referred to Caldwell (1984), who suggested that two (Kiowa – Skull Creek, Greenhorn) major transgressive-regressive cycles reflected global eustatic sea level fluctuations and have many parasequences within their transgressive phases which several authors contribute to local or regional tectonic events (Lorenz, 1982; Wagreich et al., 2016). A parasequence is defined as a conformable succession of genetically related beds or bedsets bounded by marine flooding surfaces and their correlative surfaces (Boggs, 2005). A flooding surface is defined as a surface separating younger from older strata, across which there is evidence of an abrupt increase in water depth (Boggs, 2005). A flooding surface forms in response to an increase in water depth. Reinson et al. (1994) correlated thousands of wells throughout the eastern portion of British Columbia to the southwestern portion of Manitoba. Reinson et al. (1994) correlated wells as far south as the border with Saskatchewan and Montana.

Porter et al. (1997) conducted a correlation project with the objectives of presenting six measured sections of the marine Lower Cretaceous interval at six central Montana localities; to propose the stratigraphic position and age of a late Albian lowstand sequence boundary in central Montana based on sedimentological and palynomorphic data. The work conducted by Porter et al. (1997) resulted in a cross-section from south central Montana to north central Montana and

several stratigraphic columns (including the Sweetgrass Hills) detailing the Albian unconformity. Porter et al. (1998) also determined that a low stand unconformity can be recognized at various stratigraphic positions within the sandy member, separating the marine Lower Cretaceous rocks into two stratigraphic sequences, which is expressed as black cherty pebbles that lie within coarse-grained marine sediments.

Pedersen et al. (2002) conducted a sequence stratigraphic correlation project of the Viking Formation over an area in Alberta and established the lower and middle members of the Bow Island as results of the transgressive and regressive highstand systems tracts of the basal sequence. The objectives were to establish a sequence stratigraphic framework of the Bow Island; to relate foraminiferal biofacies to depositional settings; to distinguish between autocyclic and allocyclic processes within these marginal marine and open-marine deposits. The results of this work were several sequence stratigraphic cross-sections and structure contour maps that depicted a marine environment. Pedersen et al. (2002) also recognized a potential source for these pebbles being major relative sea level fall that caused a prolonged period of sub-aerial exposure and weathering of the deposits of the Bow Island sandstones.

Croft (2012) conducted a correlation and subsurface mapping project that covered approximately the Sweetgrass 30’ x 60’ Quadrangle. Croft (2012) conducted his project with the objectives of comparing frameworks that had been established by previous works. He correlated 750 wells throughout a large area of 194 townships in Glacier, Toole, Liberty and Hill counties to create several cross-sections. The correlations were used to create a structure contour map and isopach maps of the different tops within the Bow Island to compare his results to the horizons that the Montana Board of Oil and Gas Conservation had recorded. Croft (2012) began correlation in Montana, basing his correlations off work that Reinson et al. (1994) conducted in

Alberta and Saskatchewan. The type log used in his work was log 07-02-001-21W4 located above T37N R8W that was the closest well which Reinson et al. (1994) correlated. He carried out correlations throughout the North Central Montana area covering the Sweetgrass Hills and the Kevin Sunburst Dome (Figure 5). Croft (2012) used five tops throughout the 750 wells that he correlated: Fish Scales, upper Bow Island, middle Bow Island, lower Bow Island, Flood (Figure 4). He used these correlations as a way to establish continuity because of the confusion caused by several different correlations of the same Formations (Figure 3).

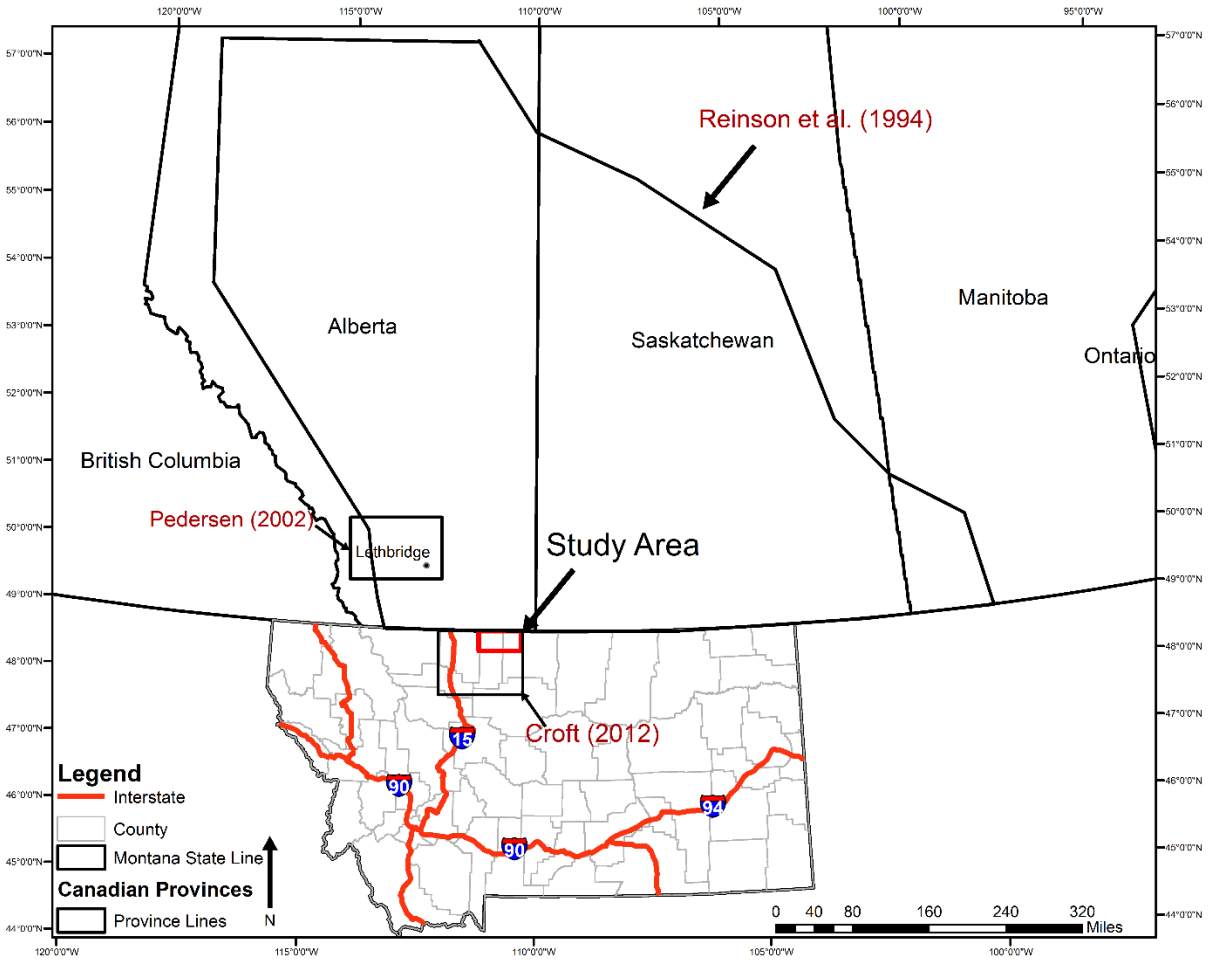

Figure 5: Black box indicates Croft (2012) study area. Red box outlines the study area for this project, the other black polygons indicate past study locations with authors highlighted in red text.

1.1.3. Sedimentology

Sedimentology of the Bow Island shows a variety of depositional systems and varying flow regimes. In Cobban (1959) the he remarks that the transition from the Skull Creek Shale and the Bow Island marks a change from a deltaic or barrier island to a marine environment. Peterson (1966) created a sedimentological summary of each geologic period and processes that drove their formation, where he described their depositional environment as being a shallow marine to marine environment. He postulated that volcanic material came from the western highlands and early emplacement of the Idaho batholith and deposited a large amount of ash within the Bow Island. Reinson et al. (1994) established the Bow Island as part of an offshore to foreshore progradational highstand systems tract. Many authors (Reinson et al, 1994; Pedersen et al., 2002) mention that the Bow Island was deposited in a lower shoreface environment that is heavily influenced by tides and storm events as evidenced by mud drapes and herringbone cross stratification (Pedersen et al., 2002). The mudstones between each sandstone contain considerable amounts of pyrite indicating a partially anoxic environment related to lower shoreface to offshore depositional environments (Pedersen et al., 2002). The lower Bow Island is characterized by a group of coarsening upward sandstones, where sediments were deposited in a lower shorface to foreshore environment and are thought to be the product of a deltaic marine margin. The middle Bow Island is characterized as a transition from a lower shoreface environment to foreshore depositional environment marked by lag pebble that underwent prolonged subaerial exposure.

1.1.4. Rock Properties

According to initial production figures, production from air-drilled wells in the Bow Island is substantial. However, after casing is completed and the well is perforated, production of

some wells decreases significantly (Leo Heath, personal communication, May 16, 2015). A study conducted by Hewitt (1963) found that smectite clays were present within the Bow Island and the water sensitivity of clays in reservoirs could explain instances of reduced production when fresh water is introduced.

Hewitt (1963) tested several different sandstones, a sandstone from the Bow Island being one of them, to find the clay content in each. The objectives of his study were to: determine the causes of water sensitivity; to develop techniques that would reveal the presences, kind and amount of water sensitivity; and to recommend production practices that are compatible with water sensitive reservoir rocks. He determined that the sandstone sample from the Bow Island had a strong sensitivity to water and that the clay minerals occupy the intergranular spaces.

1.1.5. Structure and Igneous Intrusions

The chosen location of study is outside of East Butte, a syenite laccolithic intrusion that emerged in the Eocene and titled, eroded, and exposed a significant portion of Cretaceous sediments (Figure 5; Figure 6). The intrusions that comprise the Sweetgrass Hills were controlled by pre-existing north-west-trending basement fracture systems, many of the surface faults maintain the northwest trend (Lopez, 1995). The Sweetgrass Hills are considered to be part of the central Montana alkalic province, but are anomalous in that they are isolated from the main part of the province and are aligned in a northwestern trend (Lopez, 1995). By contrast, most of the province is aligned in a northeastern trend associated with the Great Falls tectonic zone (Vuke, 1984). The structural pattern of bedrock in the hills resulted from doming of the sedimentary units by the intrusion of the laccolithic igneous bodies (Lopez, 1995). Generally, rocks from the Mississippian through the Upper Cretaceous form approximately concentric

bands surrounding the five intrusive-cored buttes (Lopez, 1995). Several sills from the intrusions fingered into the sediments and produced contact metamorphism within some sedimentary beds.

The Sweetgrass Hills are east of the Sevier fold and thrust belt and on the east flank of the Sweetgrass arch. The Sweetgrass arch (Figure 2) is a forebulge developed in front of the easterly advancing Sevier-Laramide compression which tightened and uplifted the existing arch (Lorenz, 1982) during the Cretaceous. After the period of Cretaceous deformation to the Eocene, the arch remained in the same structural position. In the Eocene, the arch was uplifted to its current position.

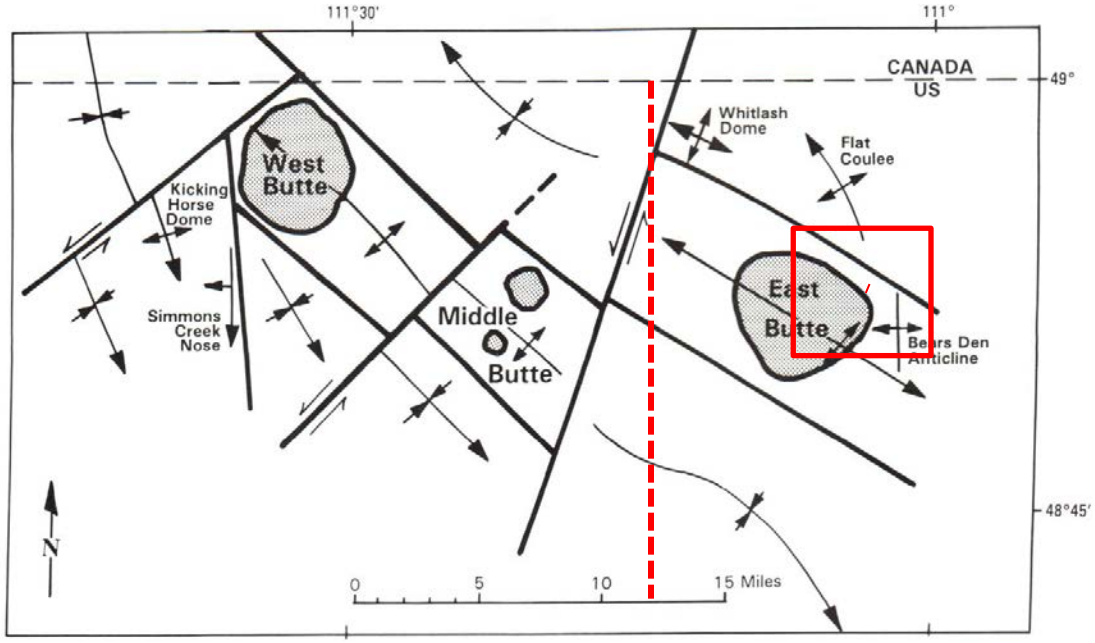

Figure 6: Sweet Grass Hills (modified from Lopez, 1995). Anticlines are related to oil and gas producing fields. Intrusions are indicated by gray areas. Red box shows the border for township 36N 5E, the red dashed line shows the approximate location of the stratigraphic section measured. East of the red dashed line is the remainder of the study area.

1.2. Statement of Purpose

The exposed stratigraphic section located on Dafoe Ranch in section 15, T36N, R5E provides a unique opportunity to tie the Bow Island from the surface to the subsurface. This has not been done in any detail in Montana. Tying the surface sedimentology to subsurface will help

to understand the sedimentology of the parasequences in the subsurface and help determine the scale of mappable cyclicity. The study area lies within the boundaries of Croft (2012) study area (Figure 5), which allows for a "zoomed in" perspective of the area that he had previously mapped in the subsurface. The correlations from Porter et al. (1997) will be used to understand the production distribution within the Bow Island and to determine change in facies throughout the study area. These correlations will be used to create structure contour maps of unit elevations, 3D visualizations of the formation tops, isochore maps to denote unit thickness, and cross sections to outline the sequence stratigraphy in the area as well as tie in the surface lithologies to the subsurface. The mineralogical data will help identify clays in the samples as well as help determine some possibilities of decreased well production in the area.

2. Methods

2.1. Field Measurements

Aligned with the goal of tying the surface lithologies to the subsurface well log data, a stratigraphic column had to be measured. An outcrop of the Bow Island is located on Dafoe Ranch in section 15, T36N, R5E Liberty County, Montana. The outcrop is on the north western flank of Mount Lebanon. Multiple reports (Porter et al., 1997; Lopez, 1995) were used to identify the contacts between the first Bow Island sandstone and the Skull Creek Shale and last Bow Island sandstone and the Shell Creek Shale. The contact between the lower portion Bow Island sandstone and the Skull Creek Shale was located and walked on both sides of the outcrop confirm location in section. The same was repeated for the contact with the upper portion of the Bow Island and the Bow Island top, however outcrop of the Bow Island top was only on the west side of the ravine (Figure 7).

Measurements of the stratigraphic column began at the contact between the Skull Creek Shale and the first Bow Island sandstone and ended at the last Bow Island sandstone and the Skull Creek Shale contact (Figure 8). Sills that were measured were kept in the stratigraphic section, although they were not included in any of the log correlations. Bed and sill thicknesses were measured using a Jacobs's staff, bedding attitudes were taken using a Suunto MC-2 Compass and recorded in a notebook. Pictures of the measurement locations were taken with an iPhone 6 Plus. The Fieldmove Clino Android mobile phone application by Midland Valley was used to take GPS coordinates of each location where measurements were taken as well as to mark the locations of samples taken from the outcrops.

Figure 7: Section of outcrop measured to create the stratigraphic column. The Bow Island lies between the black lines outlined in this section.

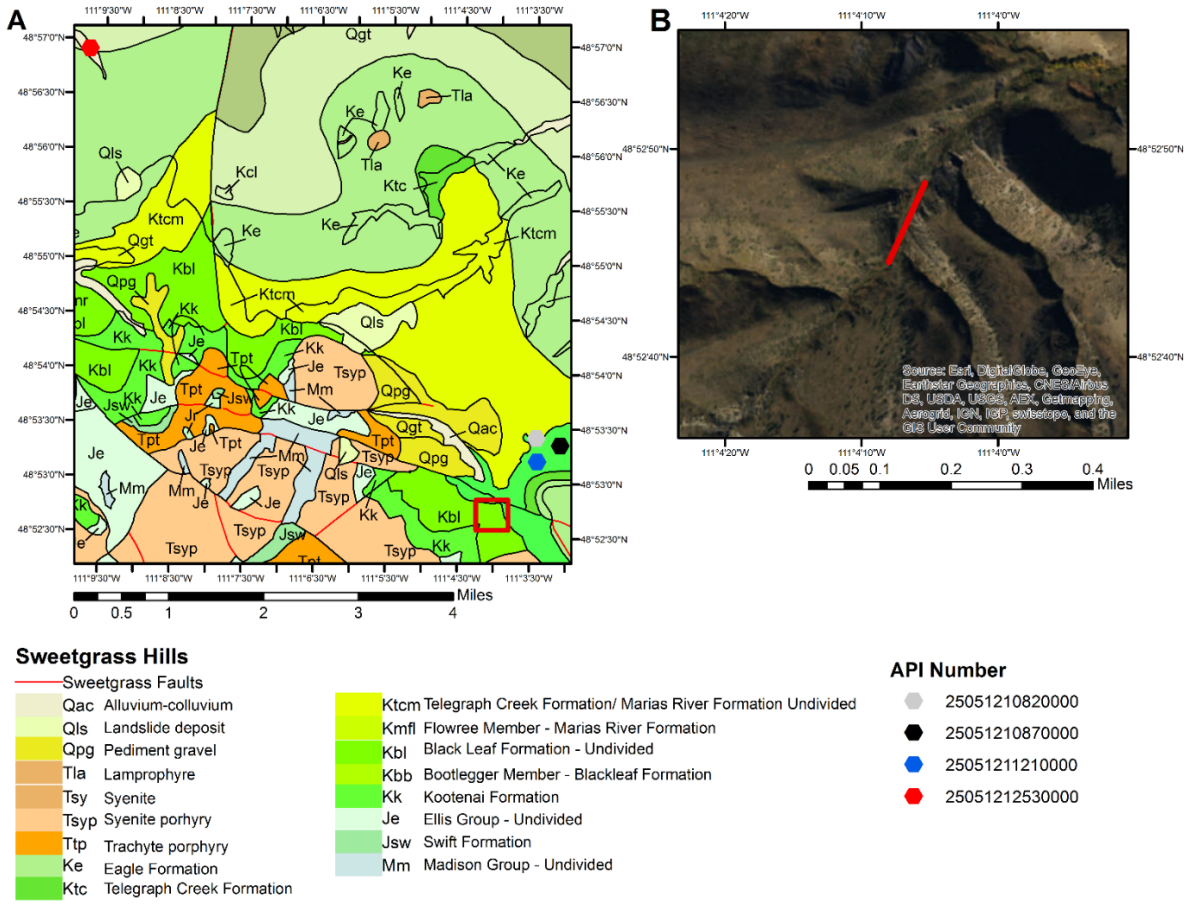

Figure 8: (A) Geology of outcrop area, red box shows general location of the study area (from Lopez, 2002). (B) Digital orthophoto of area with red line demonstrating location and length of measured section (source Esri Maps, 2016).

2.2. Correlations and Cross-sections

The log selections were created in IHS-Accumap, where the area and wells within the area were defined. Selections were made on well log availability and log type. Of the 1506 wells logs that were available, 814 wells with rasters were chosen and correlated throughout 35 townships surrounding and to the east of East Butte (Appendix B). Raster logs were imported from Log Sleuth to IHS-Petra (v4.1.1) to pick tops and create elevations of the horizons within the wells that were drilled. Petra was used to display and correlate logs in cross sections. Initially, seven tops were picked from each well: Blackleaf, Fish Scales, upper Bow Island, Bow Island top, middle Bow Island, lower Bow Island, and Skull Creek Shale. Later, focus was changed to the four informal members of interest: Bow Island top, middle Bow Island, lower Bow Island, and the Skull Creek Shale. The change in focus of tops was to better highlight the units within the Bow Island. A combination of tops from both Porter et al. (1997) and Croft (2012) were used to conduct the correlation in the wells, nomenclature from both Porter et al. (1997) and Croft (2012) were used to define the smaller scale correlations.

The type log (Figure 9) used was API# 25051212530000 which Croft (2012) modified from Porter et al. (1997). This well is located approximately 7.23 miles (11.63 km) from the location of the measured stratigraphic section (Figure 8). Wells, API#: 25051211210000 (.72 miles, 1.16 km), 25051210870000 (.94 miles, 1.51 km), 25051210820000 (1.15 miles, 1.86 km), near the stratigraphic section were the first to be correlated to see how the measured section would match up to the wells in the area (Figure 8)

Correlations were carried out in Petra using the resistivity and induction curves from each log. Spontaneous potential (Sp) logs often did not provide enough information to be reliable but were used when they provided information. Gamma logs available were uncalibrated and

provided little in terms of interpretation, very few of the logs contained calibrated gamma readings.

The first formation top to be correlated was the Blackleaf Formation and was used to create a datum for flattening. The Fish Scales was the second top to be correlated and is a horizon that most drillers used to denote depth and arrival before the Bow Island due to the large area it covers and its distinctive signature. The upper Bow Island is usually characterized by a sandstone resistivity kick with a serrated cylindrical shape (Figure 9). The Bow Island top was correlated as a shale bed that shows a V-shaped dip in resistivity before entering the sandstone of the Bow Island. The middle Bow Island was recognized as a sharp sandstone contact with a serrated funnel shape. The lower Bow Island is identified by sharp sandstone contact, recognized by a serrated cylindrical shape. The Skull Creek Shale is identified by a marked decrease in resistivity.

Six cross sections were created to identify thickening and thinning of sediments within the area. Cross sections were chosen on well log availability and areas of interest that had numerous producing wells. Cross section A-A' is oriented west to east in township 35 and ranged from R6E to R7E (5.19 miles), this cross section location was chosen because of a notable producing well trend that is oriented north to south. Cross section B-B' is oriented north to south in townships T34N, T35N, T36N, T37N, and in ranges R6E to R7E (18.76 miles). Cross section C-C' is oriented west to east and is in township T37N and in ranges R4E to R7E (17.43 miles). Cross section D-D' is oriented northwest to southeast in townships T37N, T36N, T35N, T34N and in ranges R5E to R7E (13.69 miles). Cross section E-E' is oriented north to south in townships T34N, T35N, T36N, T37N in range R4E (19.57 miles). Cross section F-F' is oriented east to west in township T35N and in ranges R4E, R5E, R6E, and R7E (19.98 miles).

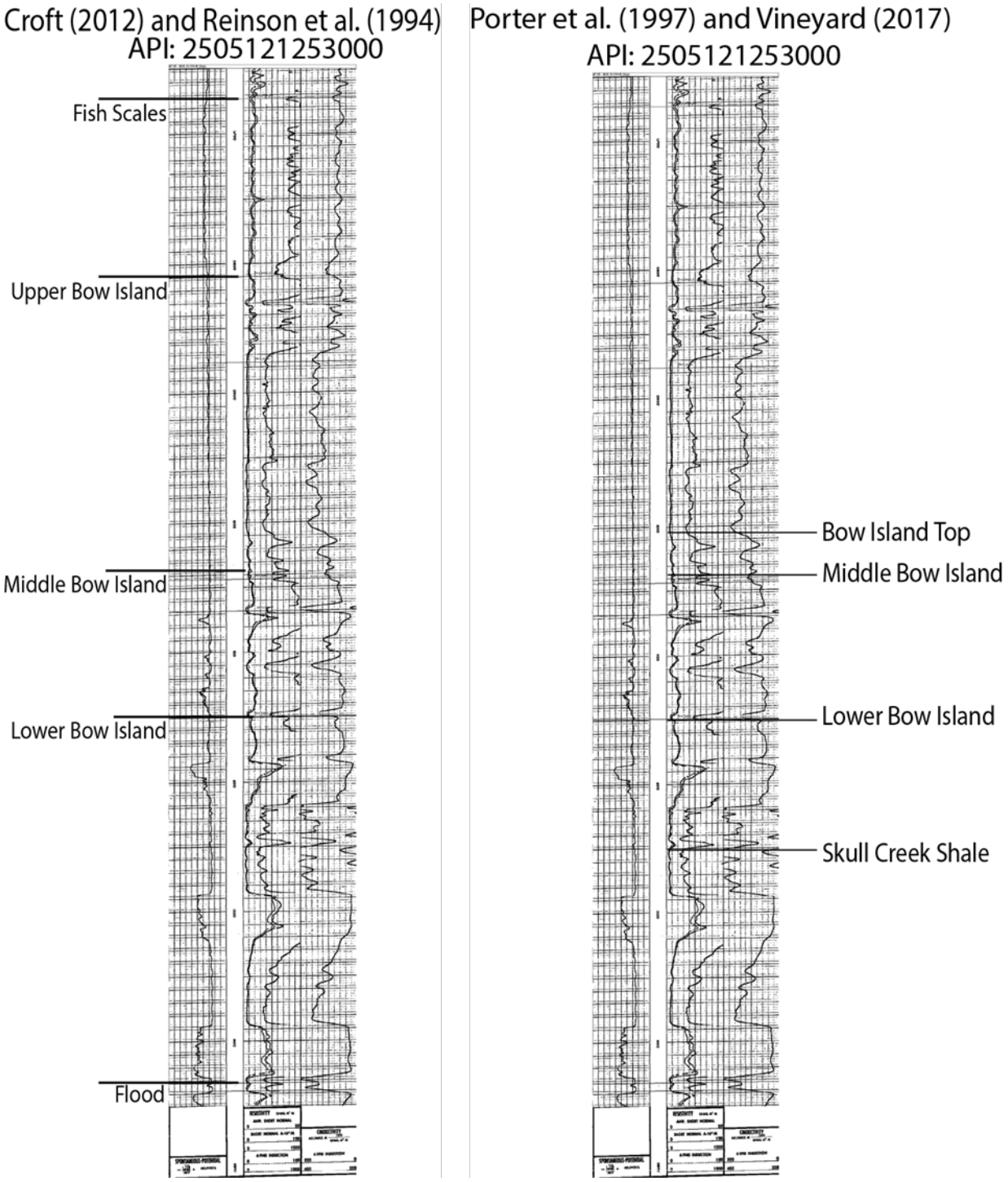

Figure 9: Type log used in correlation (modified from Croft, 2012). Left log shows the correlations Croft (2012) used, right log are correlations of Porter et al. (1997) and this research. Location of the log is shown as the red dot in figure 8a.

2.3. Contour, Isochore Maps and 3D Visualizations

Structure contour maps were created in IHS-Petra from log correlations to illustrate subsurface bedding and horizons. Elevations were determined by subtracting the Kelly Bushing (KB) from the elevation to create an accurate representation of the subsurface elevation for the 814 correlated logs. The formation tops were used to create a model of each bed individually to determine any patterns that exist in areas of the gas production in an attempt to relate thickness to gas productivity and perforation zones.

Four isochore maps were created in ArcGIS 10.4 using NAD 1927 datum by exporting formation tops from Petra to Excel. The formation tops were imported from Excel into ArcGIS where they were used to create kriging rasters. Isochore maps measure the vertical thickness of each unit. The four isochore maps are: the total thickness of the Bow Island Member, the lower Bow Island, the middle Bow Island, and the Bow Island top.

Two 3D visualzations were created in ArcScene by creating rasters and contours in ArcGIS 10.4 with data imported from the Montana Board of Oil and Gas (last accessed 25 October, 2016), vertical exaggeration was multiplied by a factor of six. Subsurface elevations for the tops were subtracted from the KB in Excel to find the horizon elevations above sea-level. The data was imported into ArcScene to create a 3D visualzation for the tops mapped in the area. The four informal units (Bow Island top, middle Bow Island, lower Bow Island, Skull Creek Shale) were mapped and separated by 2500 feet to create a better viewing angle. Contours were created in ArcGIS and imported into ArcScene. Contours are set at 100-foot intervals and range from 600 feet to 4200 feet, depending on the horizon top.

2.4. Sample Mineralogy

Rock samples taken from the field were placed in a Ziploc bag and labeled with the same name and number of the formation from the stratigraphic column (Figure 10). Mineral analysis was conducted using the PANalytical TerraSpec Halo Mineral Identifier on 17 samples to identify the clay mineralogy. The technology used to identify the minerals in each sample is near-infrared reflectance spectroscopy. This method uses the near infrared region of the electromagnetic spectrum to measure light that is scattered off and through the sample. This method is beneficial because it is quick and does not alter the sample (Maras et al., 2016)

In an attempt to be certain that the Terraspec was identifying the correct minerals, a calibration was conducted using pure samples of gypsum and kaolinite, each sample was tested three times on a different surface, the readings from the sample calibrations were accurate and the use of the instrument was validated (Table I).

Table I: Instrument calibration using samples.

Reading	Sample 1 - Gypsum	
	Gypsum	Monazite
1	3	2
2	3	2
3	3	2
	Sample 2 - Kaolinite	
	Kaolinite	Dickite
1	3	3
2	3	3
3	3	3

Each mineral reflects a certain amount of light and the light wavelength units are displayed in nanometers, where the wavelength range is between approximately 700 to 2500 nm. The readings are displayed on a small monitor on the back of the instrument in “scalar” units as well as stars that show the presence of the minerals in sample. Stars that appear next to the

mineral indicate confidence of the mineral in sample. Three stars (most confident) indicate the mineral is present and there could potentially be more of that same mineral, two stars (less confident) indicate that the mineral is there but likely is one of a few constituents and is not a predominant mineral, one star (least confident) indicates a small possibility that the mineral is in the sample or it could be a false reading.

3. Results

Within the measured stratigraphic section of the Bow Island there are five major cyclic depositional systems with some sub-cycles. The sediments range from mudstones to coarse-grained sandstone, and display different types of cross stratification.

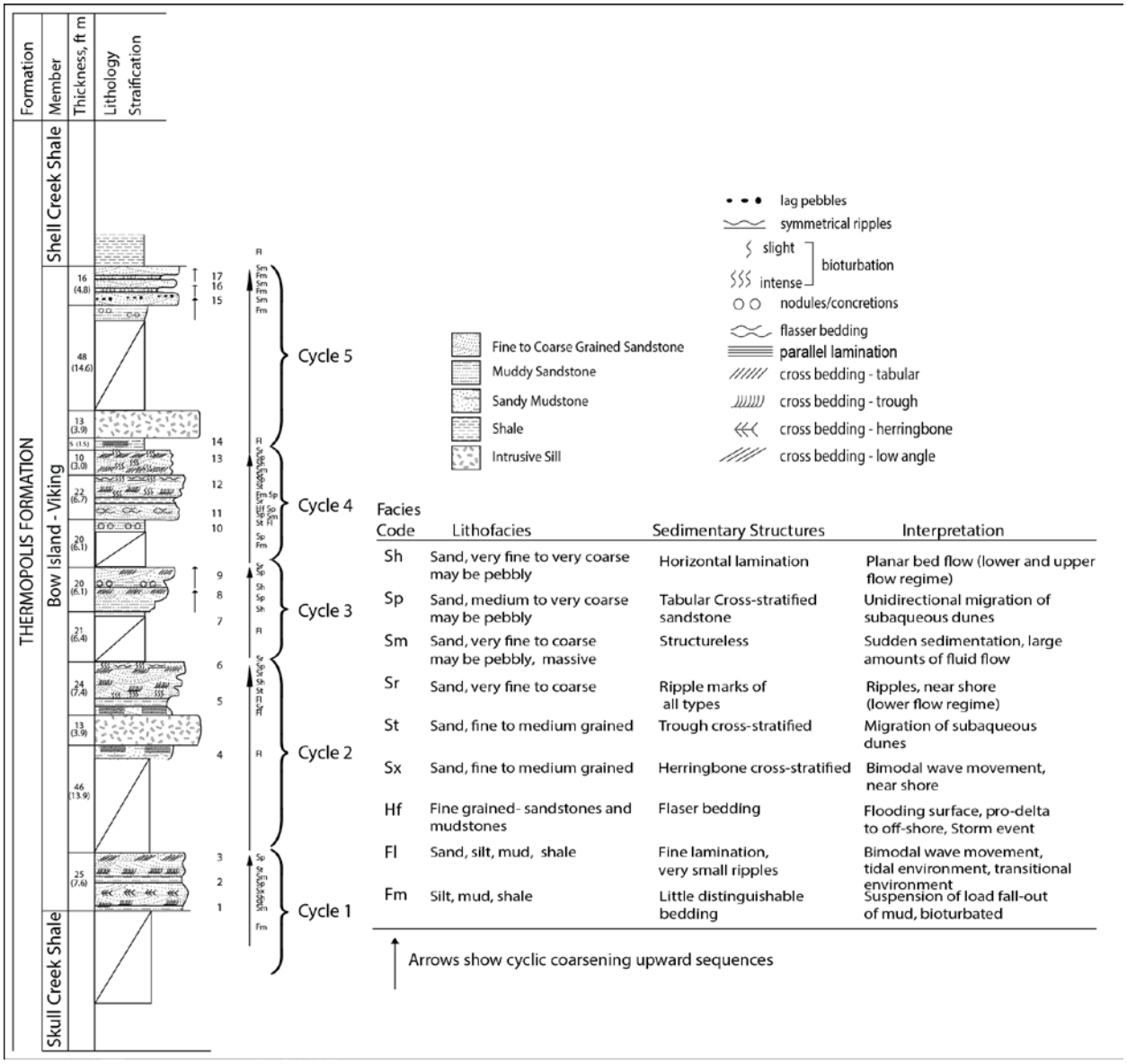

Figure 10: The stratigraphic column of the Bow Island Formation. Facies annotations and cyclic sequences annotated in the legend, each cycle is separated by a mudstone flooding surface. Numbers next to the facies units indicate the relative location of the samples taken from the stratigraphic section.

3.1. Facies Analysis and Sequence Stratigraphy

Field work conducted yielded a stratigraphic section that is approximately 270 feet thick and consists of five coarsening upward sandstones which are separated by four mudstones. The penultimate sandstone in the section is capped by a gravel lag deposit indicating a prolonged period of subaerial exposure. The Bow Island is underlain by the shelf-to-shoreface Skull Creek Shale and overlain by the shallow marine Shell Creek Shale. Throughout the column facies change is typically abrupt, so facies codes are placed on the column where the facies descriptions matched the code (Figure 10). Facies codes noted throughout the column are: Sh, Sp, Sm, Sr, St, Sx, Hf, Fl, and Fm. Table II shows the facies codes, lithofacies, sedimentary structures, and interpretations.

Table II: Facies codes, lithofacies, sedimentary structures, and interpretations of the facies (after Miall, 1999).

Facies Code	Lithofacies	Sedimentary Structures	Interpretation
Sh	Sand, very fine to very coarse may be pebbly	Horizontal lamination	Planar bed flow (lower and upper flow regime)
Sp	Sand, medium to very coarse may be pebbly	Tabular Cross-stratified sandstone	Unidirectional migration of subaqueous dunes
Sm	Sand, very fine to coarse may be pebbly, massive	Structureless	Sudden sedimentation, large amounts of fluid flow
Sr	Sand, very fine to medium grained	Ripple marks of all types	Ripples, near shore (lower flow regime)
St	Sand, fine to medium grained	Trough cross-stratified	Migration of subaqueous dunes
Sx	Sand, fine to medium grained	Herringbone cross-stratified	Bimodal wave movement, near shore
Hf	Fine-grained- sandstones and mudstones	Flaser bedding	Flooding surface, pro-delta to off-shore, Storm event
Fl	Sand, silt, mud, shale	Fine lamination, very small ripples	Bimodal wave movement, tidal environment, transitional environment
Fm	Silt, mud, shale	Little distinguishable bedding	Suspension of load fall-out of mud, bioturbated

3.1.1. Cycle One

The contact with the Skull Creek Shale (Fm) and first Bow Island sandstone (Sm) sediments abruptly transition from a sandy mudstone to a medium- to coarse-grained sandstone (Figure 11). As a whole unit, the first sandstone has numerous types of cross stratification and is composed of a fine-grained sandstone with some mud that grade upward to a coarse-grained quartzose sandstone.

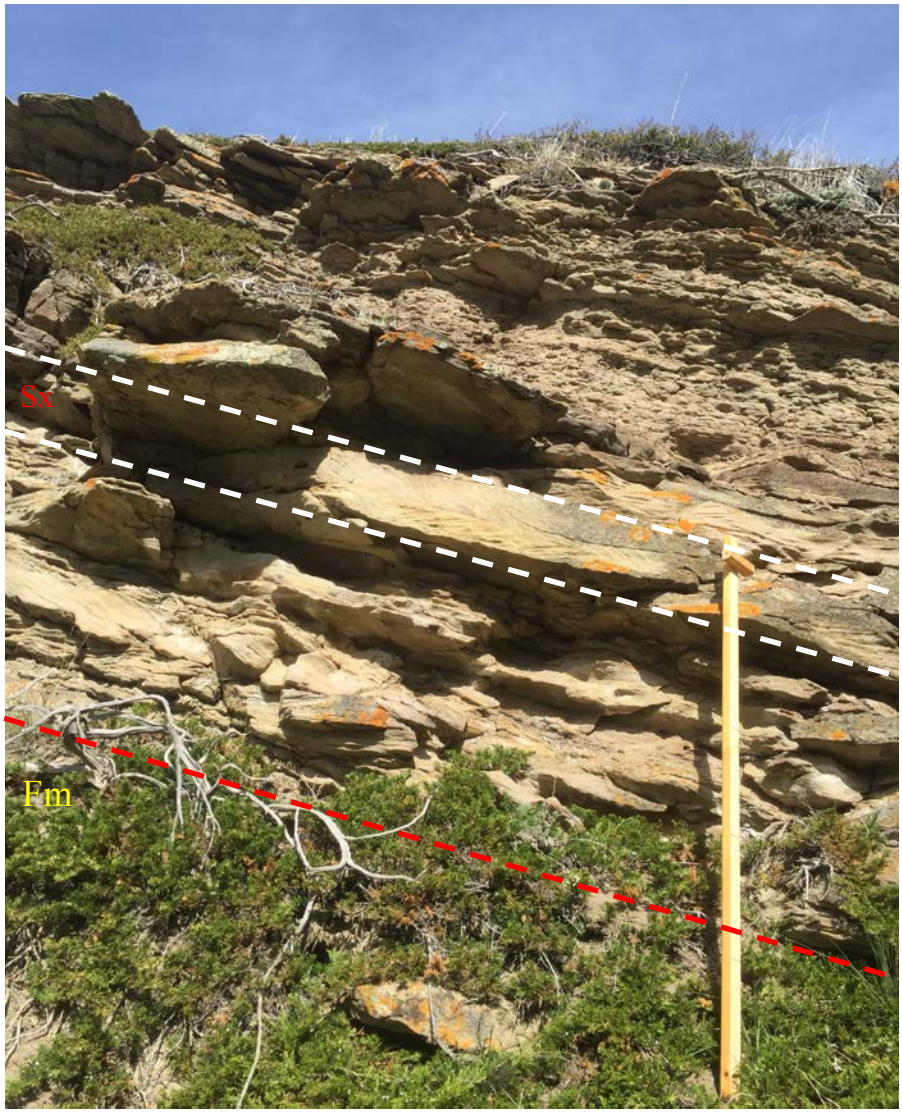

Figure 11: First sandstone unit of the Bow Island. The red line indicates the gradational contact between the Skull Creek Shale and the first Bow Island Sandstone. The white lines highlight the herringbone cross (Sx)-stratification.

Facies Sm is dominated by a very fine-grained sandstone with mud prone to erosion and is about three feet thick. Facies Sm grades upward into a medium-grained sandstone with flame structures at its base and trough cross-stratification and is about four feet thick (facies St; Figure 12). Facies St transitions to a one foot thick interval of horizontally planar coarse-grained rocks (facies Sh). Facies Sh transitions to facies Sx which displays herringbone cross-stratification and is about two feet thick (facies Sx). Above facies Sx there is a two-foot interval of facies Sp that is comprised of medium- to coarse-grained tabular sandstone. Sample 1 is a non-calcareous fine- to coarse-grained sandstone which is gray when fresh and gray-tan when weathered. The sample locations are noted on the right of the stratigraphic column on Figure 10. The portion comprised of Sm, Sh, St, Sp and Sx facies is approximately 12 feet thick.

Figure 12: Sm noted as the contact between the Skull Creek Shale and the first Bow Island sandstone. Location 1 on Figure 32.

The Sp interval transitions to a very fine-grained sandstone with mud that is massive (facies Sm) and is about five feet thick (Figure 13). Facies Sm coarsens to a fine- to medium-grained sandstone that shows trough cross-stratification (facies St). Facies St is interbedded with

mud drapes and is about two feet thick. Sample 2 (facies St) is a non-calcareous medium-grained sandstone that is gray when fresh and gray when weathered.

Figure 13: Sm facies of cycle one. Location 2 on Figure 32.

The upper portion (facies Sp) of the first sandstone is a medium- to coarse-grained sandstone that displays tabular cross-stratification (Figure 14). The sandstone becomes entirely coarse-grained with black and white chert grains in the upper two inches, which creates a prominent surface that is resistant to erosion. Sample 3 is glauconitic and non-calcareous, gray when fresh and oxidized when weathered.

Figure 14: Sp facies of cycle one, an example of the facies is highlighted in white lines. Location 3 on Figure 32.

3.1.2. Cycle Two

The coarse-grained sandstone (facies Sp) from cycle one transitions into a fine-grained sandy mudstone (facies Fl) in cycle two that is largely covered. The sediments are best exposed near a sill and display fine bedding and no cross-stratification (Figure 15). Sample four near the sill is very brittle and fissile and non-calcareous. The sill induced contact metamorphism evidenced by conchoidal fracturing. Fresh surfaces are light gray and exposed surfaces are heavily oxidized and iron stained. The approximate thickness of the sandy mudstone is 46 feet.

Figure 15: Fl facies of cycle two. Location 4 on Figure 32.

The transition from the sandy mudstone (facies Fl) to the muddy sandstone (facies Sr) is gradational, it contains beds of sandstone with no cross-stratification and is about three feet thick. Facies Fl contains parallel laminations of sandy mudstone and is about five feet thick (Figure 16). The beds are iron stained and hard due to contact metamorphism. Sample 5 is fine-grained, gray when fresh and tan when weathered. Sample 5 is non-calcareous and shows high amounts of bioturbation and burrowing.

Figure 16: Fl facies of cycle two. Location 5 on Figure 32.

The transition from facies Fl to facies St is gradational and coarsens upwards into a medium- to coarse-grained sandstone (Figure 17). The fine-grained facies St displays trough cross stratification and is about five feet thick. The sediments coarsen to facies Sh that is a coarse-grained sandstone that displays tabular cross stratification and is about eight feet thick. The tops of the sandstones are covered with ripple marks that are approximately an inch thick (facies Sr). The Sp facies is interbedded with very thin muddy layers that produce a saw tooth profile and cause more erosion in between sandstone beds this facies is about 11 feet thick. Facies Sr marks the top of the saw tooth profile and is about an inch thick. Bioturbation is visible throughout facies Sp and Sr. Sample 6 of facies Sp is non-calcareous, sample 6 is gray when fresh and iron-stained when weathered.

Figure 17: Fl facies of cycle two. Location 6 on Figure 32.

3.1.3. Cycle Three

The transition from facies Sr from cycle two to facies Fl from cycle three is abrupt, most of the mudstone is covered by detritus and vegetation and only crops out in one area near the contact with the overlying sandstone (Figure 18). The beds are composed of black mudstone with some fine lamination (facies Fl). Sample 7 shows alternating beds of sandy mudstone and soft mudstone that is non-calcareous. Facies Fl is approximately 21 feet thick.

Figure 18: Sh and Fl facies of cycle three. Location 7 on Figure 32.

The coarsening from facies Fl to the facies Sh is abrupt. Facies Sh, is a very fine-grained sandstone with some mud, and coarsens to the fine to medium grained facies Sp, this pair of facies is about 12 feet thick (Figure 19). Sample 8 (facies Sh) is oxidized with iron staining on weathered surfaces, is dark gray to gray on fresh surfaces, and is non-calcareous. Facies Sp is tan when weathered and tan when fresh and is non-calcareous.

Figure 19: Sp and Sh facies of cycle three. The white lines denote section boundaries. The yellow line indicates the break between the two coarsening upward cycles; Location 8 and 9 on Figure 32.

Facies Sp transitions into a very fine-grained sandstone with some mud (facies Sh). Facies Sh coarsens to a fine- to medium-grained sandstone (facies Sp) cycle as seen in the previous section. Facies Sh is gray when fresh and iron stained with some iron concretions when weathered. Sample 9 is a non-calcareous, fine-grained sandstone with no bioturbation. Facies Sr

is at the top of the second Sp facies and is about 2 inches thick. This section with Sh, Sp, and Sr facies is approximately eight feet thick (Figure 19).

3.1.4. Cycle Four

The facies Sr from cycle four transitions abruptly into a mudstone (facies Fm) in cycle four that is interbedded with thin beds of tabular cross stratified sandstone (facies Sp). The Sp facies are difficult to notice because they are covered by degraded overlying sediments (Figure 20). Facies Fm is poorly bedded and very fissile. Iron concretions are visible and facies Fm is gray on a fresh surface and heavily iron stained and oxidized when weathered. Facies Sp is gray on fresh surfaces and tan when weathered. Sample 10 was non-calcareous and the section with Sp and Fm facies is approximately 20 feet thick.

Figure 20: Fm facies of cycle four. Location 10 on Figure 32.

The Fm facies coarsens into a two-foot thick layer of fine-grained sandstone (facies St) with trough cross-stratification interbedded with thin layers of mudstone (facies Fl; Figure 21). Sample 11 is tan when weathered and tan when fresh. The sample is slightly calcareous and the pair of the St and Fl facies is approximately two feet thick.

Figure 21: Sp facies of cycle four example. Location 11 on Figure 32.

The fine-grained sandstone (facies St) coarsens into a fine- to medium-grained sandstone (facies Sp; Figure 22). Throughout the section there are interbedded layers of a very fine sandstone with mud (facies Sm) and fine- to medium-grained sandstone (facies Sp). The muddy

sandstone (facies Sm) erodes more readily and creates a saw tooth profile made from the (facies Sp) tabular beds. The section with both Sp and Sm facies is approximately five feet thick. The sandstone (Sp facies) is gray when fresh and weathered surfaces are tan from oxidation.

Figure 22: Sm facies of cycle four. Location 12 on Figure 32.

The Sp facies coarsens into a medium- to coarse-grained sandstone (facies Sp; Figure 23). The Sp facies sandstones are interbedded with mudstone and display flaser bedding (facies Hf) that is about a foot thick. Above facies Hf, the sandstones are medium- to coarse-grained and display trough cross-stratification (facies St) and in the upper foot of facies St the tops of the beds display small unidirectional ripple marks (facies Sr). The mudstones are dark gray to black

and weathered surfaces and black on fresh surfaces. Facies St is tan on fresh surfaces and tan on weathered surfaces. This section of facies Sp, Hf, St, and Sr is approximately 10 feet thick.

Figure 23: Hf and St facies of cycle four. Location 13 on Figure 32.

The Sr facies transitions into a five-foot thick mudstone layer (facies Fm; Figure 24). The mudstone is highly fissile and is heavily iron stained, oxidized and non-calcareous. No bedding is evident in the mudstone (facies Fm) and is interbedded with thin layers of tabular cross

stratified sandstone. The mudstone is black on weathered surfaces and gray to black on fresh surfaces.

Figure 24: Facies Fm and Sp of cycle four. The white lines show the boundaries of the shale layer. Location 14 on Figure 32.

The facies Fl coarsens into a medium- to coarse-grained sandstone (facies St; Figure 25). The St facies shows trough cross-stratification and is about four feet thick. The St facies transitions to the Sp facies. The Sp facies displays tabular cross-stratification and is about four feet thick. The tops of the beds are capped by unidirectional ripple marks and are thinly laminated (facies Sr) at about six inches. The Sr facies transitions to a massive coarse-grained

sandstone (facies Sm) and cross bedding becomes hardly visible. The Sm facies is about a foot thick. Sample 12 is non-calcareous, tan on fresh surfaces and tan on weathered surfaces.

Figure 25: St facies of cycle four. Location 15 on Figure 32.

The coarse-grained sandstone (facies Sm) transitions to a fine-grained sandstone with some mud (facies Sh) and grades to a medium- to coarse-grained sandstone (facies Sp; Figure 26). The four foot thick fine-grained sandstone with mud (facies Sh) is poorly bedded and shows

heavy burrowing. The facies Sh coarsens into a medium-grained sandstone (facies Sp) that is about five feet thick. Unidirectional ripple marks (facies Sr) cap the tops of the beds being about four inches thick and shows considerable bioturbation. Sample 13 is non-calcareous, gray-tan on fresh surfaces and tan on weathered surfaces. The group of Sh, Sp, and Sr facies is about 10 feet thick.

Figure 26: Sp facies of cycle four. Location 16 on Figure 32.

3.1.5. Cycle Five

The contact from the medium-grained sandstone (facies Sr) from cycle four to a sandy mudstone (facies Fl) in the fifth cycle is abrupt. This portion is largely covered and is only observable where there is a dike that exposes the sandy mudstone (Figure 27). The sandy mudstone is finely bedded and is non-calcareous. Sample 14 shows fresh surfaces are gray and weathered surfaces are black to gray. Facies Fl is approximately five feet thick.

Figure 27: Fl facies of cycle five. Location 17 on Figure 32.

The sandy mudstone (facies Fl) transitions to a mudstone that is mostly covered by vegetation and detritus, the only location where there is visible bedding is the transition from a mudstone to a sandy mudstone in the upper five feet (facies Fm; Figure 28). This section is the thickest of the mudstones. The mudstone (facies Fm) that is visible is dark gray on fresh surfaces and iron stained and oxidized on weathered surfaces, iron concretions makeup up a large portion of the visible bed. No signs of bioturbation are visible and this portion of the sediment is non-calcareous; there is a sulfurous smell from fresh surfaces. This section is approximately 48 feet thick.

Figure 28: Facies Fl of cycle five. Location 18 on Figure 32.

The mudstone (facies Fm) coarsens to a coarse-grained pebbly sandstone (facies Sm); the transition creates a sharp saw tooth profile. Facies Sm is coarse with white and black cherty pebbles (Figure 29). There are large rounded black chert pebbles throughout the top of the bed. The outcrop is poorly bedded and does not display cross stratification. Bioturbation is not visible

in the bedding and it is non-calcareous. Sample 15 is gray on fresh surfaces and iron stained on weathered surfaces. The pebbly sandstone is approximately six inches thick and the sandstone below is approximately eight feet.

Figure 29: Pebbly sandstone Sm facies of cycle five. Location 19 on Figure 32.

The pebbly sandstone (facies Sm) fines to a mudstone (facies Fm) that contains heavy amounts of oxidation and iron staining (Figure 30). The facies Fm is fractured and fissile, within the fractures are iron concretions and oxidized iron fill the fractures. Facies Fm coarsens upwards to a medium-grained sandstone (facies Sm). Facies Sm is massive and does not shows signs of bioturbation. Sample 16 (facies Fm) is black on fresh surfaces and black with iron

staining on weathered surfaces. This section of facies Fm is approximately five feet thick and is non-calcareous.

Figure 30: Fm facies of cycle five. Location 20 on Figure 32.

The contact with facies Sm and the mudstone (facies Fm) is abrupt. Facies Fm is fractured, fissle, and contains abundant iron concretions. Facies Fm coarsens to a fine-grained sandstone (facies Sm; Figure 31). Facies Sm is poorly bedded and does not show any cross-stratification. Sample 17 has fresh surfaces that are gray and weathered surfaces are tan with iron staining. No bioturbation was evident within the sandstone. This section is approximately three feet thick and is calcareous.

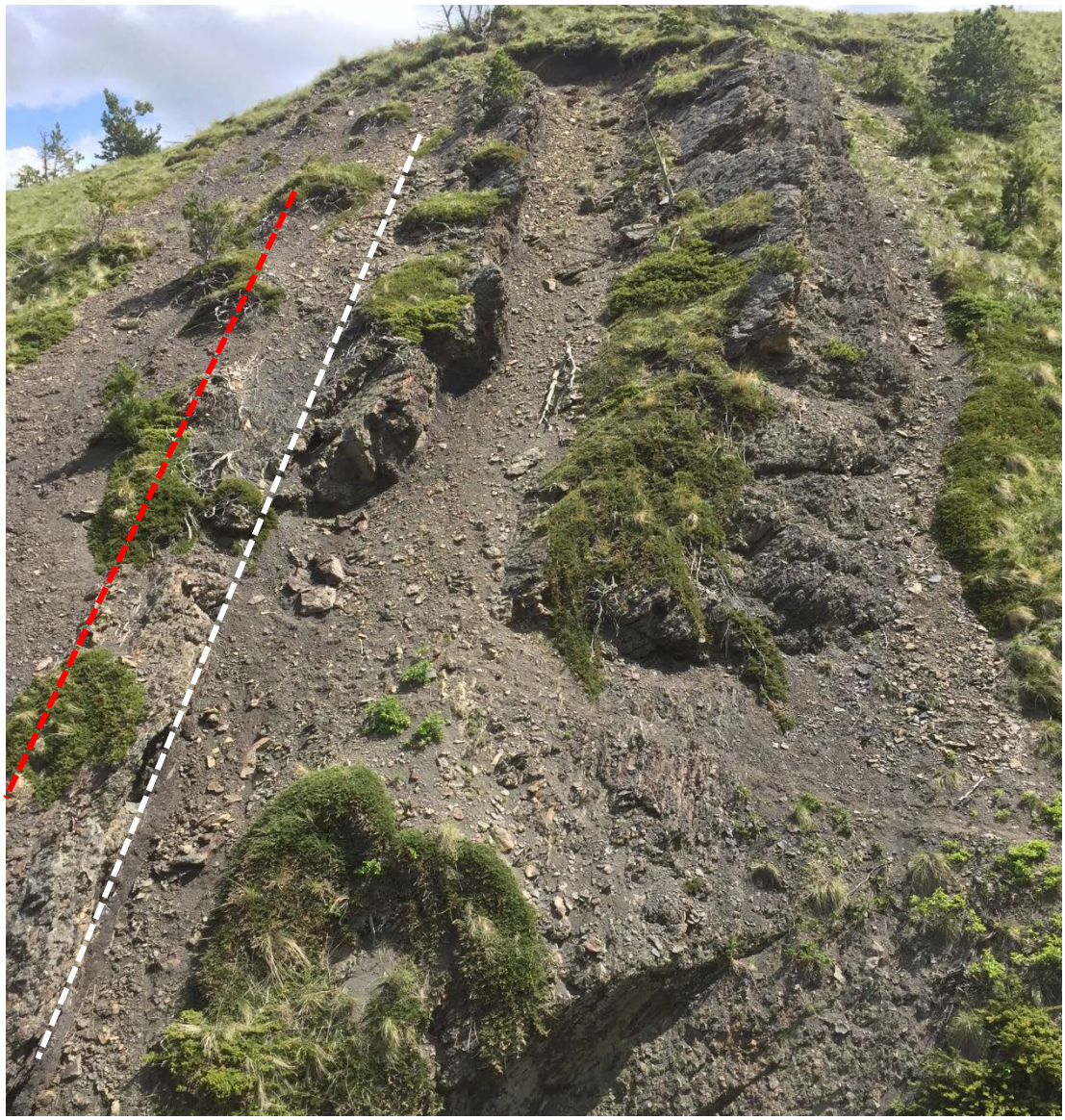

Figure 31: Uppermost sandstone, facies Sm in cycle five. Location 21 on Figure 32. The sandstone is located between red and white dashed lines. Above the red dashed line is the Bow Island top.

Locations of figures 12-31, relative to the stratigraphic section are located to the right of the stratigraphic section on Figure 32.

3.1.6. Sequence Stratigraphy

The section represents a progradationally stacked parasequence set of sandstones and mudstones. A parasequence set is a succession of genetically related parasequences that form a

distinctive stacking pattern, in this case it is a progradational parasequence set. The five coarsening upward sequences separated by mudstones represent episodes of transgression and regression of the Western Interior Seaway. Each of the mudstones represents a flooding surface, where the sea rose locally or regionally.

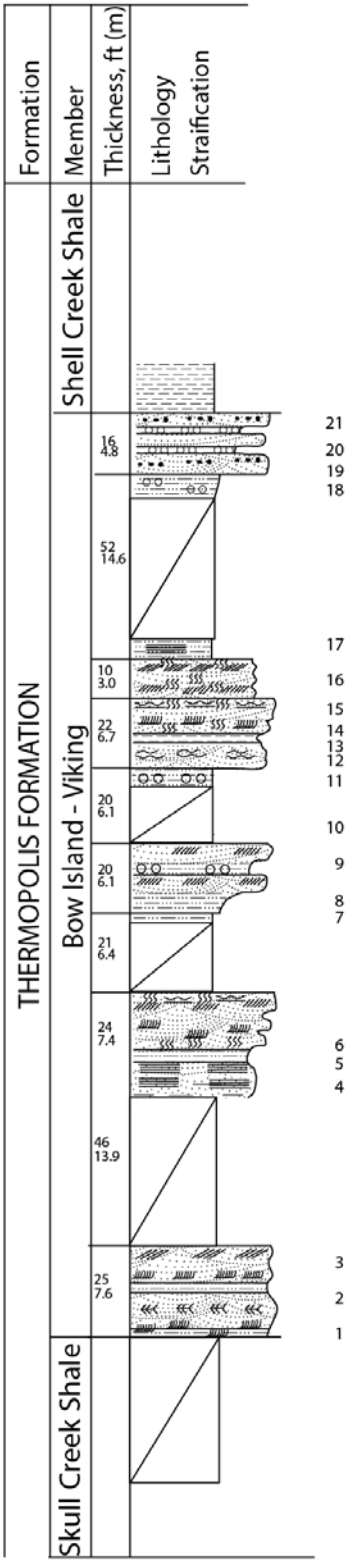

Figure 32: Figure locations relative to stratigraphic section. Numbers on the right indicate the location of the pictures and descriptions. Sills were removed to illustrate the stratigraphic section more accurately.

3.2. Correlations and Cross-sections

Cross-sections in the area were created based on well log availability and noticeable producing trends. Cross-sections are oriented north-south and west-east around East Butte in an attempt to create a box. The goal of these cross-section directions and was to use common wells whenever possible to allow for constant and consistent correlations of the formation tops. Cross-sections were created to be able to identify changes in facies and thickening/thinning patterns of sediments. Croft (2012) created cross section B-B' which was comprised of 88 wells along the northern portion of the area in Montana as well as some in southern Saskatchewan. Only one well from Crofts (2012) correlations was used in cross section C-C', API: 2505105247. A map of the cross-section lines shows locations and trend of the cross-sections (Figure 33). Cross-section A-A' location was chosen because of a notable Bow Island producing trend that is oriented north to south, perpendicular to the cross-section. Cross-section B-B' is oriented north to south and runs parallel producing trend mentioned previously. Cross-section C-C' is oriented west to east in the northern part of the area and created to intersect with cross-section B-B'. Cross-section D-D' is oriented northwest to southeast and was used to intersect wells between cross-sections B-B' and C-C'. Cross-section E-E' is oriented north to south on the western border of the area, E-E' and C-C' intersect at well 2505105315. Cross section F-F' is oriented east to west and intersects cross sections E-E', A-A', and B-B'.

Formation tops were correlative throughout the area. Only cross-section E-E' showed a significantly thicker sandstone body above the middle Bow Island top in the southern six wells of the cross-section. Being that the tops were correlative, the five cycles measured in section are consistent throughout the area. Flooding surfaces are highly correlative representing dips in

resistivity in the section. The sands are correlative throughout the area and display a similar signature throughout the area.

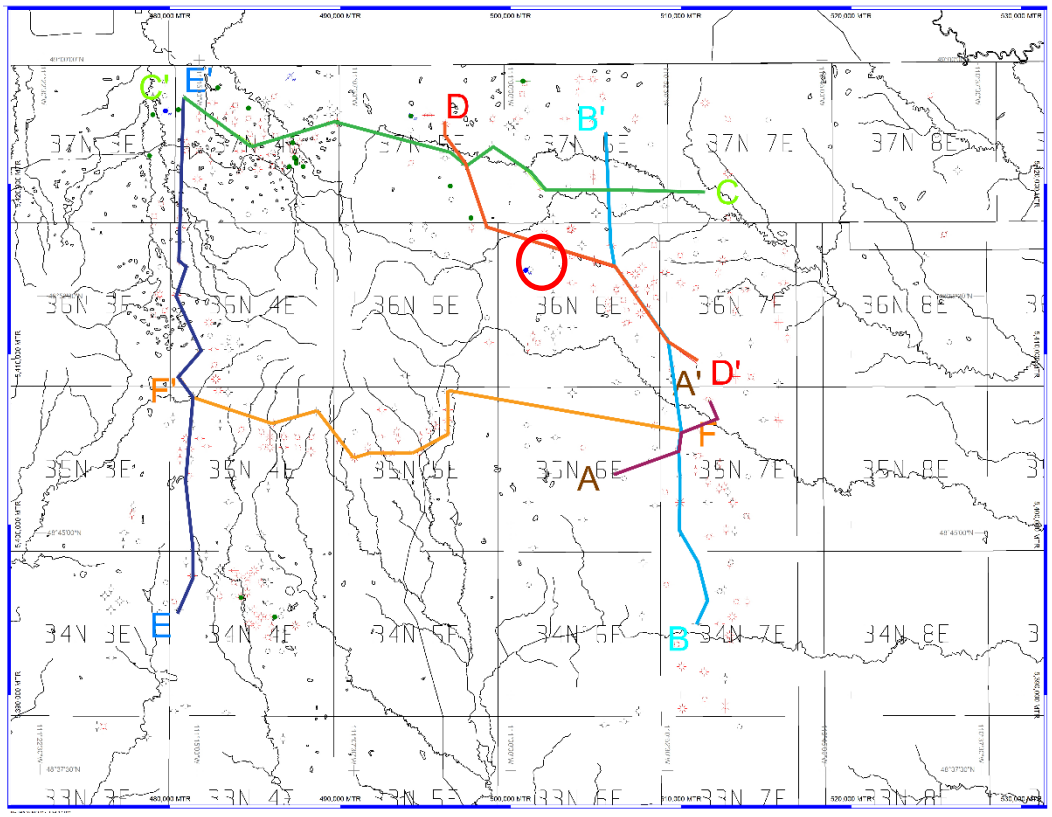

Figure 33: Cross-section lines in Hill and Liberty Counties: A-A' (dark red), B-B' (blue), C-C' (green), D-D' (bright red), E-E' (dark blue), F-F' (orange). The bright red circle shows the location of the three wells nearest to the exposed stratigraphic section.

The stratigraphic section measured near Mount Lebanon was used to tie the subsurface well log data to the exposed section of the Bow Island (Figure 33). Three wells were used to correlate the surface to the subsurface, the location of the wells is in the red circle on Figure 33. These wells were chosen because of their proximity to the exposed section and well log availability (Figure 34). Within the Bow Island section there is some thickening generally in the southeast and thinning of sands generally in the northwest. The black lines in Figure 34 represent an attempt to correlate the stratigraphic section to the subsurface. Sills were removed from the

stratigraphic section to show a more accurate representation of the stratigraphy that would be seen in the subsurface.

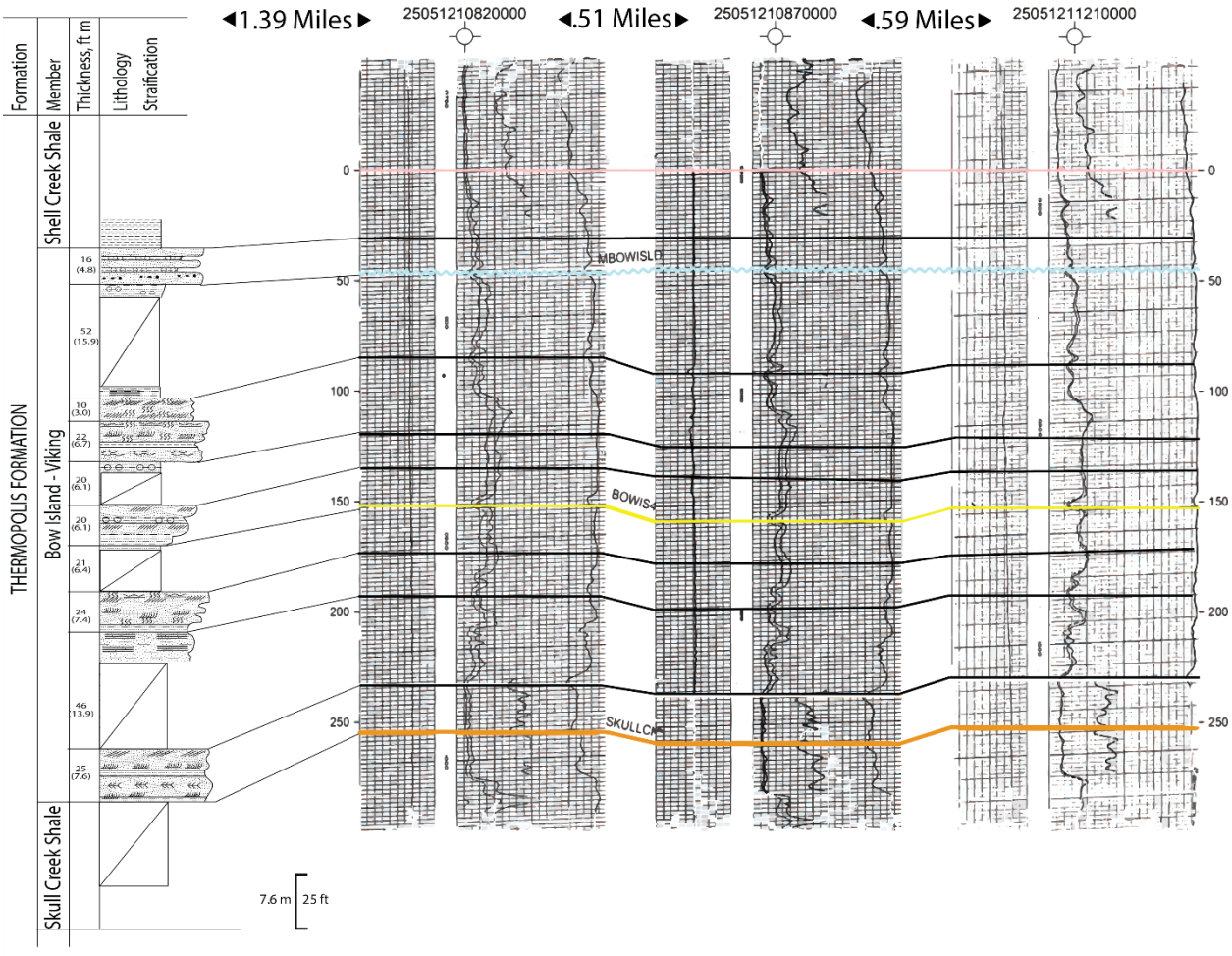

Figure 34: Correlations of four informal units. Skull Creek Shale (gold line), the lower Bow Island (yellow line), the middle Bow Island (blue line), Bow Island top (pink line). Vertical scale for the stratigraphic section and the well logs is equal. Figure details three wells closest to the exposed outcrop: 250521121, 2505121082, 2505121087.

3.2.1. Cross-section A-A'

Cross-section A-A' (Figure 33; Figure 35) is oriented east to west townships R36N T6E and R35N T7E. It consists of six logs covering 5.19 miles. Resistivity logs were the main log used; spontaneous potential (SP) readings were used to corroborate readings when they provided any information. Additional markers were correlated in each of the cross sections and were

numbered 1-4. Each line indicates the same marker in every cross section. Generally, cross-section A-A' shows moderate thickening of a sandstone located between the middle Bow Island and marker 3 from west to east. From west to east, there is a thickening of the mudstone between marker 1 and the middle Bow Island member. The sandstone that lies above the lower Bow Island maintains a similar thickness in all of the logs where the sandstone is visible. The rest of the section shows uniformity of thickness in the different mudstones and sandstones.

3.2.1.1. Gas Production

Cross-section A-A' was designed to identify a trend in productive wells. The perforation zones are distinct in all of the gas producing wells. The productive sands are located below a mudstone that acts as a seal (Figure 35). Wells 2505121383 and 25051252306 are both perforated at the same location in the log, which is directly below the middle Bow Island. Well 2505121449 has a perforation zone lower than the other two wells in the cross section.

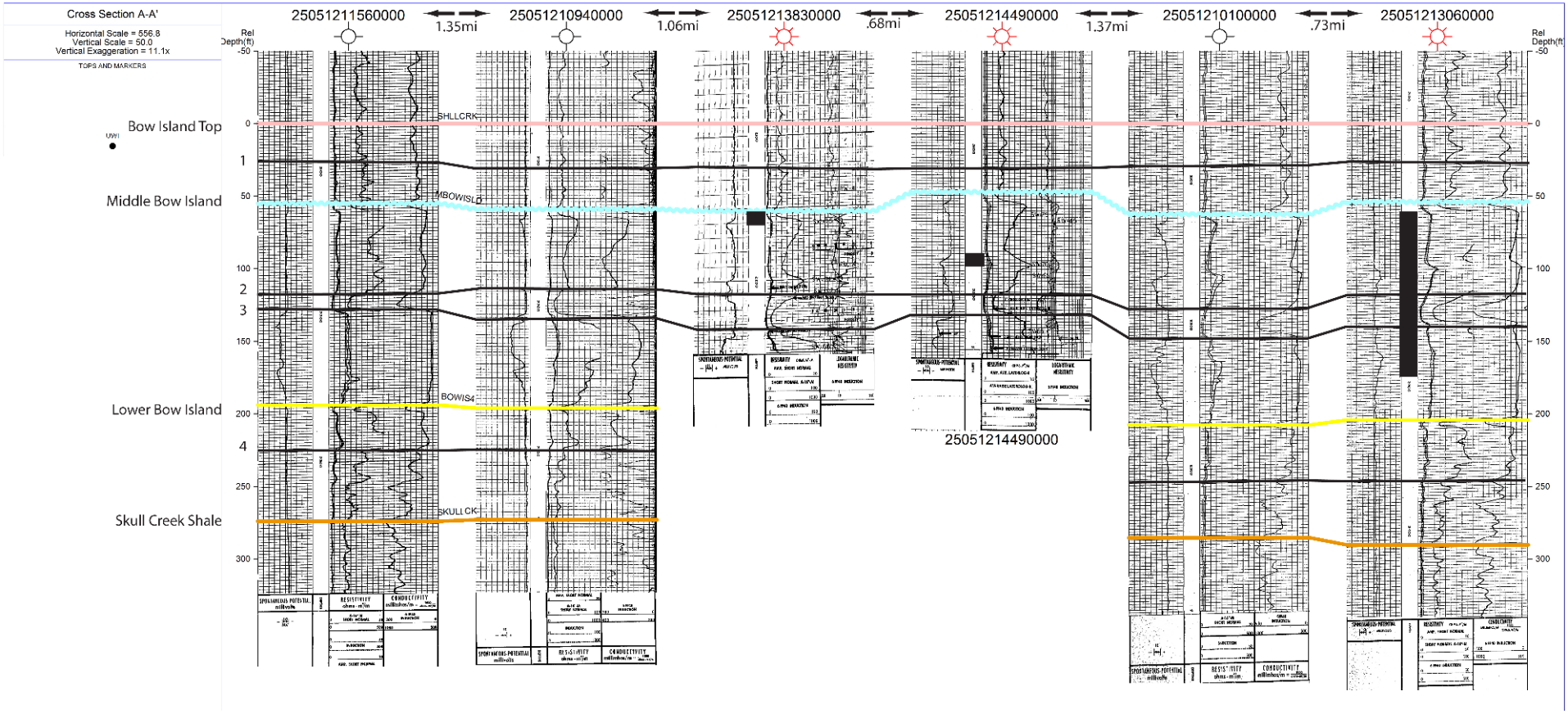

Figure 35: Cross-section A-A'. Lines 1-4 show correlative surfaces that are visible in all of the wells. Black boxes between resistivity and SP on the logs indicate perforation zones. Dry holes are marked with an empty circle and four points; producing wells are marked with the standard symbol of a gas producer, the red circle and with six points; Green dots above a well indicates an oil producer.

3.2.2. Cross-section B-B’

Cross-section B-B’ is oriented south to north through T34N R7E, T35N R7E, T36N R6E, and T37N R6E covering a distance of 18.76 miles (Figure 33; Figure 36). Cross-section B-B’ was created to possibly identify a productive well trend. The cross-section contains 11 well logs that show relative uniformity in formation thickness. Between markers 3 and 4 there is a thickening of a sandstone from north to south and thins again at the end of the cross-section. The sandstone between the lower Bow Island and marker 4 has a repeated thinning and thickening pattern from north to south. The same sedimentological patterns exist in producing and non-producing wells in the intersecting cross-sections.

3.2.2.1. Gas Production

Six of the 11 wells are gas-producing wells and four contain perforation data. The perforation zones for the wells are in distinct locations. The perforations lie below the middle Bow Island marker. Of the wells that produce from the Bow Island, perforations are located at the top of a sandstone that is capped by a mudstone layer. Overall, the logs show that the section thickness is the consistent south to north.

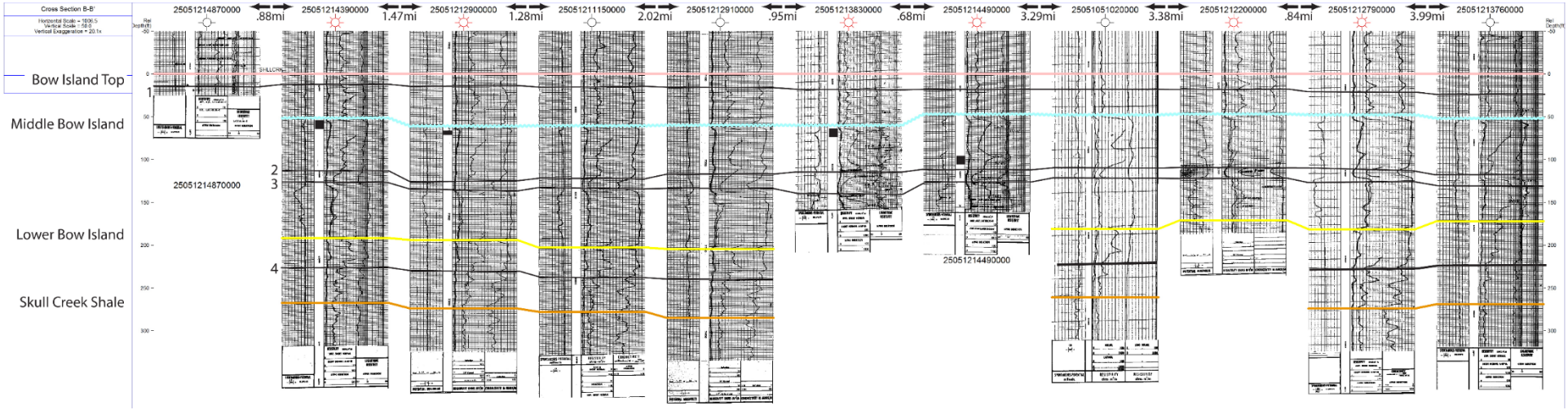

Figure 36: Cross-section B-B'. Symbols as in Figure 34.

3.2.3. Cross-section C-C’

Cross-section C-C’ is oriented west to east through T37N R4E, T37N R5E, T37N R6E, and T37N R7E covering a distance of 17.43 miles (Figure 33; Figure 37). The cross-section contains nine well logs that show a thickening of the overall section from west to east. The sandstone between the middle Bow Island and marker 3 shows substantial thickening from west to east. The sandstone between markers 2 and 3 thins substantially from west to east. The most notable feature of this cross-section is the thinning of a sandstone body from west to east, located between marker 3 and the lower Bow Island from west to east in Figure 37. The sandstone that lies above the lower Bow Island thickens west to east and thins out in the last three eastern logs.

3.2.3.1. Gas Production

In cross-section C-C’, only one well contains perforation data for the Bow Island, other wells in the cross-section produced oil and gas from the deeper Madison Formation. Petra showed that well 2505121246 was plugged and abandoned, however MBOG data (last accessed 25 October, 2016) indicate that the well has been acidized and reperforated to produce from the Bow Island. The perforation zone is the same that is seen in the other wells in cross-sections A-A’ and B-B’, which is directly above the middle Bow Island top.

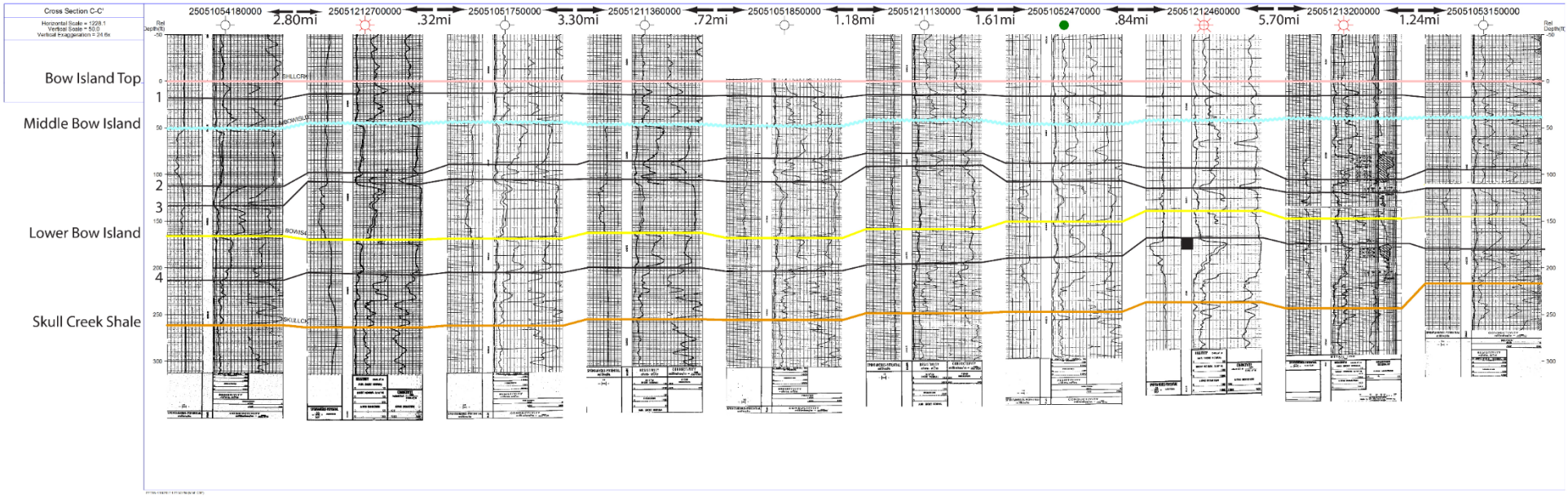

Figure 37: Cross-section C-C'. Symbols as in Figure 34.

3.2.4. Cross-section D-D’

Cross-section D-D’ is oriented northwest to southeast through T37N R5E, T36N R5E, T36N R6E, T36N R7E covering a distance of 13.69 miles (Figure 33; Figure 38). The cross-section consists of seven wells, two of which are gas-producing wells, production in these wells is not from the Bow Island. Gas comes from the Flood Member of the Blackleaf Formation in well 2505121075 and from the Madison Group in well 2505121220. There is a general thickening of the section in the logs from northwest to southeast, mainly in the large sandstone that lies above the lower Bow Island marker.

3.2.4.1. Gas Production

The perforation in well 2505121075 follows the other patterns seen in previous wells but is perforated in a different section and does not produce from the Bow Island. Gas comes from the Blackleaf Formation in well 2505121075 and from the Madison Group in well 2505121220.

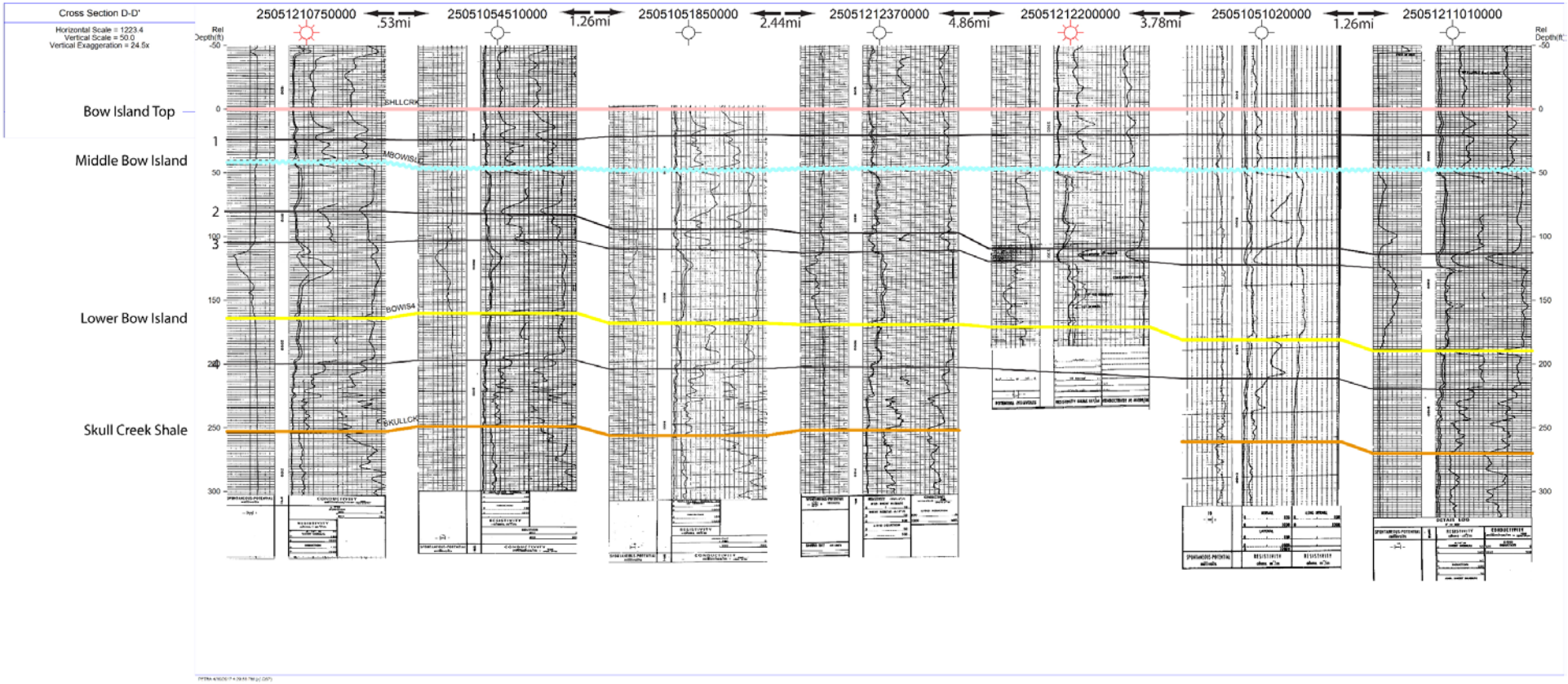

Figure 38: Cross-section D-D'. Symbols as in Figure 34.

3.2.5. Cross-section E-E’

Cross-section E-E’ is oriented from south to north through T34N R4E, T35N R4E, T36N R4E, T37N R4E covering a distance of 19.57 miles (Figure 33; Figure 39). This cross-section is composed of 12 well logs, two of which are gas producing wells, none produce from the Bow Island. Generally, the sands and mudstones displayed little change in thickening and thinning throughout the well logs. There is a thickening of a mudstone in the south above the middle Bow Island top in the south two wells and thinning the wells to the north. The sandstones and mudstones in this cross-section are the most uniform out of all the cross-sections, except for a substantial amount of thickening in the sandstone located between marker 1 and the middle Bow Island top. The sandstone unit outlined in a light green polygon shows a sandstone that is not visible on any other logs in the cross-sections. The sandstone pinches out between wells 2505105100 and 2505121441. It was designated a separate unit due to its distinctive SP and resistivity signature, identified by a serrated coarsening upward cycle in SP logs and a large jump in resistivity in the induction logs. I believe that the thickening of the section in this area is the result of a paleo-valley or a drainage system deposited during the transgression of the Shell Creek Shale after the middle Bow Island low stand event.

3.2.5.1. Gas Production

The sediment distribution is similar that of the other cross-sections in the area. There are wells near the cross-section that are productive wells but are not from the Bow Island either. Because of the fault systems in the area it is possible that faults have cut off or sprung gas reservoirs in within the Bow Island.

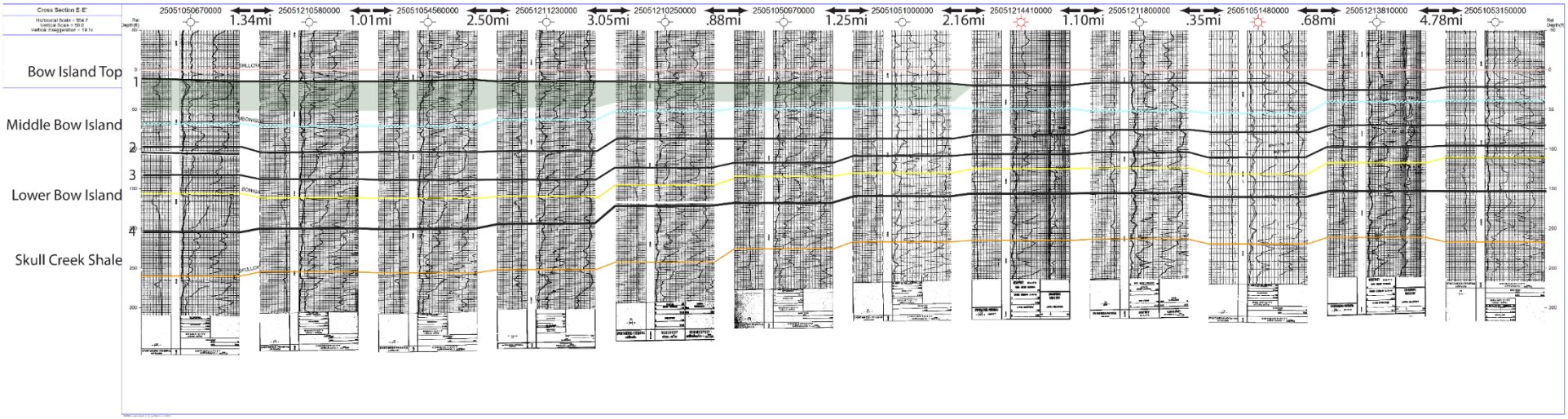

Figure 39: Cross-section E-E'. Symbols as in Figure 34. Area in green represents a sandstone body not seen in any portion of the area.

3.2.6. Cross-section F-F'

This cross section intersects cross sections E-E', A-A' and B-B'. It is oriented through T35N R4E, T35N R5E, T35N R6E, T35N R7E and covers a total distance of 19.98 miles (Figure 33; Figure 40). The cross section is composed of 11 wells with four of them being productive. Out of the four wells three of the wells have perforation zones and produce from the Bow Island. One mudstone that lies between markers two and three shows a thickening to the west. The sandstone between the lower Bow Island top and marker three show thickening towards the center of the cross section, where the sandstone is thicker in the middle and thinner towards the edges of the cross section. This cross section was created because of the many producing wells that are located against the south side of East Butte. Well logs 2505121318 and 2505121297 are the only logs in the cross sections that have calibrated gamma logs.

3.2.6.1. Gas Production

Perforations in this cross section do not follow the same pattern that is seen in the other cross sections. Gas production related to the Bow Island is obvious, but the perforation zones are unique. The sedimentological pattern in this area is the same as in the other cross sections, although the location of the middle Bow Island is not as marked as in other cross sections.

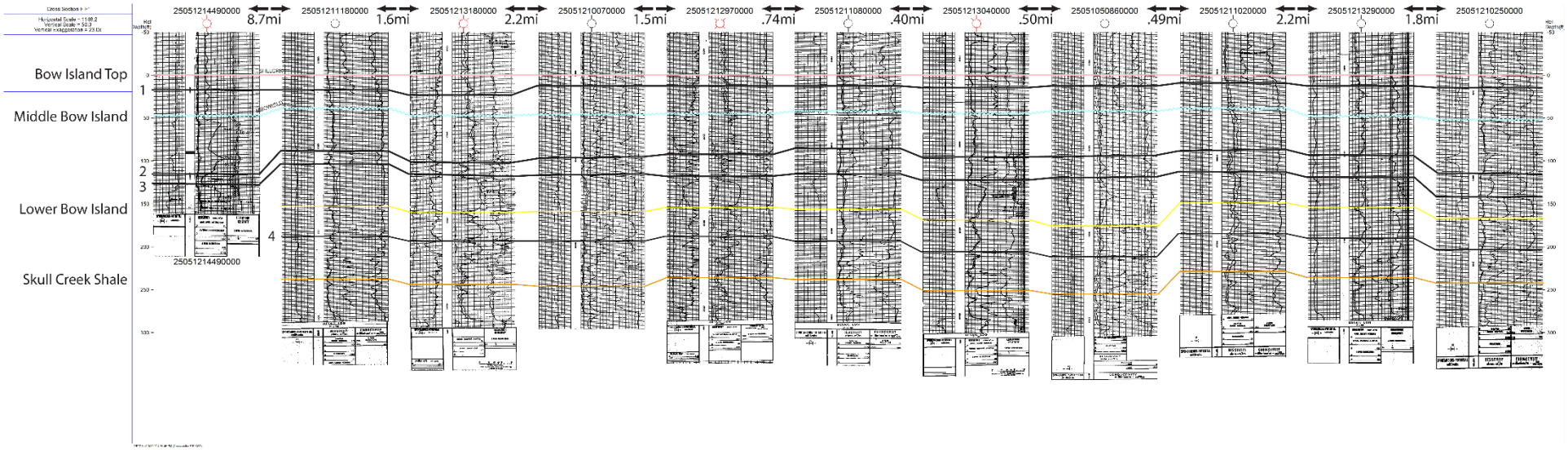

Figure 40: Cross section F-F'. Symbols as in Figure 34

3.3. Structure and Isochore Maps

A 3D visualization illustrates the high peak on the western side of East Butte. Four structure contour maps also show a subsurface domal structure. Above the domal structure, there is a high density of wells, most of which are gas producing. Although, there is a high concentration of wells located above the subsurface dome, for whatever reason, many of the wells did not provide well logs to interpret and the some of the formation heights were provided by Petra. Figure 41 shows the domal structure in a profile view, looking from south to north.

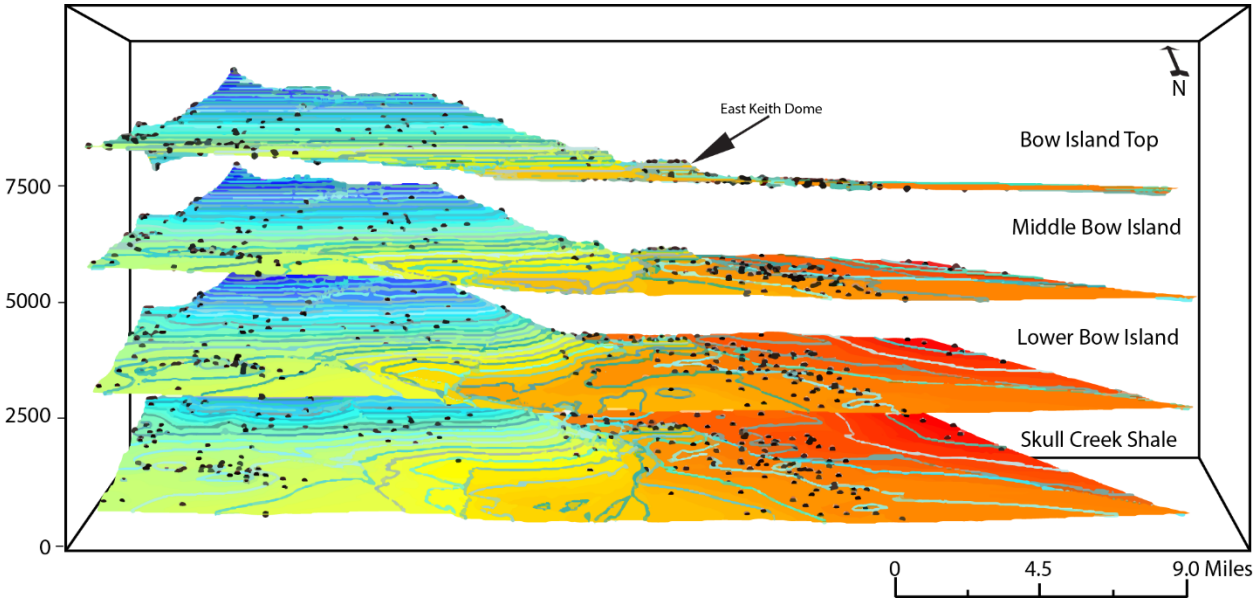

Figure 41: 3D visualization of the horizon tops facing north. Listed from bottom to top: Skull Creek Shale, lower Bow Island, middle Bow Island, and Bow Island top. Black dots indicate correlated wells; contour lines are at 100 foot intervals. The depths have been offset by 2500 feet to allow for a better viewing potential. Vertical exaggeration of 6 times.

Northwest of East Butte, Whitlash Dome has a high concentration producing wells oil and gas producing wells. Whitlash dome is one of a few places near East Butte that produces oil. Peterson suggested that the reason why oil was formed at the dome was because organic matter

was thermally matured through proximity to an instrusive igneous body (Peterson, 1966). The dome was cored by an igneous intrusion as seen in Figure 42 (Lopez, 1995).

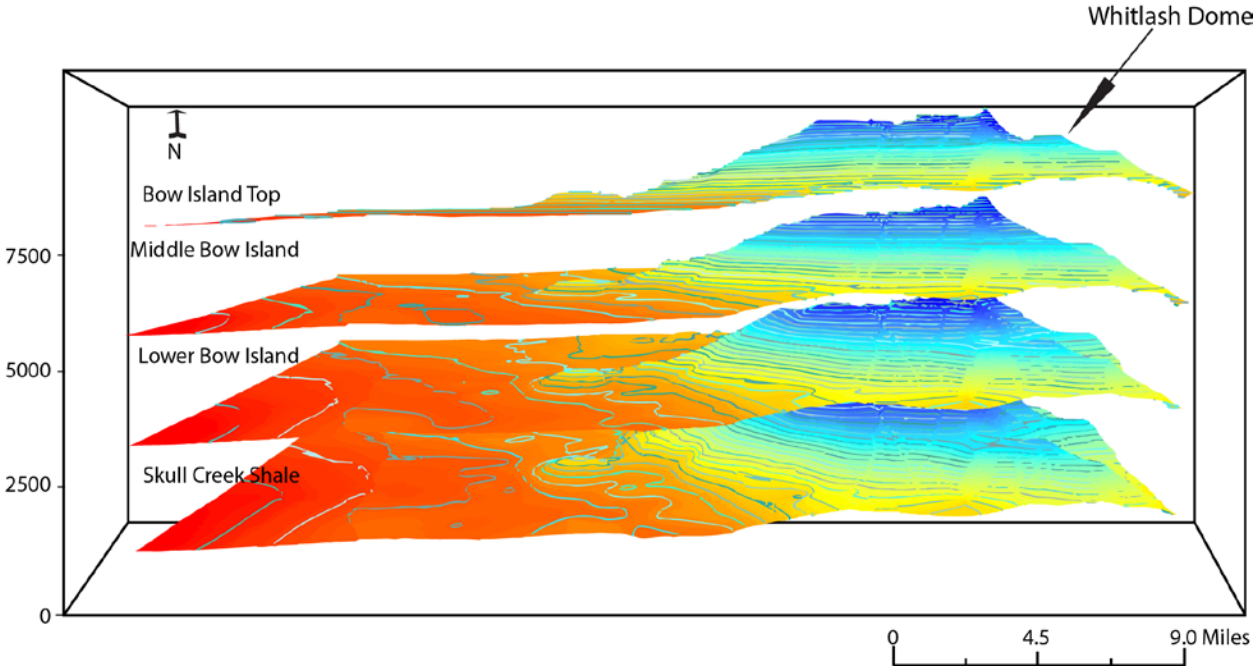

Figure 42: 3D visualization of the Formation tops facing south. Listed from bottom to top: Skull Creek Shale, lower Bow Island, middle Bow Island, and Bow Island top. Black dots indicate correlated wells; contour lines are at 100 foot intervals. The depths have been offset by 2500 feet to allow for a better viewing potential. Vertical exaggeration of 6 times.

Structure contour maps were created from well log correlations of the four units, the Bow Island top, top of the middle Bow Island, top of the lower Bow Island, and the top of the Skull Creek Shale (Figure 43; Figure 44; Figure 45; Figure 46). The Bow Island top ranges in elevation between 985-3281 feet above sea level. The red portion in the northwestern corner of the contour map indicates the igneous intrusion that formed East Butte. Elevations are measured above sea level where the igneous intrusion at East Butte is approximately 3281 feet above sea level. The eastern portion of the area that is purple is approximately 985 feet above sea level indicating that the beds are lowering in elevation to the east. The same trend can be seen in all of the other structure contour maps. The middle Bow Island has a larger range in elevations from

656-4101 feet above sea level. The lower Bow Island depths range from 492-4101 feet above sea level, the highest displayed elevation is 4101 feet due to the high peak in the left portion of the main East Butte intrusion. The Skull Creek Shale has a depth range of 328-3773 feet above sea level in the subsurface. The highest displayed elevation is 3773 feet above sea level.

Faults within the well logs were difficult to find. It is thought that the reason for this is that they are at such a high angle that they are not seen on the well logs. One log did show evidence of normal faulting, evidenced by missing log signatures near the Bears Den Anticline (Figure 6). The fault was located higher on the log than the formation tops that were focused on in this study. Dramatic changes in elevation are related to the igneous intrusion which also created many major surface faults. Mapping that Lopez (1995) conducted resulted in the location of a number of large faults and anticlines that act as trapping mechanisms in many areas surrounding the Sweetgrass Hills. Logs that did show evidence of faulting were rare. A fault model could not be created because multiple faults are needed create a fault surface or model in Petra.

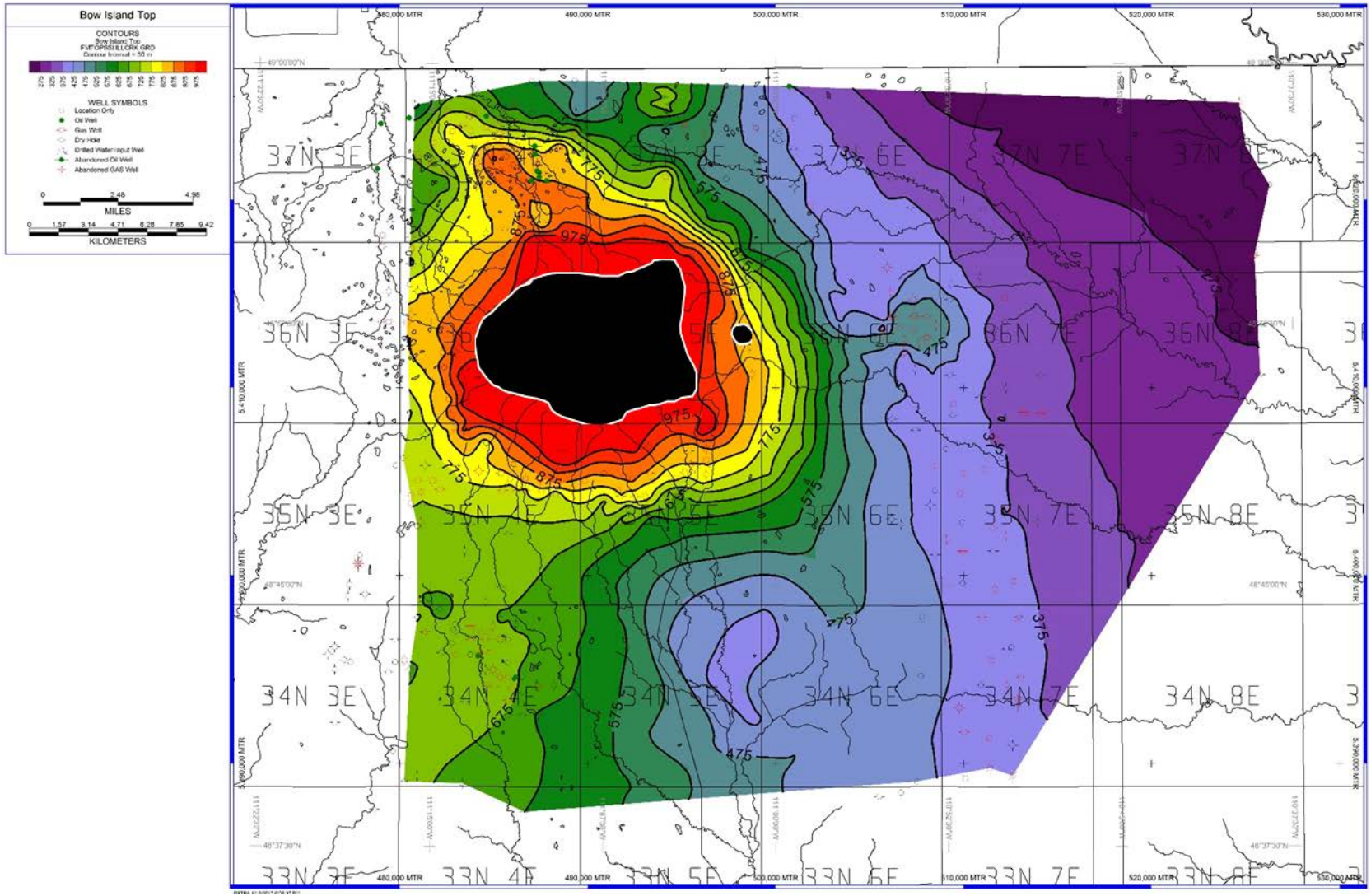

Figure 43: Bow Island top structure contour map. Elevated red surface cause by East Butte intrusion. Contour interval set at 50 feet.

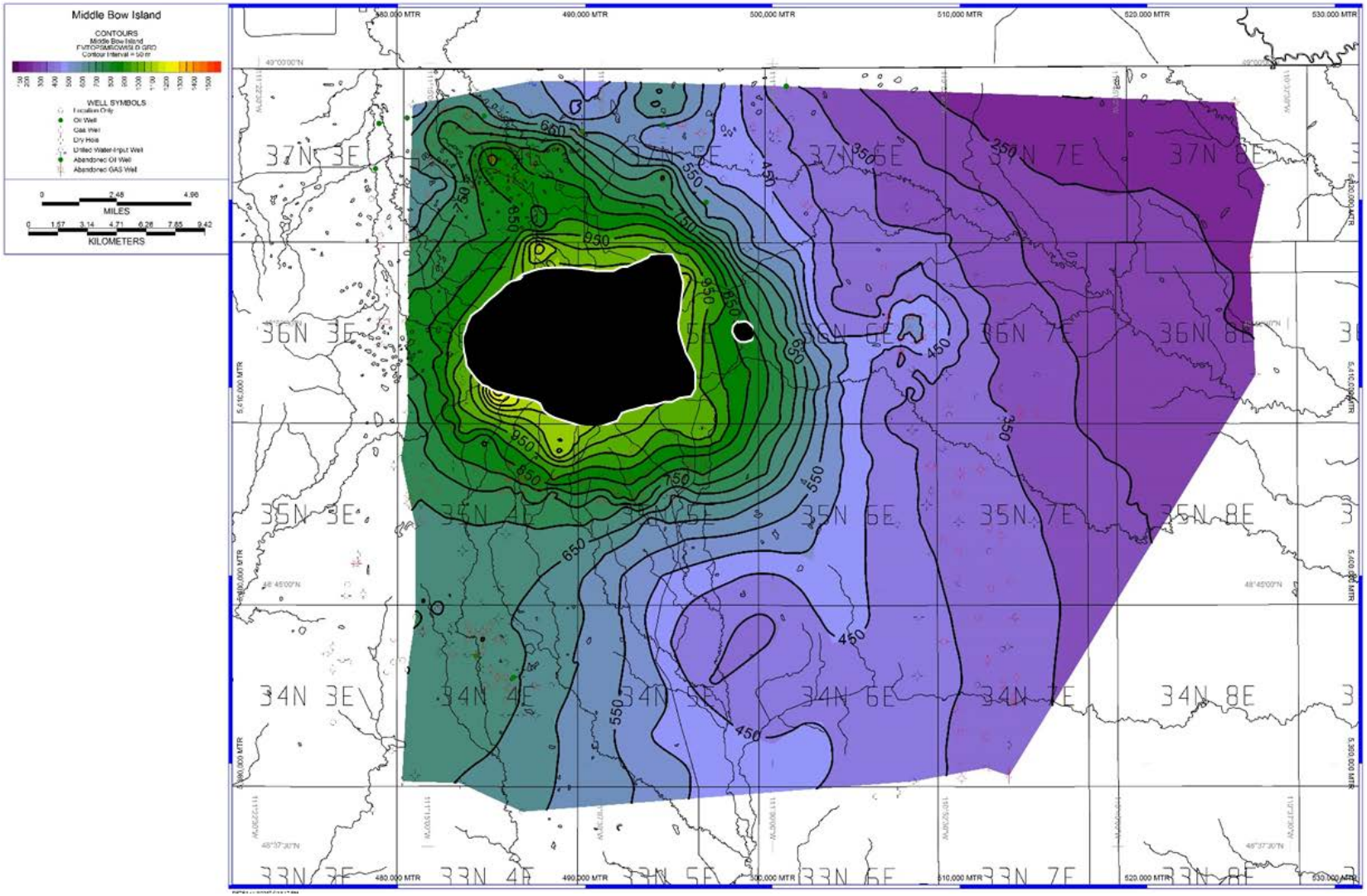

Figure 44: Middle Bow Island structure contour map. Elevated surface in green caused by East Butte intrusion. Contour interval set at 50 feet.

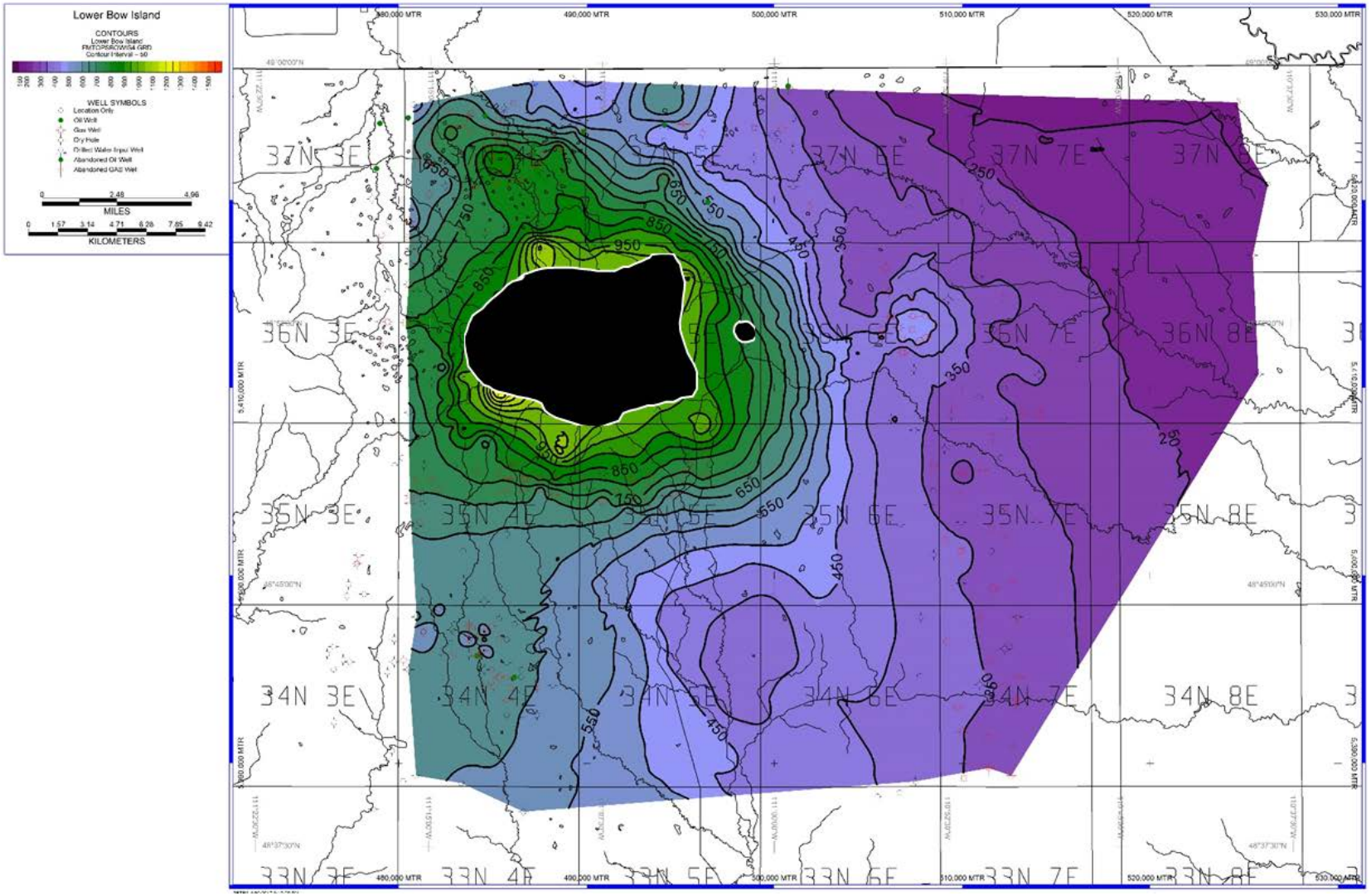

Figure 45: Lower Bow Island structure contour map. Elevated green surface caused by East Butte intrusion. Contour interval set at 50 feet.

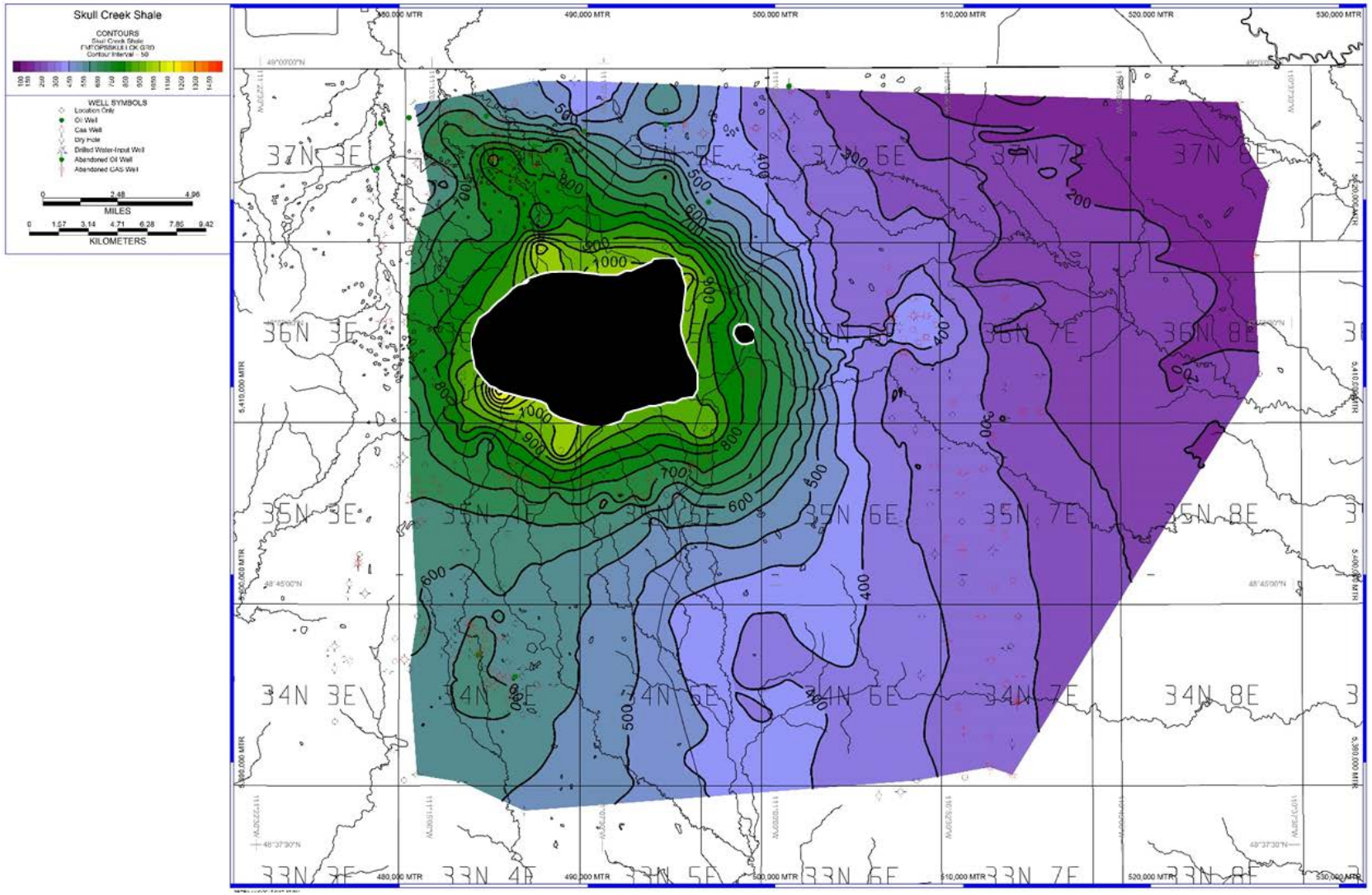

Figure 46: Skull Creek Shale structure contour map. Elevated yellow surface caused East Butte. Contour interval set at 50 feet.

The isochore map of the Bow Island shows a thickening in the east central to north central portion of the area (Figure 47). The south-central portion to the north-central portion of the area shows thinning as well as the upper north eastern corner. The thickness highlighted in this area is the entire correlated Bow Island, between the Skull Creek Shale and the Bow Island top.

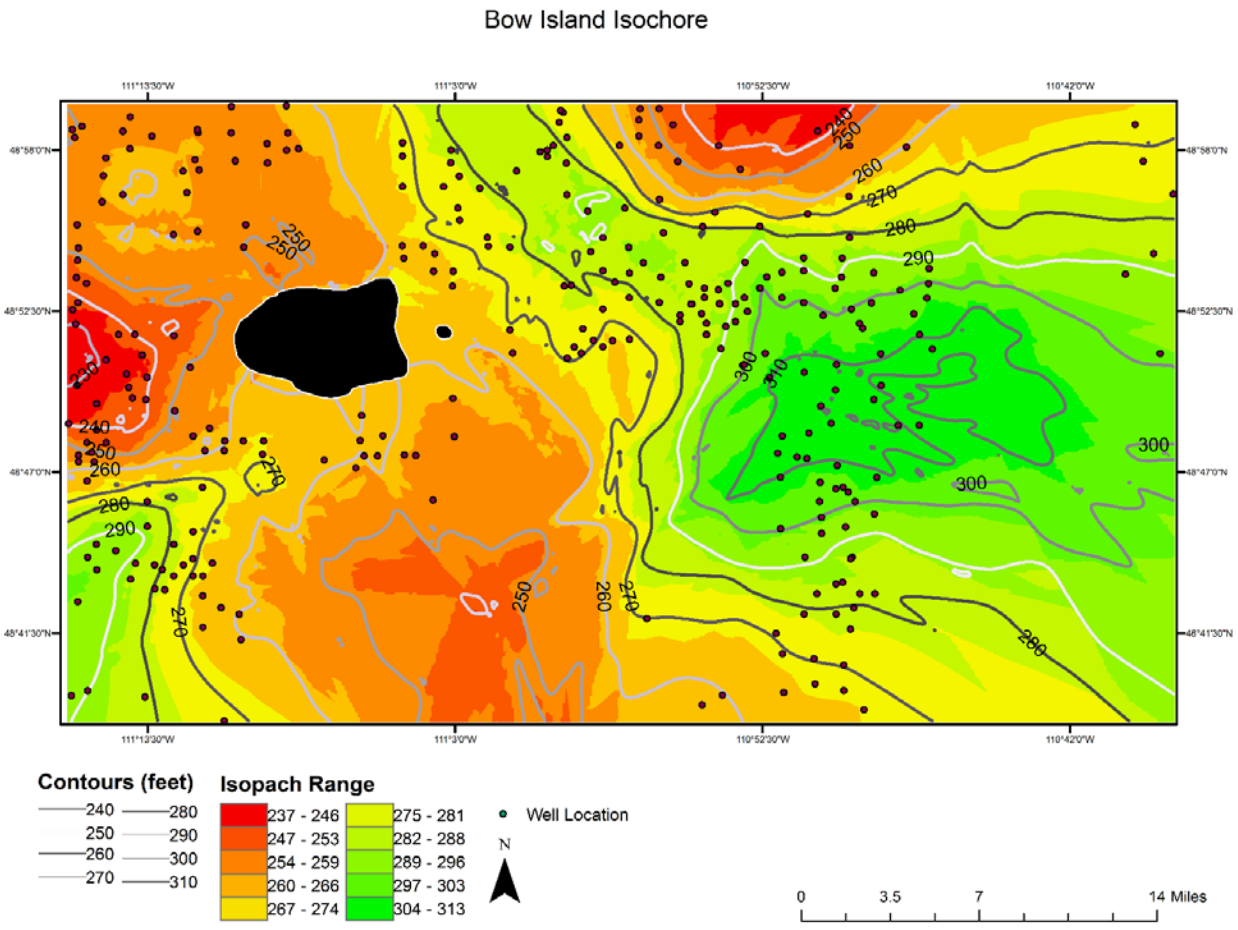

Figure 47: Entire Bow Island isochore map. The upper boundary is the Bow Island top and the lower boundary is the Skull Creek Shale. The blacked-out zone indicates the East Butte igneous intrusion and zero thickness.

The Bow Island top is the thinnest of the tops that were correlated. In general there is not a significant change in thickness between the Bow Island top and the middle Bow Island. There

is a thick trend in the southwestern portion of the map (Figure 48). The rest of the map shows a general constant thickness.

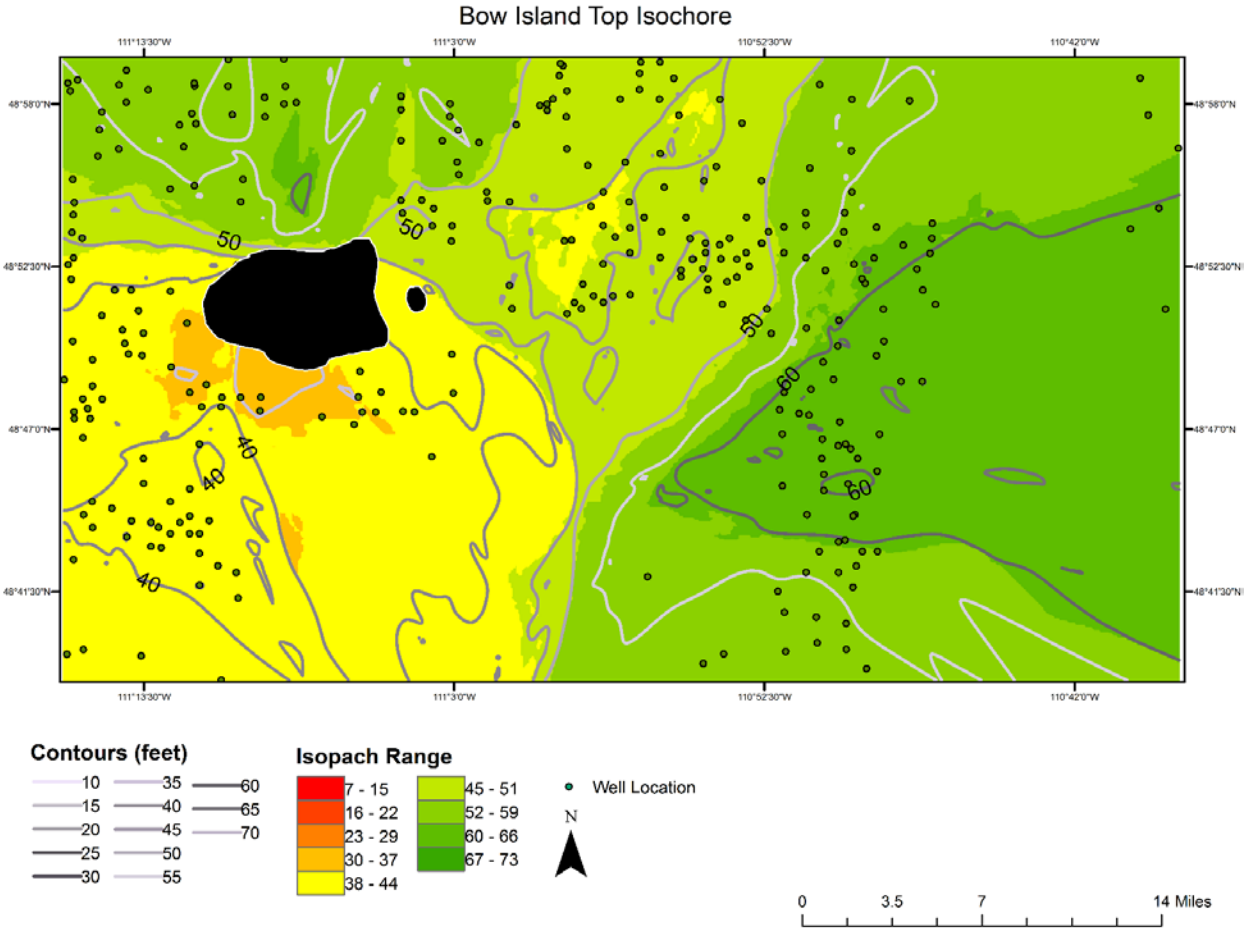

Figure 48: Bow Island top Isochore. The blacked-out zone indicates the East Butte igneous intrusion and zero thickness.

The isochore map for the middle Bow Island shows thickening in the middle portion of the area from northwest to southeast (Figure 49). The thick pattern is similar to the pattern seen in Figure 47. The northern portion, especially the northwestern corner of the area, shows substantial thinning. The thinning areas are thought to be topographic highs that were subaerially exposed during the late Albian lowstand event mention by several authors (Croft, 2012; Porter et

al., 1997; Reinson et al., 1994). The valleys are thought to be where incised valleys occurred due to the forced regression, resulting in the sandstone that is above the middle Bow Island in cross section E-E'.

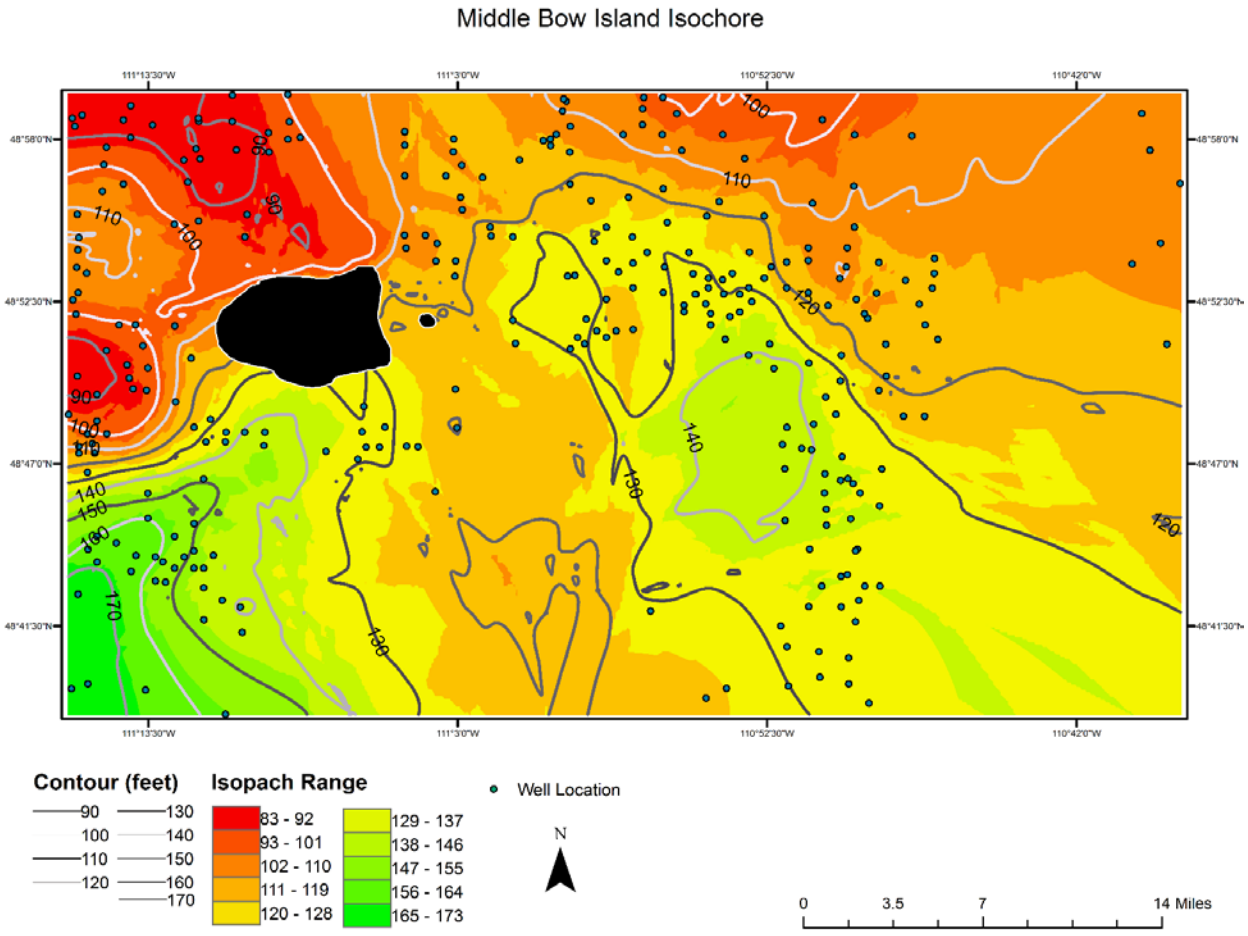

Figure 49: Middle Bow Island Isochore. The blacked-out zone indicates the East Butte igneous intrusion and zero thickness.

An isochore of the lower Bow Island shows the western-southwestern part of the area thinning (Figure 50). The northeastern portion of the area shows thickening where the middle Bow Island is thinning, and thinning where the middle Bow Island thickened. The lower Bow Island isochore displays relatively uniform deposition throughout the area, where the areas of thinner bedding are thought to be subaqueous topographic highs.

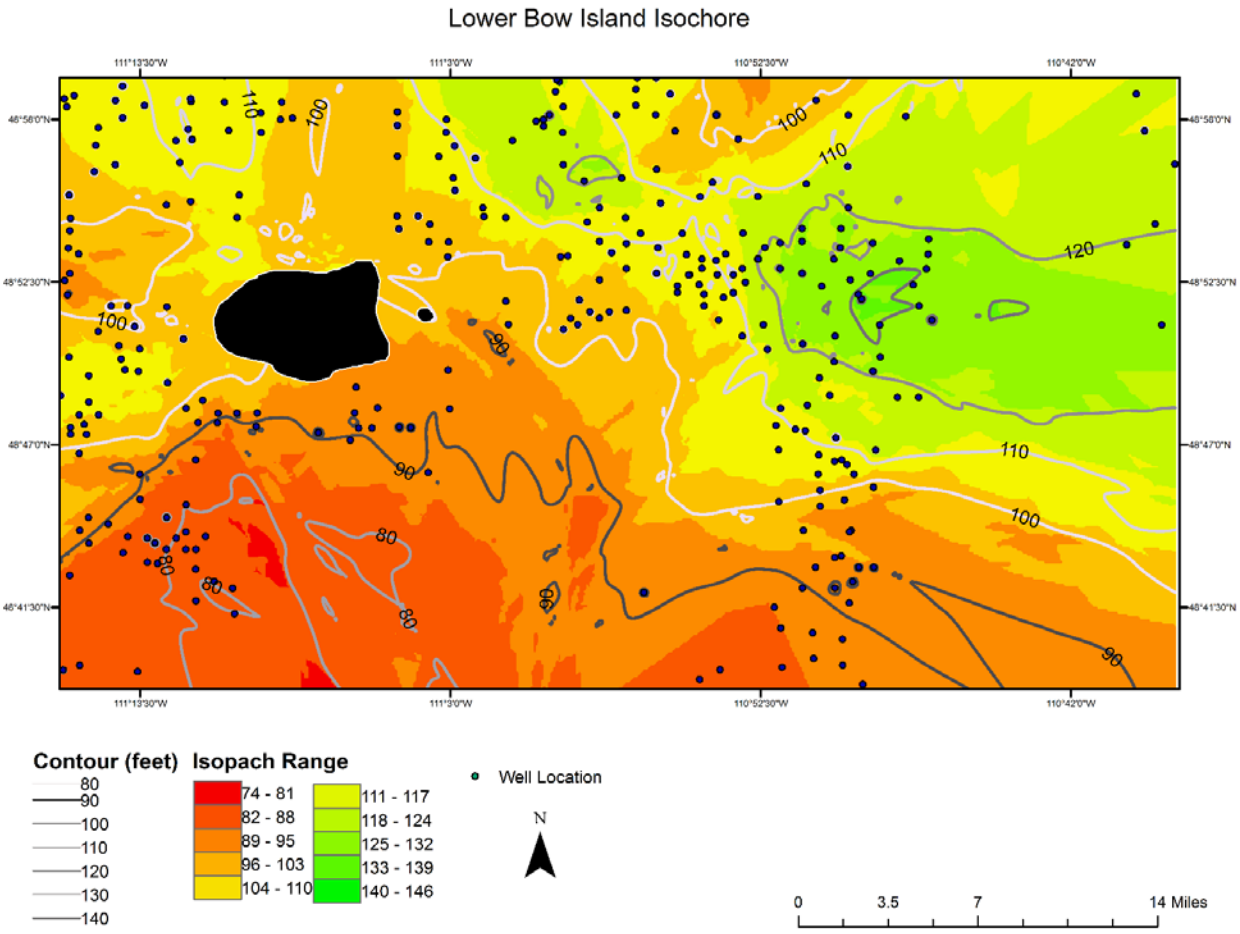

Figure 50: Lower Bow Island Isochore. The blacked-out zone indicates the East Butte igneous intrusion and zero thickness.

3.4. Mineral Analysis

Terraspec Halo short wave infrared readings were taken from each rock on a clean surface four times, each value from the readings are listed specifically and were not averaged. Minerals identified by the TerraSpec were listed in order of prevalence. Numbers indicate the number of times that the mineral appeared in the samples, not the "star number" that the panel on the back of the TerraSpec indicated (Table III).

Table III: Number of times minerals appeared summed from 68 total readings. Percentage is the number of times a mineral appears in a reading. Clays present from the minerals identified by the Terraspec. Swelling capability of the clays identified in samples.

	Minerals																					
	Mg-Illite	Muscovite	Smithsonite	Rectorite	K-Illite	FeChlorite	FeMgChlorite	Ferrihydrite	Vermiculite	Gypsum	Chabazite	Montmorillonite	Wavellite	Palygorskite	Gibbsite	Goethite	Phengite	Tourmaline	Paragonite	Calcite	Hematite	Heulandite
Occurrence	58	21	17	16	16	13	11	6	6	4	4	3	3	3	2	2	2	2	1	1	1	1
% of Clays Read	30.05	10.88	8.81	8.29	8.29	6.74	5.70	3.11	3.11	2.07	2.07	1.55	1.55	1.55	1.04	1.04	1.04	1.04	0.52	0.52	0.52	0.52
Clay	Y	N	N	Y	Y	Y	Y	N	N	N	N	Y	N	Y	N	N	N	N	N	N	N	N
Swelling Capability	N	N	N	Y	N	N	N	N	Y	N	N	Y	N	N	N	N	N	N	N	N	N	N

Table IV details the minerals as they are distributed throughout the column by sample. The scalar values of each of the readings for specific properties within the minerals are listed in Table V. Information detailing the procedure for reading the TerraSpec Halo Mineral Identifier are found in appendix B.

Minerals identified in the samples were separated into non-swelling and swelling clays groups to better identify clays that could contribute to intergranular particle plugging or swelling within the samples. Non-swelling clays and minerals from the list include: Mg-illite, K-illite, smithsonite, gypsum, wavellite, gibbsite, tourmaline, calcite, hematite, paragonite, goethite, ferrihydrite, muscovite, Fechlorite, FeMgchlorite, palygorskite, phengite. Swelling clays from the identified minerals include: rectorite, vermiculite, montmorillonite (Eggleton, 2001).

4. Discussion

4.1. Stratigraphy and Sedimentology

Aligned with the objective of tying the surface lithologies to the subsurface as previously stated in this project, the stratigraphic section was correlated to three wells nearest to the outcrop location (Figure 34). The subsurface correlations were used to create 3D visualization of the horizon tops to illustrate them in the subsurface. The cross-sections that were produced showed thickening and thinning of sandstones throughout the area and were used to determine the number of mappable cycles in the logs.

4.1.1. Sedimentology

The five coarsening upward parasequences within the Bow Island show a range of depositional environments from an offshore to foreshore environment, with some tidal influences, evidenced by the truncation of an unconformable surface associated with a lowstand event that occurred during the late Albian (Reinson et al., 1994). The cross bedding types seen in the sandstones indicate varied flow regimes associated with foreshore and offshore deltaic marine systems,as depicted in a composite section of the facies observed in the stratigraphic section (Figure 51). The herringbone cross bedding (Sx) indicates bimodal direction of forest dip caused by alternating current direction. This observation is important because of the implication that herringbone cross bedding occurs in tidally influenced areas (Boggs, 2005). It should also be noted that this is the only sandstone with herringbone cross stratification observed in the stratigraphic section. The cycle one sandstone displays changes in facies caused by fluctuations of sediment load and relative sea-level where coarsening upward subcycles occur. The unit coarsens upward to facies Sp, a coarse-grained sandstone.

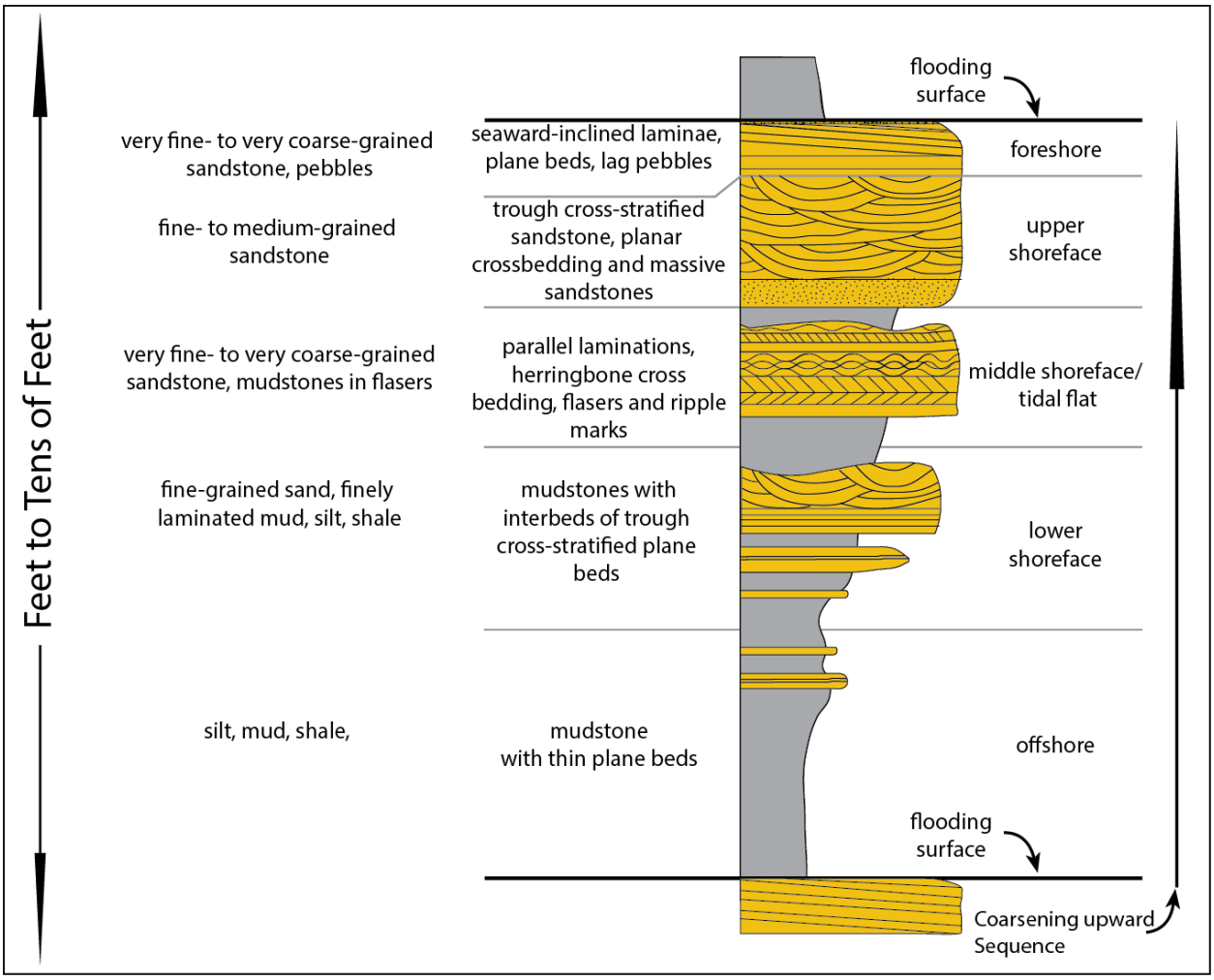

Figure 51: Generalized stratigraphic section for Bow Island cycles (modified from UGA Stratigraphy Lab, 2011).

The facies in cycle two indicate show the similar morphology as seen in the cycle one sandstone. A mudstone coarsens into a sandstone, the sandstones contain fine- to coarse-grained sandstone. The cross-stratification observed in section indicate varied flow regimes and relate to a marine deltaic depositional environment. The cycle two sandstone is not as varied in facies as the previous sandstone and contains symmetrical ripple marks on the tops of the beds indicating bidirectional currents. The ripple marks also indicate a middle to lower shoreface depositional environment.

The sediments cycle three display two coarsening upward subcycles. Cycle three shows the same coarsening upward morphology seen in the previous cycles. The repetition of the subcycles is attributed to minor rises and falls in sea level and increases in sediment load. The sandstones in this cycle are fine- to medium-grained. Fine-grained symmetrical ripples mark the tops of the beds and indicate a bidirectional current. The observed bedding structures indicate a middle shoreface to lower shoreface depositional environment.

The fourth cycle sandstone shows a wide variety of crossbedding structures such as flaser bedding (Hf) and planar cross stratification (Sp). Flaser bedding suggests deposition under fluctuating hydraulic conditions and tend to form in low energy environments where mud settles between troughs of rippled or cross stratified sands (Boggs, 2005). Alternating current and sediments supply are common conditions in marine delta front (middle shorefront) environments. The Fm facies contains nodules that are related to an offshore depositional environment. The Fm facies transitions to a fine- to medium-grained sandstone.The sandstone is abruptly transitions into a five foot thick shale layer (Fm) with interbedded planar sandstones. The shale is attributed to being deposited in an interdistributary bay, the shale is much darker in this portion than any other previous mudstone in the section. The Fm coarsens to a medium- to coarse-grained sandstone (Sp) capped by unidirectional ripple marks indicating a unidirectional current. Over all, the fourth cycle is interpreted to be part of a distributary mouth bar deposited in a marine deltaic front environment (middle shoreface). Cycle four displays the same mode as seen in the other successions, where overall, the cycle is coarsening upward.

Cycle five contains the thickest mudstone in the section. The changes in facies are not as varied as seen in the previous cycles, but follow the same mode where the section overall coarsens upward. The mudstone (Fm) coarsened to a medium- to coarse-grained massive

sandstone (Sm). The Fm facies contains nodules that are related to an offshore depositional environment. The sandstones contain black chert pebbles that are about ½ inch to about an inch long, they are noted to be related to the Albian lowstand event (Porter et al., 1997). After this sandstone (Sm) deposit there are two subcycles of a very fractured shale (Fm) and medium- to coarse-grained massive sandstone (Sm) beds. These beds are thought to have been formed as the Western Interior Seaway regressed, leading to them being subaerially exposed and are interpreted as a coastal plain deposit (backshore).

In summary, the changes in sedimentology observed in the column show a coarsening upward sequence in each succession, which is also seen in well logs. Changes in bedding structures and grain size are explained by changes in depositional environment and proximity the sediment supply. A marine deltaic front (middle shoreface to lower shoreface) environment is the dominant depositional environment in this stratigraphic section. The marine deltaic front is capped by a foreshore depositional environment that is denoted by lag pebbles that were deposited as sea level fell.

4.1.2. Stratigraphy

Holbrook and Ethridge (1996) proposed the extent of the Kiowa-Skull Creek highstand, wherein the Bow Island was deposited (Figure 52). The changes of lithologies within section can be explained by sea level and proximity to the sediment source. As mentioned in the previous section the dominant depositional system is a marine deltaic front (middle to lower shoreface). The parasequences that comprise the Bow Island show progradation of sediments into the Western Interior Seaway (Reinson et al., 1994). The cross sections in the area show the same trend that several authors have found (Croft, 2012; Pedersen, 2002; Reinson et al., 1994). The Bow Island thickens to the north west and thins to the south east. Tops remain correlative

throughout the area. Croft (2012) mentioned that the work that Reinson et al. (1994) and Pedersen (2002) had completed in Canada would transfer south of the Canadian border into Montana.

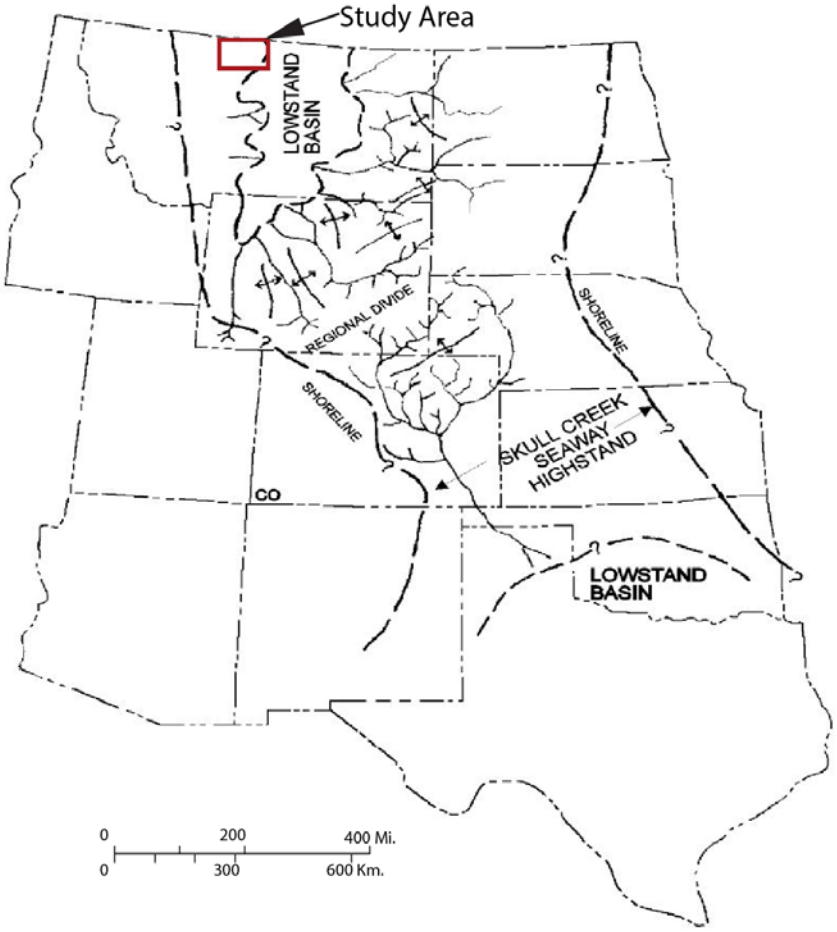

Figure 52: The extent of the highstand shoreline of the Kiowa-Skull Creek Seaway proposed by Holbrook (modified from Holbrook and Ethridge, 1996). Study area is highlighted in red.

4.1.3. Sequence Stratigraphy

During the Albian and Cenomanian stages, the boundary between late and early Cretaceous, two large scale transgressive/regressive cycles occurred in the Rocky Mountain Foreland Basin, the two cycles are referred to as the Kiowa-Skull Creek Cycle and the Greenhorn Cycle. These two cycles are separated by an unconformable erosional surface, which

is marked by the middle Bow Island horizon in this project and in other projects (Croft, 2012; Porter et al., 1997). The Kiowa-Skull Creek Cycle deposited large amounts of mudstone and marked an offshore to foreshore transition at the top of the Bow Island Member (Holbrook and Ethridge, 1996). The Greenhorn Cycle consists of a transgressive systems tract preserving the Bow Island below the Shell Creek Shale. Tectonics and/or eustatically controlled transgressions and regressions occurred throughout the deposition of the Bow Island during the Cretaceous (Kaufmann, 1977).

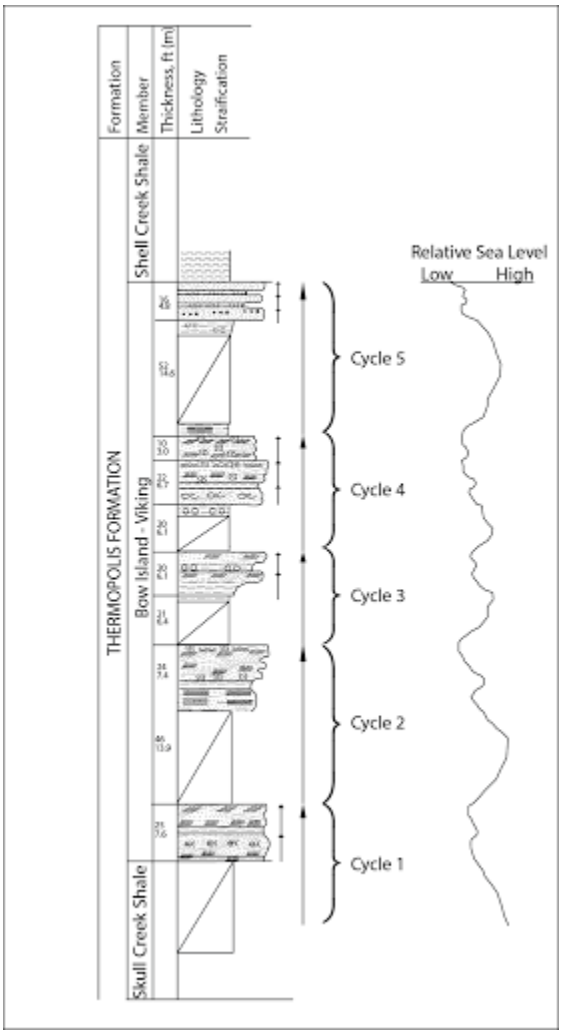

Figure 53: Stratigraphic section with relative sea level and annotation of coarsening upward cycles and subcycles.

Figure 53 illustrates the relative rise and fall in sea level in the stratigraphic section. The lithologies and changes in facies were the data used to create the curve. The relative sea level curve shows a general falling trend from the Skull Creek Shale to the Shell Creek Shale. The contact between the Bow Island and the Shell Creek Shale marks a sequence boundary where the sea level fell. A sequence boundary is defined by an unconformity that records subaerial exposure of sediments and relative fall in sea level, typically, the sequence boundary is capped by siliciclastic lag pebbles (Boggs, 2005). The Shell Creek Shale and Bow Island sequence boundary has been termed as a second order cycle sequence boundary by Porter et al. (1997). The sequence boundary is correlative throughout Alberta and northwestern Montana. Cyclicity of sequence boundaries are separated by their respective duration periods (Figure 54).

Cycle Order	Sequence Stratigraphic Unit	Duration (Ma)	Relative Sea Level Amplitude (ft)	Relative Sea Level Rise/Fall Rate (in/1000 yr)
First	Super cycle	> 100		< .4
Second	Sequence or Synthem	10-100	150-300	.4-1
Third	Mesothem	1-10	150-300	.4-4
Fourth	Cyclothem	.1-1	1-500	150-200
Fifth	Cyclothem	.01-.1	1-500	25-275

Figure 54: Cycle hierarchy of sedimentary cycles. Reproduced from Kerans and Tinker (1997).

Throughout the section there are five coarsening upward cycles with mudstones between each of the sand bodies. The mudstones are flooding surfaces that mark a rise in sea level and a transition from a foreshore to middle foreshore depositional environment to a lower shoreface to offshore depositional environment. According to Catuneanu et al. (2009) the Bow Island parasequences are thought to be fourth to fifth order. Subcycles in the parasequences are illustrated in Figure 53 as small arrows to the right of the stratigraphic section. Each of the subcycles is thought to be a fifth (?) order subcycle. A fourth and fifth order cycles are thought to

be related to rises and falls in sea level produced by retreating and advancing glaciers. However, during the Early Cretaceous there were likely not any glaciers due to the greenhouse conditions that were prevalent (Wendler et al., 2016). One theory for a fourth or fifth order cycle to occur is that aquifer eustasy plays a major role in the retaining or dispersing fluids on a large timescale (Wendler et al., 2016). When there are high precipitation rates, aquifers will retain more water, when there is less precipitation there will be less water retained. The parasequence set that comprises the Bow Island show a progradational stacking pattern where the sands thin to the east and some of the mudstones become thicker to the east. This pattern agrees with the gradual retreat of the Western Interior Seaway, where lag pebbles were deposited that mark the sequence boundary between the Bow Island and the Shell Creek Shale.

4.2. Structure and Petroleum Occurrence

The area surrounding East Butte is complex structurally. Lopez (1995) mapped several anticlines in the area and labeled East Butte as a large anticlinal structure (Figure 6). Subsurface structure from horizon elevations revealed structures that are visible in well logs and are not visible from the surface, due to being covered by glacial till (Lopez, 1995). Overall the gas fields are largely related subsurface faulting and structure. Many of the fields in the area are adjacent to faults with few exceptions. O'Brien's coulee is one of the locations that appears to be controlled by stratigraphic trapping, although stratigraphic trapping patterns could not be identified in cross-sections. Figure 55 shows gas producing fields related to the Bow Island. Some of the fields are thought to be stratigraphically controlled.

There are many structures in the area that produce oil and gas and are thought to be intrusively cored. The visualization in Figure 41 shows a domal structure, possibly related to the East Keith Field. There is a high density of wells above this domal structure which is interpreted as having been caused by an intrusion. North of East Butte is Whitlash Dome which produces gravity heavy oil and natural gas. Whitlash Dome is a doubly plunging anticline which is interpreted to have an intrusive core at depth (Erdman, 1935). Flat Coulee and Bears Den Anticlines are thought to be caused by intrusive igneous bodies due to pre-existing faults and igneous intrusions (Lopez, 1995).

Horizon elevations interpreted from the available well logs facilitated the production of four structure contour maps of two units within the Bow Island as well between the Skull Creek Shale and the Bow Island top. The structure maps all showed a down dipping trend to the east, where the horizons are much deeper than they are near East Butte (Figure 43;Figure 44; Figure 45; Figure 46). Noticing this trend on the eastern side of the area provoked the thought of gas

possibly migrating up dip to O'Brien's Coulee (Figure 55) and being trapped stratigraphically in a pinched-out sandstone. Both cross-sections A-A' and B-B' were examined carefully to find a possible pattern for traps, with no result. It should be taken into consideration that there is a possibility that wells drilled in the area were not developed because they did not produce oil and were deemed a dry hole. Many of the wells that were said to be nonproductive could have produced gas but were abandoned because they did not produce oil. Reinson et al. (1994) claimed that highly prospective explorational trends are those that occur at two different type of sequence boundaries: erosional boundaries, and parasequence boundaries. Many of the producing wells in cross-section A-A' show that perforations are located directly below or near the middle Bow Island horizon which is the sequence boundary between the Bow Island highstand systems tract and the Shell Creek Shale transgressive systems tract.

The middle Bow Island and lower Bow Island isochore maps show various thickening and thinning patterns, that are opposite of each other. The middle Bow Island shows thickening trend in the northcentral to the southcentral borders of the study area (Figure 49). The thicknesses are controlled by paleo-topographical highs and lows, possibly related to drainage valleys (Dolson et al., 1991). The middle Bow Island also shows an irregular shoreline due to the regression of the Western Interior Seaway. The lower Bow Island has subtler thickening trends throughout the area and thickens in the areas where the middle Bow Island thins (Figure 50). Although, the tops of the Formations are varied from those that Croft (2012) mapped, the pattern where sediments were deposited remains the same.

The Bow Island isochore (Figure 47) illustrates the vertical thickness of the entire Bow Island Member. This includes the portion of the Bow Island between the Bow Island top and the Skull Creek Shale tops. There is a thickening of the Bow Island section from the northcentral to

the east. This thickening trend appears to be part of a drainage system which could be tied in with the drainage systems mapped by Croft (2012) and hypothesized by Dolson et al. (1991) (Figure 47).

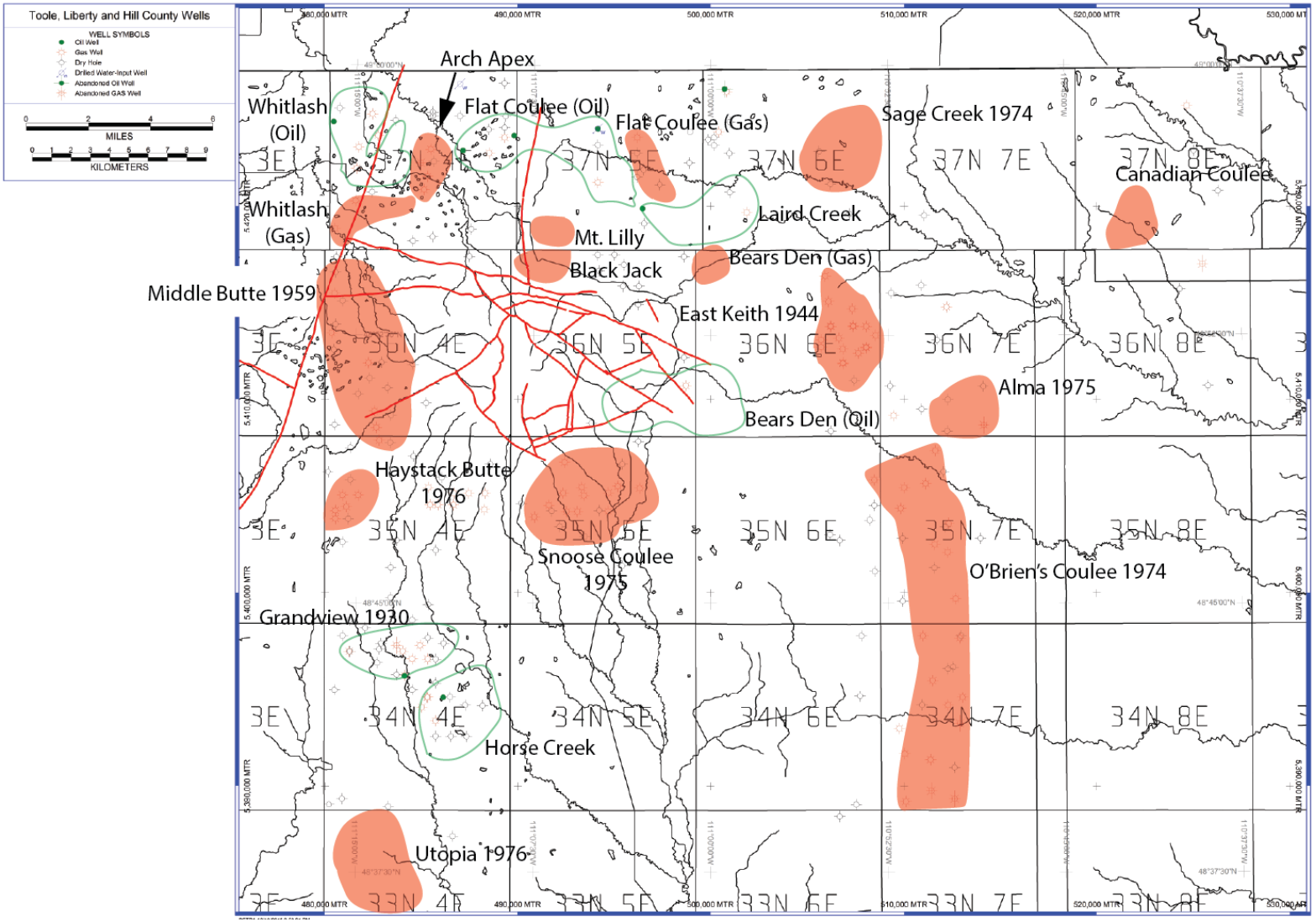

Figure 55: Bow Island gas fields and date of discovery (modified from Croft, 2012). Red lines are fault traces from Lopez (1995). Red circles indicate gas fields and green circles indicate oil fields.

4.3. Mineralogy

The Bow Island has been known as a gas producer since the 1920s (Perry, 1928). While there are many producing wells in the area, production problems have occurred in a large number of the wells (Leo Heath, personal communication, 16 May, 2015). Working from the objective statement of being able to identify potential causes for decreased well production, samples were analyzed to identify clay minerals that could contribute to the decrease in gas production. The mineralogy in the samples taken from the Bow Island were varied and contained many different types of clays. The most common type of clays found in the samples were from the illite group (Table III). Mg-illite and K-illite were present throughout the samples and could be related to intergranular particle plugging (Figure 56). Particle plugging refers to the movement of loose non-swelling particles plugging the pore of the system through rearrangement of clays (Hewitt, 1963). Other minerals commonly found throughout the column were rectorite and muscovite. Rectorite is an interstratified clay mineral that is composed of muscovite and montmorillonite. The swelling capability of this mineral is similar to that of montmorillonite. Muscovite does not swell, but could possibly be related to particle plugging. Chlorite group minerals were only found in coarse-grained sandstones. FeMgchlorite is found throughout the columns but is most present in samples that have medium to coarse-grained sandstone and could be a contributor to particle plugging within those samples. Montmorillonite would be the main contributor of swelling if it is present in any sandstone, however it is odd that it is only present in one of the sandstone samples, sample 15. It should be noted that although smithsonite appeared many times in the Terraspec readings, the readings were one star readings, meaning that the mineral was most likely a false reading. It is improbable that smithsonite formed as a secondary mineral in the samples due to smithsonite being related to zones with zinc ore.

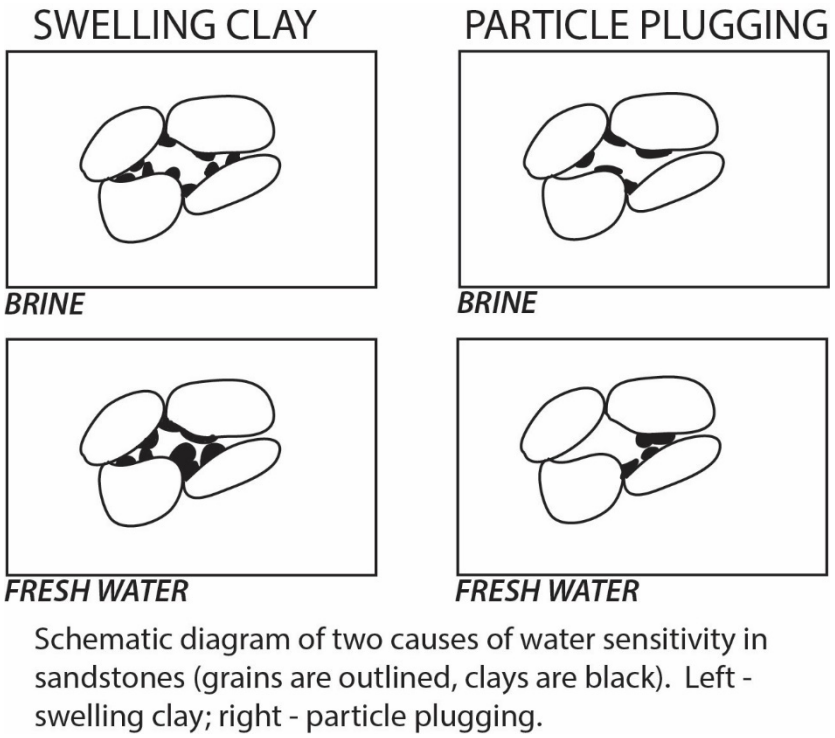

Figure 56: Diagram of clay swelling and particle plugging present in the pores of the sandstone after exposure to fresh water (modified from Hewitt, 1963).

Hewitt (1963) studied a sandstone sample of the Bow Island Formation from Alberta, Canada, although details of location and which sandstone from the formation were not provided. Hewitt (1963) tested the sandstone for water sensitivity and found that the clays are intergranular and swelling of clays is 118%, where a value of 105% was chosen as the lower limit of acceptable swelling percent. He concluded that the clays that are present in sandstones contribute to the decrease in production of the wells and classified the sandstone as strongly water sensitive. The clays that were present in the sample tested by Hewitt were by weight percent: montmorillonite (4.3%), kaolinite (2.5%), illite (3.2%), chlorite (1.3%).

One theory to account for the disparity of clays that Hewitt (1963) identified and the minerals that were identified using the Terraspec (Table III), is that there may have been alteration that occurred because of the intrusions. Meteoric and ground water may have

circulated the porous sandstone and the heated fluids caused alteration of the clay minerals present in the samples. Alteration of smectites is likely to have occurred because the heat needed to alter smectites to illites is 100°-110° C (Pollastro, 1993). The stratigraphic section where the samples were taken from is close enough to the intrusions for this to be a possibility. Two sills are also within the measured stratigraphic section, however in the field, observed contact metamorphism with the surrounding sediments is minimal.

Another question about the clays in the Bow Island is their origin, whether they are authigenic, meaning having formed in place, or whether they are allogenic, meaning that they were derived from different localities. McMannis (1964) observed an abundance of volcanic material in the Lower Cretaceous of western Montana and he suggested that volcanic material could possibly be related to an extensive deposit of similar age-equivalent rocks in Wyoming and southeastern Idaho. He noted that this appears to be correlated to the transition between non-marine and marine beds adjacent to the western highland source area caused by uplift and volcanic activity. He also suggested that the volcanic activity may be attributed to the early phase of emplacement of the Idaho batholith, which occurred in the early Cretaceous at approximately the same time as the deposition of the Bow Island sediments (Toth, 1985; Dolson et al., 1991).

Morad et al. (2013) explains that mechanical clay infiltration occurs when muddy river waters pass into sandy bodies. He mentions that in instances where clays are originally deposited as smectite clays, diagenetic alteration changes smectites to illites or chlorites, depending on depositional environments, proximity to the phreatic zone, and the original composition of the smectite clays. Illites are derived from dioctahedral smectite and chlorite is derived from trioctahedral smectite. Derivation of K^+ from the dissolution of detrital potassium feldspars can lead to the formation of illites. Derivation of Fe^{2+} and Mg^{2+} from the dissolution or replacement

of minerals such as biotite, hornblende, and from volcanic rock fragments, which will facilitate production of chlorite. He added that illites and chlorites can destroy reservoir permeability through fibers blocking pore throats thus decreasing fluid transport (Figure 56).

Wendler et al. (2016) explained that that an increase in clays as well as other chemically weathered elements is caused by an increase in precipitation where aquifer recharge is greater than aquifer discharge. Conversely, they mentioned that under dryer conditions weather sensitive minerals (feldspars, epidote, pyroxenes) are less abundant in transgressive sediments where aquifer charge is less than aquifer discharge. Wendler et al. (2016) went on to explain that a drop in sea-level during the late Albian was caused by a variety of processes, but the driving force for drop was aquifer eustasy. They suggest that during this time of increased precipitation aquifer recharge was greater than discharge and these changes in water storage were large enough to cause inflation of the aquifer and a relative drop in sea-level. If such a precipitation rate occurred at the time and the suggestions made by Wendler et al. (2016) are true, it must mean that the clays in the Bow Island are allogenic rather than authigenic, meaning that they were derived from an outside source rather than having been formed in place. This would fit in with what many authors (Dolson et al., 1991; Toth, 1985; Peterson, 1966) postulated. Clays were deposited as a result of allogenic deposition from varied sources (i.e. volcanism and hydrologic cycle).

In summary, the clays were sourced from the highlands to the west and volcanic activity in the surrounding areas, meaning that they were allogenic. However, clays near the Sweetgrass Hills were likely altered due thermal fluid circulation as well as post depositional diagenesis. The large amounts of the illites in the samples suggests that alteration in the area is substantial. Particle plugging could also be the process by which gas production in wells decreased.

5. Conclusions

Facies in the stratigraphic section indicate most of the sandstones were deposited in a tidally influenced upper shoreface to middle shoreface depositional environment and mudstones were deposited in a lower shoreface to offshore depositional environment. The sandstones in cycle five were deposited in a foreshore depositional environment as the forced regression of the Western Interior Seaway caused relative sea level to fall.

Producing wells in the area show the same sedimentological pattern that non-producing wells show. Because of this, this study was not able to determine any patterns for stratigraphic trapping in the O'Brien's Coulee producing area, but determined that many of the areas that produce in the Sweetgrass Hills area are the result of subsurface structure. Many of the structures were caused by the intrusive igneous bodies that did not reach the surface. These intrusions affected Whitlash Dome, Flat Coulee, and Bears Den Anticline. One subsurface dome thought to be related to East Keith Field was identified in this study. East Keith Dome is thought to be the reason for a dense group of gas producing wells that are directly above the dome.

Generally, the trends in thicknesses were consistent throughout the area and provided good data for correlation. This was important because it facilitated the correlation of the measured surface stratigraphic section to the subsurface. Although, the match of the stratigraphic column was not exact, it still gave insight to the subsurface lithologies in the wells. It also marked the fact that there is a large amount of sedimentological variability in a relatively small area. The horizons chosen were correlative throughout the area. This proved that the cyclicity of the parasequences within the Bow Island are mappable throughout the area, apart from the extra sandstone unit in cross section E-E'.

Clays within the Bow Island originally are considered to be mostly allogenic due to the potential volcanic sources to the west and south. Sediments from the western highlands and early emplacement of the Idaho batholith are thought to be the source of the clays within the sandstones. Alteration of clays could have occurred due to thermal fluid circulation, diagenesis, and some instances of metasomatism near the sills. Fluid circulation likely altered smectites to illites in the area surrounding the Sweetgrass Hills. It is likely that areas further out from East Butte were not affected by hydrothermal fluid circulation, but this was not determined in this project. Particle plugging by the vast amount of illites and chlorites present as well as intergranular clay swelling could likely cause decreases in pore throat closures.

6. Future Work

Many opportunities for work exist in the Bow Island Member of the Thermopolis Formation and adjacent units. Some future work suggestions are: continuing correlations throughout the area, create thin sections of the samples obtained from the outcrop on Dafoe Ranch, conduct biostratigraphic and ichnological research, petrophysical analysis and outcrop correlation from different parts of Montana (Helena, Great Falls). XRD analysis of the sandstones from the Bow Island would help to describe the actual clay content and properties of the rocks and isotope analysis to determine if minerals have been reset due to hydrothermal alteration.

7. References

Boggs, S.J., 2005, Principles of Sedimentology and Stratigraphy, 3rd edition: Harlow, Pearson 659 p.

Bremer, J.M., 2015, Stratigraphy and sedimentology of the Cretaceous Mowry Shale in the northern Bighorn Basin of Wyoming: implications for unconventional resource exploration and development [M.S. thesis]: Lincoln, University of Nebraska , 55 p.

Caldwell, W.G.E., 1984, Early Cretaceous transgressions and regressions in the southern Interior Plains. In: The Mesozoic of Middle North America, Canadian Society of Petroleum Geologists, Memoir 9, 1984, p. 173-203.

Catuneanu, O., Abreu, V., Bhattacharya, J.P., Blum M.D., Dalrymple, R.W., Eriksson, P.G., Fielding, C.R., Fisher, W.L., Galloway, W.E., Gibling, M.R., Giles, K.A., Holbrook, J.M., Jordan, R., Kendall, C.G., Macurda, B., Martinsen, O. J., Miall, A. D., Neal, J. E., Nummedal, D., Pomar, L., Posamentier, H. W., Pratt, B. R., Sarg, J. F., Shanley, K. W., Steel, R. J., Strasser, A., Tucker, M. E., and Winker C., 2009, Towards the standardization of sequence stratigraphy: Earth Science Reviews, v. 92, p. 1-33.

Cobban, W.A., and Reeside, J.B., Jr., 1952, Correlation of the Cretaceous formations of the Western Interior of the United States: Geological Society of America Bulletin, v. 3, p. 1011-1044.

Cobban, W.A., 1955, Cretaceous rocks of northwestern Montana, In: Sixth Annual Field Conference Guidebook: Billings Geological Society, p. 107-119.

Cobban, W.A., and Erdmann, C. E., 1959, Colorado Group on Sweetgrass Arch, Montana, In: Tenth Annual Field Conference Guidebook: Billings Geological Society, p. 89-92.

Cobban, W. A., Erdmann, C. E., Lemke, R. W., and Maughan, E. K., 1976, Type sections and stratigraphy of the members of the Blackleaf and Marias River Formations (Cretaceous) of the Sweetgrass Arch, Montana: U.S. Geological Survey Professional Paper P 974, 66 p.

Condon, S.M., 2000, Stratigraphic framework of Lower and Upper Cretaceous rocks in central and eastern Montana, Data Series 57, p. 1-10.

Croft, T.O., 2012, Sequence stratigraphy of the Lower Cretaceous Bow Island Sandstone in north central Montana [M.S. thesis]: Montana Tech, Butte, Montana., p. 128

Dolson, J, and Muller, D.M., 1991, Regional Paleotopographic Trends and Production, Muddy Sandstone (Lower Cretaceous), Central and Northern Rocky Mountains: AAPG Bulletin, v. 75, p. 409-435.

Erdmann, C.E. and Bartram, J.G., 1935, Natural Gas in Montana, Whitlash Dome, American Association of Petroleum Geologists, p. 271.

Eggleton, R.A., 2001, The regolith glossary: surficial geology, soils, and landscapes: Floreat Park, W.A., Cooperative Research Centre for Landscape Evolution and Mineral Exploration, 144 p.

Fisher, C.A., 1909, Geology of the Great Falls coal field, Montana: U.S. Geological Survey Bulletin 356, p. 21-89.

Glass, D.J., 1997, Lexicon of Canadian Stratigraphy Western Canada: Canadian Society of Petroleum Geologists, vol. 4, 1423 p.

Hewitt, C.H., 1963, Analytical techniques for recognizing water-sensitive reservoir rocks: Journal of Petroleum Technology, v. 15, p. 813-818.

Holbrook, J., and Ethridge F.G., 1996, Sequence Stratigraphy of the Dakota Group and Equivalents from North-Central Colorado to Northeastern New Mexico: Down-dip Variations in Sequence Anatomy: A Field Trip Guide for the 1996 GSA Annual Meeting.

Kauffman, E.G., 1977, Geological and biological overview: Western Interior Cretaceous Basin, The Mountain Geologist, v. 41, p. 407-421.

Kerans, C., and Tinker, S.W., 1997, Sequence stratigraphy and characterization of carbonate reservoirs: Tulsa, SEPM, 123 p.

Lopez, D.A., 1995, Geology of the Sweet Grass Hills, north-central Montana: Montana Bureau of Mines and Geology, Memoir 68, p. 3-27.

Lopez, D.A., 2002. Geologic map of the Sweet Grass Hills 30’ × 60′ quadrangle north-central Montana. Montana Bureau of Mines and Geology, Open File Report MBMG 443, 17 p., Plate 1, scale 1:100 000.

Lorenz, J.C., 1982, Lithospheric flexure and the history of the Sweetgrass Arch, northwestern Montana, In: Powers, R.B., ed., Geologic Studies of the Cordilleran Thrust Belt, Volume I: Rocky Mountain Association of Geologists, Denver, p. 77-89.

Maras, E.E., Caniberk, M., Odabas, M.S., Degerli, B., Maras, S.S., and Maras, H.H., 2016, An evaluation of the relationship between physical/mechanical properties and mineralogy of landscape rocks as determined by hyperspectral reflectance: Arabian Journal of Geosciences, v. 9.

McMannis, W.J., 1964, Resume of depositional and structural history of Western Montana: ABSTRACT: Bulletin AAPG Bulletin, v. 48.

Miall, A.D., 1999, Principles of Sedimentary Basin Analysis, 3rd, updated and enlarged edition: Springer, Berlin, 616 p.

Montana Board of Oil and Gas Conservation, 2016, Annual production by field database: http://www.bogc.dnrc.mt.gov/WebApps/DataMiner (accessed October, 2016).

Morad, S., Ketzer, J., and De Ros, L.D., 2013, Linking diagenesis to sequence stratigraphy: An integrated tool for understanding and predicting reservoir quality distribution: Linking Diagenesis to Sequence Stratigraphy. In: Morad, S., Ketzer, J.M., and De Ros, L.F., Wiley, p. 1–36. DOI: 10.1002/9781118485347

Pedersen, P.K., 2001, Sedimentary architecture of the Bow Island Formation, Southwestern Alberta, Canada: Canadian Society of Petroleum Geologists, p. 611-613

Pedersen, P.K., Schroder-Adams, C.J., and Nielsen, O., 2002, High resolution sequence stratigraphic architecture of a transgressive coastal succession: Albian Bow Island Formation, Southwestern Alberta: Bulletin of Canadian Petroleum Geology, v. 50, p. 441-477

Perry, E.S., 1928, The Kevin-Sunburst and other oil and gas fields of the Sweetgrass Arch: Montana Bureau of Mines and Geology, Memoir 1, p. 6-24.

Peterson, J.A., 1966, Sedimentary history of the Sweetgrass Arch: 17th Annual Field Conference Guidebook: Billings Geological Society, p. 112-132.

Pollastro, R.M., 1993, Considerations and applications of the illite/smectite geothermometer in hydrocarbon-bearing rocks of Miocene to Mississippian Age: Clays and Clay Minerals, v. 41, p. 119–133

Porter, K.W., 1998, Jurassic and Cretaceous outcrop equivalents of Shaunovon, lower Mannville, and Bow Island/Viking reservoirs, north-central Montana, a field guide, Montana Bureau of Mines and Geology: Special Publication 113, 29 p.

Porter, K.W., Dyman, T.S., Thompson, G.G., Lopez, D.A., and Cobban, W.A., 1997, Six outcrop sections of the marine Lower Cretaceous, central Montana; With a section on palynomorph stratigraphy and age of a Late Albian lowstand: Montana Bureau of Mines and Geology, Report of Investigation 3, p. 5-16.

Porter, K.W., Dyman, T.S. Cobban, W.A., and Reinson, G.E., 1998, Post-Mannville/Kootenai Lower Cretaceous rocks and reservoirs, north-central Montana, southern Alberta and Saskatchewan: Eighth International Williston Basin Symposium, Saskatchewan Geological Society Special Publication 13, p. 123-127.

Reinson, R.E, Warter, W.J., Cox, J., and Price, P.R., 1994, Cretaceous Viking Formation of the Western Canada sedimentary basin: Geological atlas of the Western Canadian Sedimentary Basin: Canadian Society of Petroleum Geologists, Ch. 21, p. 353-363.

Stebinger, E, 1918, Oil and Gas geology of the Birch Creek-Sun River Area, Northwestern Montana, U.S. Geological Survey Bulletin 691. p. 149-184

Slipper, S.E., 1918, Viking gas field, structure of the area. Geological Survey of Canada Summary Report 1917, Part C, p. 6-7.

Toth, M.I., 1985, Petrology and evolution of the Bitterroot Lobe of the Idaho batholith. Geological Society America Abstracts with Programs, vol. 17., no. 4,p. 269.

University of Georgia, 2011, UGA Stratigraphy Lab An Online Guide to Sequence Stratigraphy, http://strata.uga.edu/sequence/index.html (accessed April 2017).

Vuke, S.M., 1984, Depositional environments of the Early Cretaceous Western Interior Seaway in southwestern Montana and the northern United States: The Mesozoic of middle North America: Canadian Society of Petroleum Geologists, Memoir 9, p. 127-144.

Wagreich, M., Haq, B.U., Melinte-Dobrinescu, M., Sames, B., and Yılmaz, I.Ö., 2016, Advances and perspectives in understanding Cretaceous sea-level change: Palaeogeography, Palaeoclimatology, Palaeoecology, v. 441, p. 391–392

Weed, W.H., 1899, Geology of the Little Belt Mountains, Montana: With Notes on the Mineral Deposits of the Neihart, Barker, Yogo, And Other Districts. Washington: Govt. Print. Off., 1900.

Wendler, J.E., Wendler, I., Vogt, C., and Kuss, J., 2016, Link between cyclic eustatic sea-level change and continental weathering: Evidence for aquifer-eustasy in the Cretaceous: Palaeogeography, Palaeoclimatology, Palaeoecology, v. 441, p. 430–437.

8. Tables

8.1. Table IV: Minerals and Prevalence from Terra Spec Halo

Table IV: Minerals and their number indicators.

	Minerals																				
Sample	Mg-Illite	K-Illite	Ferrihydrite	Rectorite	Muscovite	Smithsonite	Gypsum	Paragonite	Gibbsite	FeMgChlorite	FeChlorite	Vermiculite	Goethite	Calcite	Chabazite	Phengite	Montmorillonite	Wavellite	Palygorskite	Tourmaline	Hematite	Heulandite
17	3																					
17	3			1		2																
17	3			1		2								1								
17	2																					3
16							2								3							
16										1					3	2						
16											2				3	2						
16	1										2				3						3	
15	3							2														
15		3		1									3				2					
15					2												3					
15		3															3		1			
14	2		2							1	1											
14	2										2	1								1		
14	1										2	1								1		
14	3			1							2											
13	2				1	1				3												
13					2	1				3												

Sample	Mg-Illite	K-Illite	Ferrihydrite	Rectorite	Muscovite	Smithsonite	Gypsum	Paragonite	Gibbsite	FeMgChlorite	FeChlorite	Vermiculite	Goethite	Calcite	Chabazite	Phengite	Montmorillonite	Wavellite	Palygorskite	Tourmaline	Hematite	Heulandite
13					2	1				2												
13	2	3										1	3									
12		3				1				2												
12	1	3								2												
12	1	3								3												
12	2									1	1	1										
11	2				1						1											
11	2				1	1					1											
11	3										2	1										
11	3			2							1											
10	3				3	1																
10	3				3	1																
10	3				3																	
10	1	3								3												
9	3				2																	
9	3																					
9	3			1							3											
9	2					1					1											
8	3				2																	
8	3				3																	
8	3				3																	
8	3	2				1																

Sample	Mg-Illite	K-Illite	Ferrihydrite	Rectorite	Muscovite	Smithsonite	Gypsum	Paragonite	Gibbsite	FeMgChlorite	FeChlorite	Vermiculite	Goethite	Calcite	Chabazite	Phengite	Montmorillonite	Wavellite	Palygorskite	Tourmaline	Hematite	Heulandite
7	3				2	1																
7	3				3																	
7	3		2																			
7	3			2		1				1												
6	3				3																	
6	3	2				1																
6	3				2																	
6	3			2																		
5	3				1	1			1													
5	3			1					1													
5	3				3																	
5	3			2																		
4	3				3																	
4	3				3																	
4	3			2														1				
4	3	2				1	1															
3	3			2																		
3	2			2			1															
3	3																					
3	3			2														1				
2	2	3					3															
2	3	3										1										

Sample	Mg-Illite	K-Illite	Ferrihydrite	Rectorite	Muscovite	Smithsonite	Gypsum	Paragonite	Gibbsite	FeMgChlorite	FeChlorite	Vermiculite	Goethite	Calcite	Chabazite	Phengite	Montmorillonite	Wavellite	Palygorskite	Tourmaline	Hematite	Heulandite
2		3	3																3			
2	3			2														1				
1	2	3	3																3			
1	3	3	3																			
1	3			2		1																
1	3	3	2																			

8.2. Table V: Spectral measurements

Table V: Spectral measurements

Wavelength Scalar (nm)								
Sample	Al-OH	Mg-OH	Al-Fe-Mg	Fe-OH	ISM	CSM	Fe3t	Fe3i
1	2200.5	2345	2200.5		1.017		908.4	1.45
1	2199.6	2344.1	2199.6		1.007			
1	2203.7	2345.7	2203.7		1.029			
1	2200.6	2345.2	2200.6		1.021			
2	2203.1	2344.7	2203.1		1.234			
2	2199.4	2345.6	2199.4		1.026			
2	2200.8	2345.7	2200.8		1.006			
3	2199.3	2345.5	2199.3		1.056			
3	2200.5	2345.7	2200.5		1.066			
3	2200.9	2346	2200.9		1.023			
3	2198.8	2343.9	2198.8		1.075			
4	2204.5	2349.5	2204.5		1.016			
4	2205	2345.6	2205		1.013			
4	2199.7	2344	2199.7		1.047			
4	2204.49	2342.1	2204.9		1.021			
5	2204.3	2345.1	2204.3		1.048	2.873		
5	2208.4	2345.9	2208.4		1.018			
5	2205	2347	2205		1.039			
5	2204.4	2351.5	2204.4		1.043	2.851		
6	2208.8	2346.4	2208.8		1.036			
6	2209	2349.1	2209		1.028			
6	2204.7	2349	2204.7		1.029			
6	2207.5	2345.9	2207.5		1.067			
7	2205.1	2347	2205.1		1.024			
7	2205	2346.6	2205		1.026			
7	2209.2	2348.7	2209.2	2247.2	1.045	2.866		
7	2205.4	2351	2205.4		1.044	2.856		
8	2204.8	2345.3	2204.8		1.037			
8	2206.6	2345.8	2206.6		1.033			
8	2204.9	2347.6	2204.9		1.038			
8	2205.9	2350.5	2205.9		1.019			
9	2209.1	2346.2	2209.1		1.037	2.871		
9	2209.2	2348.7	2209.2		1.056	2.897		
9	2208.7	2353	2208.7		1.037			
9	2202.9	2341.9	2202.9		1.007			

Sample	Al-OH	Mg-OH	Al-Fe-Mg	Fe-OH	ISM	CSM	Fe3t	Fe3i
10	2204.9	2347.8	2204.9		1.008			
10	2205.1	2347	2205.1		1.011			
10	2207	2346.8	2207		1.025			
10	2208.3	2347	2208.3		1.002			
11	2211	2349.1	2211		1.031			
11	2205.3	2347.1	2205.3		1.024			
11	2205.5	2350.3	2350.3		1.064			
11	2204.5	2350.7	2204.5		1.031	2.819		
12	2206.5	2347.1	2206.5		1.001			
12	2205.8	2345.3	2205.8		1.004			
12	2206.2	2346	2206.2		1.005			
12	2205.4	2351.8	2205.4		1.034	2.823		
13		2348.2	2348.2	2254	0.997	2.684		
13		2349.5	2349.5	2255.9	0.996	2.684		
13		2352.9	2352.9	2253.1	0.997	2.688		
13	2202.2	2343.8	2202.2		1.02			1.373
14		2355.8	2355.8	2253.4	1.015	2.738		
14		2357.4	2357.4	2254.2	1.012			
14		2357	2357		1.021			
14	2201.3	2341.3	2201.3		1.012			
15	2202.9	2346.7	2202.9		1.014			
15	2202.4	2345.6	2202.4		1.022			1.35
15	2202.2	2340.3	2202.2		1.027			
15	2203.3	2344.1	2203.3		1.009			
16								
16	2208	2346.8	2208	2246.5	1.112	3.013		
16	2206.1				1.2			
16	2205.9	2357.8	2205.9		1.161		918.6	1.342
17	2202.8	2343.8	2202.8		1.014			
17	2203.9	2342.6	2203.9		1.033	2.845		
17	2204.1	2343.2	2204.1		1.038			
17	2203	2344.8	2203					

9. Appendices

9.1. Appendix A: 2015 Annual well production by field from the Bow Island.

FIELD	YEAR	FMTN CODE	PROD ZONE	BBLS OIL	MCF GAS	REPORTED WELLS	REPORTED WELL DAYS
Amanda	2015	BI	Bow Island	0	13258	10	2608
Antelope Coulee	2015	BI	Bow Island	0	56	1	32
Arch Apex	2015	BI	Bow Island	0	75606	29	8276
Bear's Den	2015	BI	Bow Island	0	1203	1	365
Big Rock	2015	BI	Bow Island	0	31320	6	2170
Bradley	2015	BI	Bow Island	0	1066	1	355
Cut Bank	2015	BI	Bow Island	0	85862	21	7173
Devon	2015	BI	Bow Island	0	27408	21	5358
Devon, East	2015	BI	Bow Island	0	30972	10	3341
Devon, South Unit	2015	BI	Bow Island	0	2168	7	2555
Dry Fork	2015	BI	Bow Island	0	8988	6	1582
Dunkirk, North	2015	BI	Bow Island	0	38287	26	8441
Eagle Spring	2015	BI	Bow Island	0	2787	4	818
Ethridge	2015	BI	Bow Island	0	3708	1	362
Ethridge, North	2015	BI	Bow Island	0	3544	4	1314
Fitzpatrick Lake	2015	BI	Bow Island	0	27705	9	3006
Flat Coulee	2015	BI	Bow Island	0	1580	2	486
Fort Conrad	2015	BI	Bow Island	0	3026	6	1071
Fred & George Creek	2015	BI	Bow Island	0	22310	3	1054
Galata	2015	BI	Bow Island	0	6744	4	946
Grandview	2015	BI	Bow Island	0	19550	6	2084
Hardpan	2015	BI	Bow Island	0	5799	7	781
Haystack Butte	2015	BI	Bow Island	0	19148	10	3650
Haystack Butte, West	2015	BI	Bow Island	0	25088	9	3163
Keith Area	2015	BI	Bow Island	0	162	1	31
Keith, East	2015	BI	Bow Island	0	118218	17	5658
Kevin Southwest	2015	BI	Bow Island	0	2463	1	334
Kevin Sunburst-Bow Island	2015	BI	Bow Island	0	20804	10	3269
Kevin, East Bow Island Gas	2015	BI	Bow Island	0	11398	6	2190
Kevin, East Gas	2015	BI	Bow Island	0	15766	2	730
Kevin-Sunburst	2015	BI	Bow Island	0	44849	34	11616
Kicking Horse	2015	BI	Bow Island	0	54272	11	3956
Lake Francis	2015	BI	Bow Island	0	47731	24	7344

FIELD	YEAR	FMTN CODE	PROD ZONE	BBLS OIL	MCF GAS	REPORTED WELLS	REPORTED WELL DAYS
Ledger	2015	BI	Bow Island	0	69078	36	9790
Little Rock	2015	BI	Bow Island	0	9349	1	359
Marias River	2015	BI	Bow Island	0	8147	10	2060
Middle Butte	2015	BI	Bow Island	0	14332	3	1073
Miners Coulee	2015	BI	Bow Island	0	19827	8	2647
Mt. Lilly	2015	BI	Bow Island	0	2073	1	329
O'Briens Coulee	2015	BI	Bow Island	0	35310	7	2229
Old Shelby	2015	BI	Bow Island	0	19224	8	2212
Police Coulee	2015	BI	Bow Island	0	31808	10	3548
Prairie Dell	2015	BI	Bow Island	0	18081	7	2301
Sage Creek	2015	BI	Bow Island	0	3512	1	365
Shelby, East	2015	BI	Bow Island	0	4888	1	365
Snoose Coulee	2015	BI	Bow Island	980	22271	11	4015
Strawberry Creek Area	2015	BI	Bow Island	0	42	1	210
Tiber	2015	BI	Bow Island	0	1222	2	517
Tiber, East	2015	BI	Bow Island	0	18385	11	3769
Trail Creek	2015	BI	Bow Island	0	17688	5	1750
Utopia	2015	BI	Bow Island	0	16656	4	1367
West Butte	2015	BI	Bow Island	0	14259	3	994
West Butte Shallow Gas	2015	BI	Bow Island	0	3748	2	517
Whitlash	2015	BI	Bow Island	468	212098	31	10347
Williams	2015	BI	Bow Island	0	45087	18	6268
Willow Ridge	2015	BI	Bow Island	0	5548	6	1908
Willow Ridge, West	2015	BI	Bow Island	0	4979	3	701

9.2. Appendix B: Formation Elevations Above Sea-level in Feet by API.

Depths to each horizon in each well. Depths are feet below KB (Kelly bushing).

Well API	KB	Bow Island top	Lower Bow Island	Middle Bow Island	Skull Creek Shale
25041050810000	3202	2159	2343	2205	2434
25041050820000	3113	2172	2365	2228	2464
25041051070000	3119	2297	2464	2359	2562
25041051660000	3120	2211	2395	2280	2480
25041051700000	3204	2152	2333	2198	2418
25041051740000	3104	2208	2392	2270	2533
25041051750000	3162	2264	2431	2343	2516
25041051810000	3175	2254	2438	2320	2585
25041211770000	3170	2182	2369	2228	2464
25041212580000	3199	0	2592	0	0
25041213110000	3211	2096	2290	2156	2388
25041213890000	3103	2080	2280	2139	2408
25041213980000	3147	2267	2428	2333	2546
25041214190000	3236	2369	2507	2434	2628
25041214530000	3144	2280	2438	2352	2556
25041216340000	3172	2087	2264	2129	2352
25041216350000	3180	2156	2346	2205	2441
25041216840000	3312	2369	2533	2457	2657
25041216950000	3274	2372	2516	2438	2635
25041217030000	3142	2192	2375	2254	2513
25041217050000	3158	2244	2425	2316	2513
25041217080000	3241	2365	2539	2434	2631
25041217840000	3263	2379	2536	2421	2664
25041218180000	3080	2139	2333	2205	2470
25041218500000	3140	2182	2379	2238	0
25041219150000	3194	2192	2375	2231	2451
25041219220000	3105	2208	2395	2277	2477
25041219410000	3087	2073	2280	2139	2408
25041219420000	3100	2287	2461	2339	2536
25041219540000	3140	2260	2418	2326	2530
25041219940000	3195	0	0	0	0
25041219950000	3227	2146	2333	2201	2415

25041220130000	3177	2169	2320	2228	0
Well API	KB	Bow Island top	Lower Bow Island	Middle Bow Island	Skull Creek Shale
25041220180000	3117	2169	2362	2218	2457
25041220200000	3151	2329	2464	2375	2579
25041220310000	3198	2162	2356	2218	2438
25041220420000	3231	2369	2490	2415	2615
25041220450000	3233	2372	2539	2454	2648
25041220910000	3181	2116	2316	2178	2411
25041220920000	0	2333	2523	2425	2644
25041220930000	3126	2260	2428	2333	2605
25041221070000	3109	0	0	0	0
25041221310000	3122	2303	2480	2365	2559
25041221480000	3133	2283	2444	2349	2533
25041221490000	3111	0	0	0	0
25041221880000	3152	2297	2484	2365	2556
25041222600000	3175	2369	2546	2421	2641
25041222900000	3197	2306	2484	2372	2562
25041223290000	3134	2241	2385	2293	2480
25041600050000	3098	2162	2346	2208	0
25051050510000	3396	1591	1821	1631	1893
25051050520000	3290	2113	2277	2149	2343
25051050570000	0	0	0	0	0
25051050590000	3648	0	0	0	0
25051050600000	3624	0	0	0	0
25051050610000	3660	1683	1834	1713	1893
25051050660000	3612	0	0	0	0
25051050670000	3627	1414	1634	1444	1732
25051050680000	3654	1447	1598	1476	1667
25051050720000	3679	0	0	0	0
25051050750000	3306	2057	2267	2113	2349
25051050760000	3703	0	0	0	0
25051050770000	3338	2073	2231	2142	2365
25051050790000	3299	2083	2251	2136	2320
25051050810000	3746	0	0	0	0
25051050830000	3310	2087	2280	2129	0
25051050840000	3950	1591	1795	1614	1909
25051050850000	0	1713	1870	1749	1998
25051050860000	4111	0	0	0	0
25051050870000	3990	0	0	0	0

25051050880000	3900	0	0	0	0
Well API	KB	Bow Island top	Lower Bow Island	Middle Bow Island	Skull Creek Shale
25051050890000	4118	1696	1798	1713	1903
25051050910000	4104	1683	1814	1722	1913
25051050930000	4107	0	0	0	0
25051050950000	3948	0	0	0	0
25051050970000	4151	1827	1873	1847	2011
25051050990000	4434	0	0	0	0
25051051000000	4288	1640	1749	1680	1847
25051051010000	0	0	0	0	0
25051051020000	3450	2116	2293	2159	2408
25051051030000	3602	0	0	0	0
25051051040000	3917	1955	2106	1985	2205
25051051050000	3625	1781	1939	1821	2034
25051051060000	3745	1791	1978	1834	2024
25051051070000	3645	0	1969	0	2018
25051051080000	4282	1467	1654	1512	1736
25051051090000	3592	1978	2136	2018	2238
25051051100000	4452	1322	1490	1352	1601
25051051110000	4318	1207	1385	1247	1555
25051051120000	3433	1752	1929	1788	2037
25051051130000	3912	1581	1749	1617	1857
25051051140000	3350	2228	2405	2277	2543
25051051150000	3461	1755	1939	1798	2051
25051051160000	3817	1808	1969	1847	2080
25051051170000	3480	1795	1982	1841	2090
25051051170001	3480	0	0	0	0
25051051180001	0	1759	1946	1811	2051
25051051200000	3457	1788	1972	1831	2083
25051051240000	3442	1762	1939	1804	2051
25051051260000	4110	1358	1493	1398	1565
25051051340000	3199	2146	2323	2195	2438
25051051350000	0	2080	2267	2133	2402
25051051390000	3456	1969	2156	2018	2270
25051051420000	3806	1506	1663	1545	1752
25051051430000	3127	2090	2270	2146	2411
25051051460000	3791	1568	1732	1608	1834
25051051470000	3871	1640	1804	1677	1906
25051051480000	4039	1490	1627	1526	1709

25051051500000	3816	1722	1886	1759	1988
Well API	KB	Bow Island top	Lower Bow Island	Middle Bow Island	Skull Creek Shale
25051051510000	3898	1526	1690	1562	1791
25051051520000	3732	1617	1788	1657	1886
25051051520001	3732	0	0	0	0
25051051530000	3545	2185	2349	2224	2497
25051051540000	4124	925	1070	981	1168
25051051580000	4150	1181	1322	1247	1434
25051051590000	4154	1437	1578	1496	1690
25051051630000	3643	1972	2133	2011	2218
25051051730000	3554	1923	2077	1969	2165
25051051740000	4019	1001	1135	1063	1260
25051051750000	0	2014	2182	2054	2303
25051051780000	0	1106	1243	1175	1375
25051051790000	3970	0	0	0	0
25051051820000	3669	1519	1677	1562	1785
25051051830000	3404	2119	2290	2159	2415
25051051840000	3338	0	0	0	0
25051051850000	3490	1854	2021	1896	2110
25051051900000	0	1604	1752	1663	1864
25051051920000	3415	1801	1975	1854	2090
25051051930000	0	0	0	0	0
25051052020000	4094	2106	2257	2149	2356
25051052070000	3317	2231	2395	2274	2507
25051052090000	3890	876	1024	938	1125
25051052100000	3906	1821	1972	1867	2083
25051052140000	3296	899	1043	965	1142
25051052180000	0	1129	1273	1201	1385
25051052190000	3409	2178	2352	2224	2454
25051052210000	3508	2018	2188	2070	2333
25051052220000	4002	1132	1273	1207	1378
25051052240000	3581	2018	2238	2123	2306
25051052260000	3850	1161	1329	1240	1480
25051052270000	0	0	0	0	0
25051052280000	3747	1637	1795	1683	1913
25051052290000	3900	1270	1424	1342	1594
25051052310000	0	1588	1713	1624	1837
25051052320000	3655	1818	1982	1864	2093
25051052340000	3848	1155	1371	1227	1457

25051052420000	4124	1818	1962	1886	2067
Well API	KB	Bow Island top	Lower Bow Island	Middle Bow Island	Skull Creek Shale
25051052430000	3918	1985	2123	2024	2228
25051052450000	4035	2156	2303	2195	2408
25051052470000	4032	2047	2195	2090	2303
25051052490000	3854	1962	2110	1998	2221
25051052500000	3960	0	0	0	0
25051052520000	3648	0	0	0	0
25051052530000	4070	2247	2392	2287	2497
25051052540000	3940	2090	2234	2129	2333
25051052550000	3934	1870	2011	1932	2119
25051052560000	3754	1818	1985	1867	2096
25051052570000	3724	0	0	0	0
25051052590000	3466	0	0	0	0
25051052660000	3699	2001	2162	2044	2280
25051052670000	3983	2018	2159	2077	2267
25051052680000	3510	2172	2339	2215	2451
25051052690000	3971	2241	2379	2306	2484
25051052710000	3703	2008	2165	2051	2287
25051052720000	0	0	0	0	0
25051052730000	3572	1788	1949	1831	2047
25051052740000	3773	1883	0	1926	2126
25051052750000	3913	1903	2044	1962	2152
25051052760000	0	2395	2536	2457	2625
25051052770000	3754	1831	1985	1877	2103
25051052780000	3958	0	0	0	0
25051052790000	3950	2119	2260	2185	2369
25051052820000	3804	1873	0	1913	2136
25051052840000	3746	1339	1453	1375	1578
25051052850000	3922	0	0	0	0
25051052870000	0	0	0	0	0
25051052890000	0	0	0	0	0
25051052910000	4036	0	0	0	0
25051052930000	0	0	0	0	0
25051052950000	3697	2064	2224	2103	2343
25051052960000	3686	2028	2169	2064	2283
25051052970000	3720	2028	2182	2070	2297
25051052980000	3810	0	2067	0	2182
25051052990000	3767	1877	2028	1916	2142

25051053000000	3744	1926	2090	1972	2205
Well API	KB	Bow Island top	Lower Bow Island	Middle Bow Island	Skull Creek Shale
25051053010000	3758	1877	2031	1923	2149
25051053020000	3674	2073	2238	2116	2356
25051053030000	4013	0	0	0	0
25051053040000	3729	0	0	0	0
25051053070000	0	1184	1348	1240	1437
25051053080000	3766	1939	2093	1985	2208
25051053090000	3788	1657	1778	1696	1903
25051053100000	0	0	0	0	0
25051053110000	3777	1926	2080	1972	2188
25051053140000	3162	0	0	0	0
25051053150000	3650	1811	1926	1870	2041
25051053160000	3633	0	0	0	0
25051053160001	3625	0	0	0	0
25051053170000	3651	0	0	0	0
25051053180000	3692	0	0	0	0
25051053190000	3724	2011	2165	2054	2277
25051053200000	3639	2300	2467	2346	2582
25051053210000	3698	0	0	0	0
25051053220000	3704	0	0	0	0
25051053230000	3747	1923	2070	1962	2188
25051053240000	3775	1949	2106	1995	2224
25051053250000	3797	1982	2129	2028	2244
25051053260000	3767	1972	2123	2014	2241
25051053270000	3543	0	0	0	0
25051053280000	3759	2021	2178	2067	2283
25051053320000	3622	0	0	0	0
25051053330000	3716	2126	2280	2172	2385
25051053360000	3620	0	0	0	0
25051053370000	3625	0	0	0	0
25051053390000	0	2083	0	2126	2359
25051053410000	3457	0	0	0	0
25051053420000	3656	1716	1821	1749	1955
25051053450000	3616	0	0	0	0
25051053460000	3628	0	0	0	0
25051053470000	0	1896	2041	1952	2152
25051053490000	3616	0	0	0	0
25051053510000	3931	2031	2165	2096	2274

25051053540000	3678	1791	1900	1831	2037
Well API	KB	Bow Island top	Lower Bow Island	Middle Bow Island	Skull Creek Shale
25051053550000	4073	2119	2257	2185	2365
25051053560000	3664	1795	1903	1834	2044
25051053570000	3618	1785	1903	1827	2044
25051053580000	3655	1818	1929	1857	2067
25051053610000	3846	1982	2152	2021	2228
25051054150000	4052	0	0	0	0
25051054160000	4049	2349	2484	2415	2595
25051054170000	3691	1942	2106	1982	2221
25051054180000	3242	2149	2316	2198	2411
25051054210000	3554	1391	1617	1430	1709
25051054220000	3906	1969	2116	2031	2224
25051054230000	4172	1647	1791	1713	1903
25051054240000	3803	1870	2011	1909	2110
25051054250000	3725	1916	2077	1959	2195
25051054260000	3604	2054	2224	2100	2336
25051054270000	3289	2162	2326	2208	2418
25051054280000	3829	2175	2352	2215	2438
25051054290000	3742	1913	2080	1949	2162
25051054310000	3607	0	0	0	0
25051054340000	3820	1667	1906	1726	2060
25051054350000	3589	0	0	0	0
25051054360000	3766	0	0	0	0
25051054370000	3668	1811	1955	1847	2060
25051054380000	3702	1854	2001	1890	2100
25051054390000	3781	2165	2310	2208	2428
25051054400000	3270	2087	2260	2129	2362
25051054410000	3782	1929	2100	1965	2175
25051054430000	3846	0	0	0	0
25051054440000	3720	1503	1726	1535	1808
25051054450000	3326	2064	2247	2103	2339
25051054460000	3951	1670	1824	1703	1942
25051054470000	3570	0	0	0	0
25051054480000	3578	2146	2310	2185	2418
25051054490000	3666	1709	1932	1749	2024
25051054500000	4033	0	0	0	0
25051054510000	3623	1880	2037	1926	2136
25051054520000	3883	1955	2106	1998	2211

25051054530000	3554	0	0	0	0
Well API	KB	Bow Island top	Lower Bow Island	Middle Bow Island	Skull Creek Shale
25051054540000	3668	1719	1824	1752	1965
25051054550000	3625	0	0	0	0
25051054560000	3789	1552	1788	1601	1877
25051054580000	3759	1834	1991	1880	2113
25051054590000	3949	2123	2260	2185	2372
25051054600000	4024	2310	2451	2375	2559
25051054610000	4013	1942	2083	1982	2185
25051054630000	3653	1755	1896	1791	2001
25051054700000	3732	1988	2149	2028	2260
25051054720000	3870	1909	2051	1978	2126
25051054730000	3798	1522	1690	1565	1795
25051064750000	0	873	1040	955	1135
25051064770000	0	1591	1791	1667	1860
25051064800000	0	1125	1243	1165	1368
25051100110000	4233	636	778	705	886
25051210010000	3932	1654	1831	1693	1936
25051210020000	3588	0	0	0	0
25051210050000	3680	1998	2192	2044	2267
25051210060000	3636	1883	2070	1955	2172
25051210070000	3901	0	0	0	0
25051210080000	4179	1847	2001	1886	2100
25051210090000	3718	1854	2018	1890	2126
25051210100000	3310	2064	2270	2119	2395
25051210120000	3586	1955	2116	1991	2205
25051210130000	3585	2247	2408	2290	2523
25051210140000	3310	2201	2382	2254	2467
25051210150000	3689	1421	1604	1453	1699
25051210160000	3666	1519	1752	1572	1837
25051210170000	3898	2067	2218	2106	2320
25051210180000	3656	1742	1857	1785	1991
25051210200000	3696	1762	1923	1808	2008
25051210210000	3647	0	0	0	0
25051210230000	3677	1453	1634	1483	1729
25051210240000	4228	1955	2100	1995	2205
25051210250000	4140	0	0	0	0
25051210260000	3637	1975	2133	2008	2221
25051210270000	3757	1759	1919	1804	2087

25051210280000	3615	1670	1841	1696	1942
Well API	KB	Bow Island top	Lower Bow Island	Middle Bow Island	Skull Creek Shale
25051210290000	3585	1978	2152	2024	2260
25051210300000	3667	1696	1857	1729	1978
25051210310000	3636	1788	1949	1821	2014
25051210320000	3675	1768	1919	1808	2008
25051210330000	3678	1749	1906	1791	1991
25051210340000	3665	1647	1814	1693	1903
25051210370000	3569	1903	2067	1949	2152
25051210380000	3579	1913	2077	1959	2165
25051210390000	3606	2530	2694	2572	2802
25051210400000	3682	1788	1949	1837	2054
25051210410000	3738	1811	1972	1857	2083
25051210420000	3704	1749	1909	1795	2011
25051210430000	3706	1808	1975	1857	2077
25051210440000	3446	1808	1969	1847	2077
25051210450000	3523	1873	2037	1919	2126
25051210470000	3619	1952	2110	1998	2198
25051210490000	3664	1680	1837	1722	1942
25051210500000	3861	1594	1752	1637	1870
25051210510000	3999	1470	1614	1503	1703
25051210520000	3766	1640	1844	1703	1923
25051210530000	4051	1175	1496	1204	1585
25051210540000	3541	1841	2001	1886	2087
25051210550000	3058	2096	2238	2129	2343
25051210560000	3995	1765	1900	1804	1998
25051210570000	3412	2011	2188	2057	2280
25051210580000	0	1526	1739	1555	1834
25051210590000	3655	1401	1581	1427	1670
25051210600000	3688	1834	2001	1880	2106
25051210630000	4385	1125	1230	1158	1352
25051210640000	3916	1512	1663	1552	1768
25051210650000	4110	955	1106	994	1211
25051210660000	3938	1749	1903	1788	2001
25051210680000	4094	886	1040	925	1138
25051210690000	4137	745	899	784	1001
25051210700000	4190	1867	2008	1906	2110
25051210710000	4196	1575	1775	1594	1926
25051210720000	3942	1621	1759	1647	1860

25051210730000	3539	1893	2041	1942	2129
Well API	KB	Bow Island top	Lower Bow Island	Middle Bow Island	Skull Creek Shale
25051210740000	3708	2087	2247	2133	2356
25051210750000	3614	1821	1978	1857	2087
25051210760000	3637	1713	1877	1759	1991
25051210780000	4125	850	1001	892	1093
25051210790000	3995	2152	2300	2224	2411
25051210800000	3988	2028	2169	2067	2274
25051210810000	3983	1247	1404	1286	1486
25051210820000	4087	719	883	781	981
25051210830000	4173	1099	1240	1138	1329
25051210840000	3819	1969	2116	2011	2224
25051210850000	3996	1302	1460	1348	1572
25051210860000	3997	948	1106	991	1191
25051210870000	4131	906	1053	945	1155
25051210880000	3629	1745	1906	1791	2005
25051210890000	3600	2093	2254	2139	2365
25051210900000	3802	1693	1857	1729	1959
25051210910000	3640	1381	1506	1411	1663
25051210920000	3879	1362	1516	1404	1617
25051210930000	4071	1509	1640	1558	1722
25051210940000	3422	0	0	0	0
25051210950000	3574	0	0	0	0
25051210960000	3309	2067	2267	2126	2356
25051210970000	0	2172	2356	2224	2493
25051210980000	3249	2178	2362	2231	2533
25051210990000	3490	2149	2320	2192	2421
25051211000000	3836	0	0	0	0
25051211010000	3395	2142	2352	2211	2461
25051211020000	4399	0	0	0	0
25051211050000	3722	1460	1683	1490	1739
25051211060000	3818	1588	1824	1637	1880
25051211070000	3315	2057	2260	2113	2362
25051211080000	4127	0	1798	0	0
25051211090000	0	2126	2320	2192	2428
25051211100000	3220	2149	2329	2205	2464
25051211110000	3929	1667	1827	1703	1932
25051211130000	3558	2014	2172	2054	2290
25051211140000	3723	0	2513	0	0

25051211150000	3402	2064	2260	2119	2362
Well API	KB	Bow Island top	Lower Bow Island	Middle Bow Island	Skull Creek Shale
25051211160000	4287	1722	1860	1778	1962
25051211170000	3361	2070	2277	2126	2405
25051211180000	4241	906	1073	958	1165
25051211190000	3298	2208	2385	2257	2507
25051211200000	3455	2064	2234	2103	2326
25051211210000	4099	761	935	807	1024
25051211220000	3573	2260	2418	2297	2533
25051211230000	4019	1670	1867	1709	1962
25051211240000	0	669	837	738	942
25051211250000	3333	2041	2267	2116	2372
25051211260000	3360	2077	2277	2142	2392
25051211270000	3770	0	0	0	0
25051211280000	3348	2080	2251	2136	2379
25051211310000	3600	0	0	0	0
25051211330000	3297	2195	2362	2247	2510
25051211340000	3304	2034	2270	2096	2372
25051211350000	3541	2100	2260	2139	2398
25051211360000	3515	1919	2083	1965	2201
25051211370000	4376	0	0	0	0
25051211380000	3684	0	0	0	0
25051211390000	3355	1870	2047	1919	2126
25051211400000	3613	1703	1919	1739	2014
25051211410000	4460	1398	1499	1430	1621
25051211420000	4124	1047	1211	1099	1306
25051211430000	4110	1463	1588	1509	1677
25051211440000	3766	0	0	0	0
25051211450000	4005	1601	1841	1657	1982
25051211460000	3473	2116	2293	2156	2402
25051211490000	3303	2034	2231	2077	2336
25051211500000	3945	0	0	0	0
25051211510000	3390	2434	2579	2493	2687
25051211520000	3401	2136	2316	2178	2388
25051211530000	3448	0	0	0	0
25051211540000	3355	2067	2260	2126	2362
25051211550000	3420	1903	2021	1972	2090
25051211560000	3497	0	0	0	0
25051211600000	3986	1670	1798	1729	1913

25051211610000	3532	1706	1867	1749	1955
Well API	KB	Bow Island top	Lower Bow Island	Middle Bow Island	Skull Creek Shale
25051211620000	3538	2024	2192	2067	2316
25051211630000	3665	1690	1798	1722	1932
25051211660000	3411	2024	2201	2073	2339
25051211670000	3500	1903	2028	1978	2093
25051211690000	3547	2119	2300	2175	2438
25051211710000	3353	2283	2457	2346	2625
25051211720000	3392	1535	1693	1581	1788
25051211740000	3668	0	2490	0	0
25051211750000	3821	0	2710	0	0
25051211770000	3544	0	0	0	0
25051211780000	3677	1663	1778	1699	1913
25051211790000	3738	1683	1827	1742	1932
25051211800000	4085	1407	1539	1440	1624
25051211820000	3320	2116	2293	2162	2434
25051211830000	0	0	0	0	0
25051211840000	3724	0	0	0	0
25051211850000	3718	1719	1860	1749	1962
25051211860000	4221	1490	1631	1529	1755
25051211870000	3702	1752	1900	1785	2005
25051211880000	3711	1660	1775	1699	1909
25051211890000	3414	2142	2316	2185	2457
25051211900000	3733	1680	1827	1713	1926
25051211910000	3398	2106	2333	2156	2425
25051211920000	3345	2359	2503	2382	2608
25051211940000	3460	1411	1624	1440	1719
25051211960000	3655	1673	1788	1719	1923
25051212000000	4262	988	1155	1020	1263
25051212010000	0	0	2133	0	0
25051212020000	3802	1745	1903	1801	2011
25051212040000	3365	2208	2379	2254	2543
25051212050000	3550	1959	2129	0	2224
25051212060000	3338	2192	2356	0	2480
25051212070000	3827	1890	2067	1929	2142
25051212080000	3945	0	0	0	0
25051212100000	3350	2395	2556	2434	2694
25051212110000	3436	1988	2169	2028	2287
25051212120000	3523	2110	2280	2159	2418

25051212130000	0	2162	2343	2208	2448
Well API	KB	Bow Island top	Lower Bow Island	Middle Bow Island	Skull Creek Shale
25051212150000	3323	2411	2556	2480	2687
25051212160000	4698	440	604	472	673
25051212170000	3982	0	0	0	0
25051212180000	3692	1847	2008	1886	2093
25051212200000	3488	2185	2352	2234	2438
25051212220000	4045	2142	2283	2205	2392
25051212230000	3265	2359	2500	2431	2628
25051212240000	3495	2260	2431	2303	2579
25051212260000	3612	1575	1739	1604	1788
25051212280000	3607	0	0	0	0
25051212300000	3927	1132	1273	1198	1378
25051212310000	3800	1191	1322	1253	1437
25051212320000	3912	0	0	0	0
25051212330000	3907	2218	2356	2283	2464
25051212340000	4027	1260	1404	1352	1506
25051212350000	3508	2192	2365	2238	2510
25051212360000	3335	2251	2418	2320	2566
25051212370000	3695	1791	1978	1831	2090
25051212380000	3528	1867	2034	1913	2123
25051212390000	3593	2241	2398	2277	2503
25051212400000	4068	2251	2395	2320	2503
25051212410000	3529	2116	2290	2159	2408
25051212420000	4119	2096	2238	2162	2346
25051212430000	0	2139	2280	2198	2388
25051212440000	0	1427	1549	1480	1640
25051212450000	3328	2149	2323	2208	0
25051212460000	3932	873	1014	938	1122
25051212470000	3733	1749	1880	1788	1965
25051212480000	4091	2185	2323	2244	2434
25051212500000	3488	2175	2349	2215	2461
25051212510000	3451	0	0	0	0
25051212520000	0	2129	2290	2169	2402
25051212530000	3934	1001	1152	1066	1253
25051212540000	4300	774	919	846	1007
25051212550000	4047	1493	1634	1562	1742
25051212570000	3915	2024	2175	2093	2280
25051212580000	3313	2188	2382	2238	2530

25051212590000	3848	2188	2372	2247	2464
Well API	KB	Bow Island top	Lower Bow Island	Middle Bow Island	Skull Creek Shale
25051212600000	3578	0	0	0	0
25051212610000	0	0	0	0	0
25051212620000	3306	2159	2333	2208	2526
25051212640000	3553	0	0	0	0
25051212650000	3366	2234	2405	2277	2549
25051212660000	3338	2100	2283	2142	2323
25051212680000	4604	440	610	472	679
25051212690000	3635	2316	2477	2359	2585
25051212700000	3449	2073	2244	2119	2382
25051212710000	3367	2077	2267	2133	2369
25051212720000	3291	2201	2372	2247	2510
25051212730000	3903	1991	2139	2051	2247
25051212740000	3229	2156	2339	2205	2477
25051212750000	3886	0	0	0	0
25051212760000	3270	2175	2283	2231	2385
25051212780000	3921	2077	2218	2139	2329
25051212790000	3450	2188	2365	2231	2487
25051212800000	3333	2077	2247	2139	2402
25051212810000	3519	2165	2343	2205	2467
25051212820000	3503	2087	2264	2133	2402
25051212830000	3353	2159	2336	2201	2428
25051212840000	3356	1867	2044	1923	2119
25051212860000	3884	0	0	0	0
25051212870000	3914	1345	1486	1404	1594
25051212880000	3411	2005	2136	2093	2339
25051212890000	3639	2270	2428	2310	2530
25051212900000	3365	2034	2228	2096	2329
25051212910000	3409	2096	2303	2159	2431
25051212920000	3904	0	0	0	0
25051212930000	4186	1273	1460	1302	0
25051212940000	3605	0	0	0	0
25051212950000	3828	2024	2175	2067	2274
25051212960000	3329	2152	2352	2215	2467
25051212970000	4028	1467	1617	1503	1742
25051212990000	3903	2156	2297	2198	2405
25051213000000	3514	2142	2313	2182	2402
25051213010000	4042	1194	1381	1224	0

25051213020000	3371	2067	2274	2129	2379
Well API	KB	Bow Island top	Lower Bow Island	Middle Bow Island	Skull Creek Shale
25051213030000	3344	2320	2448	2369	2589
25051213040000	4080	1755	1886	1818	1985
25051213050000	4469	1224	1407	1253	0
25051213060000	3340	2119	2323	2172	2428
25051213070000	3615	0	0	0	0
25051213080000	4126	1749	1926	1788	2047
25051213090000	3988	1322	1437	1257	0
25051213100000	3452	2041	2215	2083	2306
25051213110000	3884	0	0	0	0
25051213120000	3380	2169	2336	2208	2464
25051213130000	4111	2165	2306	2228	2415
25051213140000	3289	2159	2343	2218	2477
25051213160000	3867	0	0	0	0
25051213170000	4008	0	0	0	0
25051213180000	4011	1368	1490	1424	1588
25051213190000	4090	2106	2260	2146	0
25051213200000	3741	1122	1240	1161	1378
25051213230000	3916	1250	1391	1312	1499
25051213240000	3341	2182	2382	2257	2493
25051213250000	3525	2159	2343	2218	2487
25051213260000	4442	554	646	581	761
25051213280000	3924	2054	2195	2110	2297
25051213290000	4133	1319	1460	1352	1562
25051213300000	3912	1417	1519	1480	1667
25051213310000	3873	0	0	0	0
25051213320000	3898	1634	1857	1677	1926
25051213340000	3819	1680	1919	1739	2067
25051213350000	3802	1772	2018	1827	2126
25051213380000	4001	1368	1555	1404	1644
25051213390000	4050	1201	1407	1234	1490
25051213400000	3844	1640	1883	1703	2028
25051213410000	3874	0	2267	0	0
25051213430000	3729	1555	1759	1624	1831
25051213440000	3587	2470	2635	2516	2749
25051213450000	3526	2382	2552	2425	2667
25051213460000	3498	0	0	0	0
25051213470000	3411	2142	2375	2211	2461

25051213480000	4149	1480	1614	1539	1719
Well API	KB	Bow Island top	Lower Bow Island	Middle Bow Island	Skull Creek Shale
25051213490000	3161	2077	2260	2149	2405
25051213500000	3833	1781	2028	1844	2146
25051213530000	3747	1624	1785	1670	1906
25051213550000	3921	1621	1772	1696	1877
25051213590000	3894	1942	2087	2011	2198
25051213600000	0	2188	2336	2228	2444
25051213610000	3361	2051	2228	2096	2359
25051213620000	4327	597	679	623	781
25051213640000	3704	1463	1686	1526	1765
25051213650000	4074	0	0	0	0
25051213660000	3327	1591	1818	1644	1877
25051213670000	4004	922	1047	974	1155
25051213680000	4008	1512	1644	1562	1726
25051213690000	3627	1545	1709	1572	1759
25051213700000	3922	0	0	0	0
25051213720000	4161	1165	1352	1188	1430
25051213730000	3522	2402	2513	2444	2526
25051213740000	4022	1460	1667	1473	1729
25051213750000	3472	2228	2365	2264	2454
25051213760000	3373	2231	2392	2270	2503
25051213770000	3392	1837	1952	1909	2021
25051213780000	3479	2290	2454	2333	2562
25051213790000	3687	1486	1703	1539	1781
25051213800000	3591	2503	2595	2562	2635
25051213810000	3976	1631	1778	1683	1883
25051213830000	3391	2093	2336	2152	2405
25051213840000	3717	1506	1657	1568	1752
25051213850000	3485	2260	2454	2303	2474
25051213860000	3463	2192	2362	2231	2375
25051213870000	3411	1877	1995	1949	2064
25051213880000	3672	1722	1939	1755	2034
25051213890000	4031	1404	1555	1453	0
25051213900000	3340	2054	2195	2113	2356
25051213920000	3487	2408	2589	2461	2605
25051213930000	3310	2205	2320	2257	2448
25051213950000	3623	2438	2556	2480	2605
25051213970000	3274	2224	2395	2277	2464

25051213980000	3319	2133	2310	2178	2448
Well API	KB	Bow Island top	Lower Bow Island	Middle Bow Island	Skull Creek Shale
25051213990000	3795	2231	2379	2274	2477
25051214000000	3253	0	0	0	0
25051214010000	0	2162	2300	0	2467
25051214020000	3201	2178	2300	0	2493
25051214030000	4094	0	0	0	0
25051214040000	3395	2303	2408	2346	2425
25051214050000	3725	1483	1699	1516	1755
25051214070000	3441	2379	2539	2428	2638
25051214080000	3235	2165	2346	2218	2513
25051214090000	3291	2260	2425	2306	2562
25051214100000	3312	2303	2454	2339	2539
25051214110000	3361	2339	2464	2395	2549
25051214120000	0	0	0	0	0
25051214130000	3371	2297	2418	2346	2530
25051214140000	3638	0	0	0	0
25051214180000	3742	1496	1713	1558	1791
25051214190000	3372	2198	2333	2241	2457
25051214200000	3204	2195	2339	2228	2392
25051214210000	3231	2172	2326	2224	2405
25051214220000	3271	2129	2306	2201	0
25051214260000	3298	2205	2365	2257	2549
25051214270000	3145	2096	2260	2152	0
25051214280000	3095	2080	2234	2142	2382
25051214290000	3150	2106	2290	2165	2457
25051214330000	4183	1483	1660	1519	1732
25051214380000	3385	2356	2477	2388	2572
25051214390000	0	2083	2274	2133	2382
25051214410000	4145	1378	1512	1427	1604
25051214420000	3866	1670	1837	1713	1942
25051214430000	3306	2156	2392	2260	2493
25051214440000	3272	2231	2425	2297	2582
25051214450000	3311	2028	2224	2080	2310
25051214480000	3409	0	0	0	0
25051214490000	3377	2070	2313	2129	2408
25051214500000	3502	1381	1526	1417	1657
25051214510000	3466	2362	2480	2398	2520
25051214520000	3521	2434	2507	2464	2467

25051214530000	3485	2247	0	2303	0
Well API	KB	Bow Island top	Lower Bow Island	Middle Bow Island	Skull Creek Shale
25051214580000	0	1444	1581	1496	1686
25051214630000	3921	2001	2146	2070	2247
25051214640000	3778	1657	1834	1706	1939
25051214650000	3658	1709	1824	1759	1949
25051214660000	3677	1713	1860	1752	1952
25051214700000	3453	2431	2559	2480	2628
25051214720000	3363	2323	2490	2385	2566
25051214730000	4153	1299	1440	1332	1581
25051214740000	3462	0	0	0	0
25051214750000	3359	1886	2021	1969	2083
25051214760000	3438	0	2205	0	0
25051214770000	3314	2041	2247	2113	2352
25051214780000	3377	2083	2251	2119	2339
25051214790000	3428	0	0	0	0
25051214800000	3211	1939	2119	1978	2211
25051214810000	3480	1969	2152	2014	2264
25051214820000	3360	2100	2228	2136	0
25051214860000	3501	1978	2198	2037	2326
25051214870000	0	2011	2231	2090	2264
25051214880000	3341	2064	2221	2123	2310
25051214890000	0	1637	1795	1673	1847
25051214920000	3301	2041	0	2103	0
25051214930000	3449	2044	2257	2106	2362
25051214940000	3729	1273	1371	1329	1499
25051214950000	3694	0	1726	1663	1811
25051214960000	4020	1473	1598	1509	1670
25051214970000	3553	0	0	0	0
25051214980000	0	2133	2293	2205	2398
25051214990000	3732	1499	1670	1562	1739
25051215000000	3831	1562	1791	1608	1837
25051215010000	3662	0	0	0	0
25051215020000	3792	1273	1371	1329	1499
25051215030000	3738	0	0	0	0
25051215050000	3316	2067	2254	2116	2303
25051215070000	3307	2014	2169	2103	2283
25051215080000	3329	2054	2247	2119	2303
25051215090000	3288	2064	2198	2123	2320

25051215110000	3310	2054	2228	2110	2313
Well API	KB	Bow Island top	Lower Bow Island	Middle Bow Island	Skull Creek Shale
25051215140000	0	2024	2156	2090	2254
25051215150000	3937	2051	2152	2123	2254
25051215190000	3898	1775	2018	1827	2139
25051215230000	0	0	0	0	0
25051215240000	3410	0	0	0	0
25051215250000	3889	0	0	0	0
25051215260000	3890	0	0	0	0
25051215270000	3341	2047	2211	2119	2306
25051215280000	3342	2077	2287	2136	2388
25051215310000	0	2080	2238	2139	2349
25051215320000	3536	1296	1522	1325	1594
25051215360000	3717	0	0	0	0
25051215440000	3641	0	0	0	0
25051215460000	0	1362	1519	1430	1608
25051215470000	3672	2001	2175	2057	2290
25051215480000	4163	0	0	0	0
25051215490000	3558	2156	2326	2208	2431
25051215500000	0	2139	2313	2192	2411
25051215510000	4118	1575	1690	1627	1811
25051215520000	3357	2067	2244	2106	2349
25051215530000	0	2077	2254	2116	2352
25051215540000	0	2057	2241	2106	2336
25051215550000	0	0	0	0	0
25051215560000	0	0	0	0	0
25051215570000	3290	2139	2352	2234	2470
25051215580000	3629	0	0	0	0
25051215620000	3833	2228	2362	2280	2441
25051215680000	0	2100	2329	2178	2438
25051215690000	3888	1788	2028	1841	2139
25051215750000	3516	1952	2152	2011	2293
25051215760000	4061	0	0	0	0
25051215770000	3870	2165	2303	2218	2382
25051215780000	3470	1860	2018	1909	2152
25051215790000	0	1831	1952	1916	2018
25051215820000	3880	1276	1375	1329	1506
25051215850000	3944	1627	1781	1683	1886
25051215930000	0	0	0	0	0

25051215940000	3960	1532	1703	1588	1788
Well API	KB	Bow Island top	Lower Bow Island	Middle Bow Island	Skull Creek Shale
25051216050000	3585	2326	2503	2369	2595
25051216060000	3603	0	0	0	0
25051216070000	3762	1565	1726	1624	1778
25051216110000	4044	1214	1335	1270	1430
25051216130000	3469	1962	2156	2008	2251
25051216140000	3443	1962	2139	2005	0
25051216150000	3800	1781	2034	1847	2142
25051216170000	4116	0	0	0	0
25051216190000	3237	2241	2369	2297	2490
25051216220000	3881	0	0	0	0
25051216240000	3991	2346	2503	2408	2585
25051216250000	3563	0	0	0	0
25051216270000	3332	1627	2051	1680	2136
25051216290000	3572	2103	2260	2142	2290
25051216320000	3952	1660	1818	1696	1896
25051216360000	0	1424	1608	1460	1647
25051216370000	0	2067	2169	2156	2369
25051216380000	4227	1411	1512	1460	1621
25051216390000	4029	978	1142	1047	1260
25051216410000	3820	2188	2372	2238	2451
25051216430000	3648	1434	1611	1460	1634
25051216460000	3825	0	0	0	2051
25051216480000	4306	571	741	600	814
25051216540000	3838	1772	2024	1827	2133
25051216560000	3791	1654	1880	1690	1946
25051216570000	4048	2044	2185	2087	2293
25051216580000	4061	1490	1644	1532	1742
25051216590000	3512	1991	2260	2110	2365
25051216600000	3758	2077	2251	2113	2346
25051216630000	4141	1716	1834	1755	1955
25051216640000	3518	2067	2224	2113	2343
25051216660000	3520	1260	1490	1296	1555
25051216680000	3688	1670	1896	1719	2001
25051216690000	4158	1699	1801	1745	1955
25051216700000	4077	1191	1352	1234	1450
25051216710000	4135	1686	1795	1729	1883
25051216730000	3430	1801	1975	1847	2080

25051216740000	3513	1890	2051	1962	2198
Well API	KB	Bow Island top	Lower Bow Island	Middle Bow Island	Skull Creek Shale
25051216760000	3681	1535	1680	1552	1736
25051216770000	3730	1736	1900	1768	1991
25051216800000	4241	1322	1421	1371	1529
25051216810000	3705	1716	1883	1768	1929
25051216830000	3568	0	0	0	0
25051216840000	4121	1503	1660	1552	1755
25051216850000	3814	1657	1831	1706	1909
25051216860000	4321	1608	1709	1647	1811
25051216870000	4295	1473	1677	1532	1831
25051216880000	3828	1545	1713	1585	1821
25051216890000	3823	1427	1591	1463	1693
25051216900000	4320	0	1919	0	0
25051216910000	3454	1749	1965	1795	2064
25051216920000	3457	2113	2297	2165	2411
25051216930000	3493	1752	1923	1795	2018
25051216950000	3767	1365	1591	1401	1696
25051216960000	3456	1749	1919	1788	2028
25051216970000	3438	1752	1952	1804	2064
25051216980000	4096	1650	1808	1683	1932
25051216990000	4044	1266	1440	1299	1555
25051217000000	4077	2142	2287	2205	2388
25051217010000	3276	2359	2490	2415	2602
25051217020000	3263	2320	2441	2372	2493
25051217040000	3408	2320	2464	2372	2546
25051217050000	3325	2287	2418	2333	2526
25051217060000	3282	2110	2241	2215	0
25051217070000	3412	2142	2382	2208	2454
25051217080000	3422	2323	2454	2375	2543
25051217090000	3344	1978	2205	2037	2247
25051217100000	3332	2077	0	0	0
25051217110000	3313	2293	2441	2339	2513
25051217120000	0	1447	1585	1480	1663
25051217130000	4006	0	0	0	0
25051217190000	3531	1552	1719	1604	1795
25051217200000	0	0	0	0	0
25051217210000	0	0	0	0	0
25051217220000	4171	0	0	0	0

25051217260000	3699	1355	1509	1385	1677
Well API	KB	Bow Island top	Lower Bow Island	Middle Bow Island	Skull Creek Shale
25051217270000	4428	554	656	594	781
25051217280000	4218	1401	1529	1463	1644
25051217290000	3727	0	1923	0	0
25051217300000	4421	581	676	620	801
25051217310000	4229	531	643	571	748
25051217330000	3620	0	0	0	0
25051217340000	3479	2116	2293	2175	0
25051217350000	3484	2119	2300	2172	2402
25051217360000	3458	2116	2290	2159	2402
25051217370000	3435	1749	1939	1791	2047
25051217390000	3445	1768	1952	1818	2064
25051217400000	3457	1759	1932	1811	2041
25051217510000	3261	2047	2208	2064	0
25051217540000	3393	2064	2244	2110	2349
25051217580000	3547	2106	2290	2149	0
25051217590000	3596	1365	1526	1388	1565
25051217610000	3373	1886	2024	1972	2093
25051217650000	3163	2077	2303	2149	2428
25051217660000	3289	2188	2320	2247	2470
25051218300000	3893	0	1952	0	0
25051600080000	3651	1978	2126	2021	2244

9.3. Appendix C: Spectral Readings Information

Mineralogical data information: Scalars that are measured are: Al-OH, Mg-OH, Al-Fe-Mg, and Fe-OH. Scalars listed have subtle variations that are indicative of fluids present at the time of alteration. Each of these scalars pertain to minerals with slight compositional variations that have differing spectral shifts. The compositional variations result in wavelength shifts of the Al-OH absorption spectrum at approximately 2200 nm. Mg-OH indicates fluids present at the time of alteration, the spectral shift is around 2350 nm. Fe-OH has an absorption feature near 2260 nm. Al-Fe-Mg scalar reports the wavelength of the deepest absorption feature of these three and has a larger range of scalar number 2160 nm to 2370 nm (Maras et al. 2016).

ISM and CSM are other scalars that are included in the reading, they the maturity of the clays in the sample. ISM (Illite Spectral Maturity) with increasing metamorphic grade, the reflectance spectrum of these minerals indicate a loss of molecular water and an increase of crystallinity, scalar values greater than one indicate a low grade metamorphic illite which indicate relatively low temperature of Formation, a number below one indicates a higher temperature alteration event.

CSM (Chlorite Spectral Maturity) with increasing metamorphic grade, the reflectance spectrum of these minerals indicate a loss of molecular water and an increase of crystallinity. Fe^3t describes iron oxides that form over a large range of geologic conditions the most common of which are hematite and goethite, they both have a spectral range of 750-1000 nm, the position of the feature shifts depending on the identity of the Fe^{3+} mineral. Fe^3i scalar tracks the intensity of this future, the higher the Fe3i value, the more intense the Fe^{3+} absorption (Maras et al. 2016).

SIGNATURE PAGE

This is to certify that the thesis prepared by Michael Vineyard entitled "Sequence Stratigraphic Correlation of the Bow Island Member of the Thermopolis Formation Using Surface and Subsurface Data, Liberty and Hill Counties, Montana" has been examined and approved for acceptance by the Department of Geological Engineering, Montana Tech of The University of Montana, on this 13th day of April, 2017.

Larry Smith, PhD, Associate Professor and Department Head
Department of Geological Engineering
Chair, Examination Committee

Chris Gammons, PhD, Professor
Department Geological Engineering
Member, Examination Committee

Curtis Link, PhD, Professor Emeritus and Director of Freshman Engineering
Department of Freshman Engineering
Member, Examination Committee